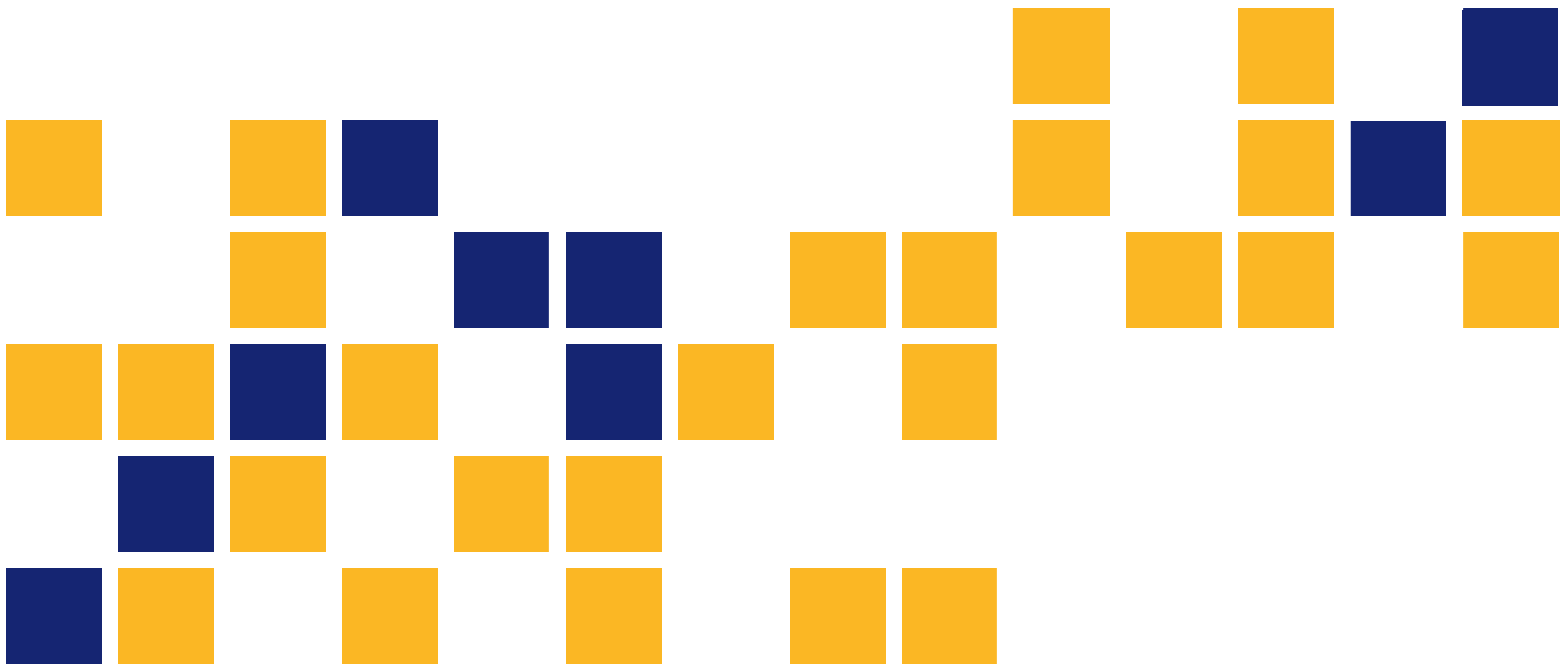


# Rational Load Rating of Deck-Girder Bridges with Girder End Shear Cracks in Reverse Orientation

Andrew Bernica  
Hayder Rasheed, Ph.D., P.E.

*Kansas State University Transportation Center*





<b>1 Report No.</b> K-TRAN: KSU-15-2	<b>2 Government Accession No.</b>	<b>3 Recipient Catalog No.</b>	
<b>4 Title and Subtitle</b> Rational Load Rating of Deck-Girder Bridges with Girder End Shear Cracks in Reverse Orientation		<b>5 Report Date</b> April 2017	<b>6 Performing Organization Code</b>
		<b>7 Performing Organization Report No.</b>	
<b>7 Author(s)</b> Andrew Bernica, Hayder Rasheed, Ph.D., P.E.		<b>10 Work Unit No. (TRAIS)</b>	
<b>9 Performing Organization Name and Address</b> Kansas State University Transportation Center Department of Civil Engineering 2126 Fiedler Hall Manhattan, Kansas 66506		<b>11 Contract or Grant No.</b> C2046	
		<b>13 Type of Report and Period Covered</b> Final Report August 2014–July 2016	
<b>12 Sponsoring Agency Name and Address</b> Kansas Department of Transportation Bureau of Research 2300 SW Van Buren Topeka, Kansas 66611-1195		<b>14 Sponsoring Agency Code</b> RE-0653-01	
		<b>15 Supplementary Notes</b> For more information write to address in block 9.	
<p>Reverse diagonal shear cracking at reinforced concrete girder supports affects many low-volume bridges built in the early 1900s in Kansas. This phenomenon, however, is not addressed in the American Association of State Highway and Transportation Officials (AASHTO, 2002) Standard Specifications for Highway Bridges or American Concrete Institute specifications. This study investigates causes of this cracking and develops Bridge Rating of Inclined Damage at Girder Ends (BRIDGE), an Excel-based software, to determine load rating of a user-specified bridge with reverse diagonal shear cracking at girder supports. A user interface creates a grillage model of an existing bridge and places various rating trucks on the bridge. Equivalent flexibility analysis distributes truck live loads within deck panels to surrounding girders and diaphragms. Stiffness matrices are utilized to find nodal displacements and reactions at the girder supports caused by truck live loads and bridge dead load. These reactions are checked against RISA software models to test the accuracy of the stiffness matrix application. ABAQUS FE models and Mohr's circle stress distribution determine driving and clamping forces on the crack due to resolution of dead and live load reactions and friction force generated between the concrete girder and rusty steel bearing pad along the shear crack orientation. In addition to the simplified modified compression field theory, these clamping and driving forces are used to determine the shear capacity of each girder at the reverse cracks. A modified version of Equation 6B.4.1 from the Manual for Bridge Evaluation (AASHTO, 2011) is used to find operating and inventory rating factors (RFs) for the bridge.</p> <p>The BRIDGE program, used to load rate Bridge No. 54-104-15.45, yielded reasonable RFs for various trucks and reduced girder widths. The operating RFs were consistently above 1 and the inventory RFs were below 1, indicating that the decision to load post this bridge is based on the engineer's judgment.</p>			
<b>17 Key Words</b> Load Rating, Reverse Diagonal Shear Cracking, Deck-Girder Bridges		<b>18 Distribution Statement</b> No restrictions. This document is available to the public through the National Technical Information Service <a href="http://www.ntis.gov">www.ntis.gov</a> .	
<b>19 Security Classification (of this report)</b> Unclassified	<b>20 Security Classification (of this page)</b> Unclassified	<b>21 No. of pages</b> 132	<b>22 Price</b>

Form DOT F 1700.7 (8-72)

This page intentionally left blank.

# **Rational Load Rating of Deck-Girder Bridges with Girder End Shear Cracks in Reverse Orientation**

Final Report

Prepared by

Andrew Bernica  
Hayder Rasheed, Ph.D., P.E.

Kansas State University Transportation Center

A Report on Research Sponsored by

THE KANSAS DEPARTMENT OF TRANSPORTATION  
TOPEKA, KANSAS

and

KANSAS STATE UNIVERSITY TRANSPORTATION CENTER  
MANHATTAN, KANSAS

April 2017

© Copyright 2017, **Kansas Department of Transportation**

## **PREFACE**

The Kansas Department of Transportation's (KDOT) Kansas Transportation Research and New-Developments (K-TRAN) Research Program funded this research project. It is an ongoing, cooperative and comprehensive research program addressing transportation needs of the state of Kansas utilizing academic and research resources from KDOT, Kansas State University and the University of Kansas. Transportation professionals in KDOT and the universities jointly develop the projects included in the research program.

## **NOTICE**

The authors and the state of Kansas do not endorse products or manufacturers. Trade and manufacturers names appear herein solely because they are considered essential to the object of this report.

This information is available in alternative accessible formats. To obtain an alternative format, contact the Office of Public Affairs, Kansas Department of Transportation, 700 SW Harrison, 2<sup>nd</sup> Floor – West Wing, Topeka, Kansas 66603-3745 or phone (785) 296-3585 (Voice) (TDD).

## **DISCLAIMER**

The contents of this report reflect the views of the authors who are responsible for the facts and accuracy of the data presented herein. The contents do not necessarily reflect the views or the policies of the state of Kansas. This report does not constitute a standard, specification or regulation.

## Abstract

Reverse diagonal shear cracking at reinforced concrete girder supports affects many low-volume bridges built in the early 1900s in Kansas. This phenomenon, however, is not addressed in the American Association of State Highway and Transportation Officials (AASHTO, 2002) *Standard Specifications for Highway Bridges* or American Concrete Institute specifications. This study investigates causes of this cracking and develops Bridge Rating of Inclined Damage at Girder Ends (BRIDGE), an Excel-based software, to determine load rating of a user-specified bridge with reverse diagonal shear cracking at girder supports. A user interface creates a grillage model of an existing bridge and places various rating trucks on the bridge. Equivalent flexibility analysis distributes truck live loads within deck panels to surrounding girders and diaphragms. Stiffness matrices are utilized to find nodal displacements and reactions at the girder supports caused by truck live loads and bridge dead load. These reactions are checked against RISA software models to test the accuracy of the stiffness matrix application. ABAQUS FE models and Mohr's circle stress distribution determine driving and clamping forces on the crack due to resolution of dead and live load reactions and friction force generated between the concrete girder and rusty steel bearing pad along the shear crack orientation. In addition to the simplified modified compression field theory, these clamping and driving forces are used to determine the shear capacity of each girder at the reverse cracks. A modified version of Equation 6B.4.1 from the *Manual for Bridge Evaluation* (AASHTO, 2011) is used to find operating and inventory rating factors (RFs) for the bridge.

The BRIDGE program, used to load rate Bridge No. 54-104-15.45, yielded reasonable RFs for various trucks and reduced girder widths. The operating RFs were consistently above 1 and the inventory RFs were below 1, indicating that the decision to load post this bridge is based on the engineer's judgment.

## **Acknowledgements**

Thanks are extended to KDOT for sponsoring this research. Special thanks to John Culbertson, John Jones, Calvin Reed, and Mark Hoppe for providing valuable feedback and suggestions that kept this project moving forward.



# Table of Contents

Abstract .....	v
Acknowledgements .....	vi
Table of Contents .....	vii
List of Tables .....	x
List of Figures .....	xiii
Chapter 1: Introduction .....	1
1.1 Background .....	1
1.2 Objective .....	2
Chapter 2: Literature Review .....	3
2.1 Load Ratings .....	3
2.2 Dead Load .....	5
2.3 Live Load .....	5
2.3.1 Truck Types .....	5
2.3.2 Impact Factor .....	7
2.3.3 Capacity .....	7
2.4 Friction Coefficients .....	11
2.4.1 Steel-to-Concrete .....	11
2.4.2 Cracked Concrete-To-Cracked Concrete .....	12
2.5 Transformation of Stress .....	13
2.5.1 Transformation of Stress Block .....	14
2.5.2 Formulation of Mohr's Circle .....	15
2.5.3 Principal Stresses and Maximum Shearing Stress .....	17
2.6 Effective Flange Width .....	19
2.7 Poisson's Ratio .....	20
Chapter 3: KSU BRIDGE Input/Output Interface .....	21
3.1 Mesh & Alignment Sheet .....	21
3.1.1 Lane Alignment .....	22
3.1.2 Bridge Mesh .....	23
3.1.3 Background Functions of the Mesh & Alignment Sheet .....	25

3.2 Section Geometry and Material Properties Sheet .....	27
3.2.1 Section Geometry.....	27
3.2.2 Material Properties.....	28
3.2.3 Crack Properties.....	28
3.2.4 Background Computations of Section Geometry Sheet .....	30
3.3 Section Properties Sheet .....	31
3.4 Truck Input Sheet.....	32
3.4.1 Truck Selection and Placement.....	33
3.4.2 Multiple Lane Presence Factor .....	38
3.4.3 Background of the Truck Input Sheet .....	39
3.4.4 Bridge Creation and Placement of Trucks on the Bridge .....	41
3.5 Reaction Input Sheet.....	42
3.6 Results Sheet.....	43
Chapter 4: KSU BRIDGE Functionality.....	45
4.1 Mesh Creation.....	45
4.1.1 Creating Grid and Assigning Member and Node Numbers.....	45
4.1.2 Assigning Coordinates to Nodes and End Nodes to Members .....	46
4.1.3 Identifying Boundary Members for Panels.....	47
4.1.4 Determining Truck-Load Paths.....	47
4.1.5 Placing Trucks on Bridge.....	48
4.1.6 Determining Multiple Presence Factor .....	49
4.1.7 Determining Load Length.....	50
4.2 Placement of Trucks on Bridge .....	50
4.2.1 Identifying Panels under Each Load and Location of Load on the Panel.....	50
4.2.2 Distributing Each Load to Members Surrounding the Panel .....	50
4.2.3 Determining Fixed End Reactions at Each Node Caused by Live Loads.....	62
4.2.4 Determining Reactions at Nodes Caused by Dead Loads.....	63
4.2.5 Printing $k_{ff}$ and $k_{sf}$ Reactions for the Bridge Matrix .....	64
4.3 Load Rate Bridge .....	65
4.3.1 Assigning Properties to Each Member.....	65
4.3.2 Creating Assembled Stiffness Matrix for Bridge.....	66

4.3.3 Creating $k_{ff}$ and $k_{sf}$ Matrices .....	67
4.3.4 Creating $k_{ff}^{-1}$ Matrix .....	67
4.3.5 Finding Displacements at Each Node .....	67
4.3.6 Finding Reactions at Each Support.....	67
4.3.7 Determining Governing Live Load at Each Support .....	68
4.3.8 Calculating the Impact Factor .....	68
4.3.9 Determining Girder Capacity.....	68
4.3.10 Calculating the Rating Factor at Each Support.....	74
Chapter 5: Analysis and Results .....	75
5.1 Support Reactions: BRIDGE versus RISA 3D.....	75
5.2 Capacity .....	77
5.2.1 ABAQUS Setup Confirmation .....	77
5.2.2 Girder Length versus S/N ratio .....	80
5.2.3 S/N Relationships.....	81
5.2.4 Estimation of Crack Propagation Angle .....	83
5.2.5 Predicted Crack Propagation Angle versus Actual Propagation Angle.....	84
5.3 Analysis of Bridge No. 54-104-15.45.....	85
Chapter 6: Conclusions .....	87
References.....	88
Appendix A: Truck Types .....	90
Appendix B: Stiffness Matrix .....	92
Appendix C: Support Reactions: Program versus RISA .....	93
Appendix D: ABAQUS Models: Shear and Normal Forces .....	110
Appendix E: RF and Truck Ratings for Bridge # 54-104-15.45.....	113

## List of Tables

Table 2.1: Multiple Presence Factor .....	6
Table 4.1: Comparison of Load Distribution to Girders and Diaphragms using Various Analysis Methods .....	58
Table 4.2: Comparison of the Centroid of Reaction along Girders and Diaphragms using Various Analysis Methods .....	59
Table 4.3: $f_G/f_{Gmax}$ Values for $x/a$ Locations and Aspect Ratios .....	61
Table 4.4: $f_D/f_{Dmax}$ Values for $y/b$ Locations and Aspect Ratios .....	61
Table 4.5: $f_G/f_{Gmax}$ and $f_D/f_{Dmax}$ Values for Load Location on Panel .....	62
Table 4.6: ABAQUS Parameter Variation .....	70
Table 5.1: BRIDGE versus RISA 3D Model Parameter Variations.....	75
Table 5.2: Support Reaction Comparison #1: BRIDGE Input .....	76
Table 5.3: Support Reaction Comparison #1: Results.....	76
Table 5.4: S/N Ratios at Bearing Pad for L/h Ratios for ABAQUS Models 12-0.4-6-L and 18-0.4-6-L.....	80
Table 5.5: Load on Corresponding ABAQUS Models as Shown in Tables 5.6 through 5.11 ..	82
Table 5.6: S/N Ratio Tables for ABAQUS Models with $b_w = 12$ inches and $L/h = 7$ .....	82
Table 5.7: S/N Ratio Tables for ABAQUS Models with $b_w = 12$ inches and $L/h = 12$ .....	82
Table 5.8: S/N Ratio Tables for ABAQUS Models with $b_w = 15$ inches and $L/h = 7$ .....	82
Table 5.9: S/N Ratio Tables for ABAQUS Models with $b_w = 15$ inches and $L/h = 12$ .....	83
Table 5.10: S/N Ratio Tables for ABAQUS Models with $b_w = 18$ inches and $L/h = 7$ .....	83
Table 5.11: S/N Ratio Tables for ABAQUS Models with $b_w = 18$ inches and $L/h = 12$ .....	83
Table 5.12: Principal Stresses, Maximum Shear Stress, and Angle of Maximum Shear Plan for Seven ABAQUS Models .....	84
Table 5.13: Location and Geometry of Seven Girder Supports for Bridge No. 54-104- 317.27-(0005) .....	85
Table 5.14: Observed Propagation Angles of Reverse Diagonal Crack for Seven Supports for Bridge No. 54-104-317-27-(0005).....	85
Table 5.15: Rating Factors for Spans #1 and #5 for 50% and 100% Girder Width .....	86
Table 5.16: Truck Ratings for Spans #1 and #5 for 50% and 100% Girder Width.....	86

Table A.1: Truck Axle Loads and Spacings.....	90
Table C.1: Support Reaction Comparison #2: BRIDGE Input .....	93
Table C.2: Support Reaction Comparison #2: Results.....	93
Table C.3: Support Reaction Comparison #3: BRIDGE Input .....	94
Table C.4: Support Reaction Comparison #3: Results.....	94
Table C.5: Support Reaction Comparison #4: BRIDGE Input .....	95
Table C.6: Support Reaction Comparison #4: Results.....	95
Table C.7: Support Reaction Comparison #5: BRIDGE Input .....	96
Table C.8: Support Reaction Comparison #5: Results.....	96
Table C.9: Support Reaction Comparison #6: BRIDGE Input .....	97
Table C.10: Support Reaction Comparison #6: Results.....	97
Table C.11: Support Reaction Comparison #7: BRIDGE Input .....	98
Table C.12: Support Reaction Comparison #7: Results.....	98
Table C.13: Support Reaction Comparison #8: BRIDGE Input .....	99
Table C.14: Support Reaction Comparison #8: Results.....	99
Table C.15: Support Reaction Comparison #9: BRIDGE Input .....	100
Table C.16: Support Reaction Comparison #9: Results.....	100
Table C.17: Support Reaction Comparison #10: BRIDGE Input .....	101
Table C.18: Support Reaction Comparison #10: Results.....	101
Table C.19: Support Reaction Comparison #11: BRIDGE Input .....	102
Table C.20: Support Reaction Comparison #11: Results.....	102
Table C.21: Support Reaction Comparison #12: BRIDGE Input .....	103
Table C.22: Support Reaction Comparison #12: Results.....	103
Table C.23: Support Reaction Comparison #13: BRIDGE Input .....	104
Table C.24: Support Reaction Comparison #13: Results.....	104
Table C.25: Support Reaction Comparison #14: BRIDGE Input .....	105
Table C.26: Support Reaction Comparison #14: Results.....	105
Table C.27: Support Reaction Comparison #15: BRIDGE Input .....	106
Table C.28: Support Reaction Comparison #15: Results.....	106
Table C.29: Support Reaction Comparison #16: BRIDGE Input .....	107
Table C.30: Support Reaction Comparison #16: Results.....	107

Table C.31: Support Reaction Comparison #17: BRIDGE Input .....	108
Table C.32: Support Reaction Comparison #17: Results.....	108
Table C.33: Support Reaction Comparison #18: BRIDGE Input .....	109
Table C.34: Support Reaction Comparison #18: Results.....	109
Table D.1: Forces at One Support for ABAQUS Models with Girder Width of 12 inches .....	110
Table D.2: Forces at One Support for ABAQUS Models with Girder Width of 15 inches .....	111
Table D.3: Forces at One Support for ABAQUS Models with Girder Width of 18 inches .....	112
Table E.1: Rating Factors for Spans #2 and #4 for 50% and 100% Girder Width .....	113
Table E.2: Truck Ratings for Spans #2 and #4 for 50% and 100% Girder Width.....	113
Table E.3: Rating Factors for Span #3 for 50% and 100% Girder Width .....	114
Table E.4: Truck Ratings for Span #3 for 50% and 100% Girder Width .....	114

## List of Figures

Figure 1.1: Reverse Diagonal Shear Cracking.....	1
Figure 1.2: Normal Diagonal Shear Cracking .....	1
Figure 2.1: Clearance and Load Lane Width.....	6
Figure 2.2: Crack Width at Girder C, Left Side, Pier 1 of Bridge No. 54-104-317.27 .....	8
Figure 2.3: Support Rockers at Pier 4, Left Side, Span 5 of Bridge No. 54-104-317.27 .....	12
Figure 2.4: General State of Stress at a Point .....	14
Figure 2.5: Plane Stresses .....	14
Figure 2.6: Transformed Plane Stresses .....	15
Figure 2.7: Mohr’s Circle of Plane Stresses .....	16
Figure 2.8: Principal Stresses.....	17
Figure 2.9: Maximum Shearing Stress .....	19
Figure 3.1: Bridge Mesh and Alignment User Interface.....	21
Figure 3.2: Drop-Down Menu for Number of Lanes.....	22
Figure 3.3: Drop-Down Menu for Median between Lanes .....	22
Figure 3.4: “Check Diaphragms” Error Message .....	24
Figure 3.5: “Check Diaphragms” Virtual Diaphragm Adequacy Message .....	24
Figure 3.6: Effective and Actual Slab Widths .....	25
Figure 3.7: Numerical Value for User-Specified Number of Lanes.....	26
Figure 3.8: Median Placement Drop-Down Menu Facilitation .....	26
Figure 3.9: Numerical Representation of Median Placement.....	26
Figure 3.10: Section Geometry and Material Properties User Interface.....	27
Figure 3.11: Angle of Crack Propagation.....	29
Figure 3.12: Use Input or Calculated Angle? Drop-Down Menu.....	29
Figure 3.13: Background of Section Geometry and Material Properties Sheet.....	30
Figure 3.14: Methods to Calculate the Torsional Constant .....	31
Figure 3.15: Section Properties Sheet.....	32
Figure 3.16: Truck Input User Interface .....	33
Figure 3.17: Truck Input and Information Section .....	34
Figure 3.18: Truck Type Drop-Down Menu .....	35

Figure 3.19: Lane Number Drop-Down Menu .....	36
Figure 3.20: Warning Message for Multiple Trucks in a Lane.....	36
Figure 3.21: Direction of Travel Drop-Down Menu .....	37
Figure 3.22: Truck Location Drop-Down Menu .....	38
Figure 3.23: Multiple Lane Presence Factor Drop-Down Menu .....	38
Figure 3.24: Number of Trucks .....	39
Figure 3.25: Numerical Representation of Truck Placement User Inputs .....	39
Figure 3.26: Trucks that Share a Lane .....	39
Figure 3.27: Lanes Occupied by a Truck.....	40
Figure 3.28: Number of Loaded Lanes .....	40
Figure 3.29: User-Specified Number of Lanes .....	40
Figure 3.30: Possible Lane Numbers .....	40
Figure 3.31: Spacing and Loads on Each Truck Axle .....	41
Figure 3.32: First Two Buttons that Run BRIDGE .....	41
Figure 3.33: Reaction Input User Interface.....	42
Figure 3.34: Use Calculated or Input Reactions Drop-Down Menu .....	42
Figure 3.35: Results Sheet .....	44
Figure 3.36: Bridge Mesh Graphic .....	44
Figure 4.1: Bridge Mesh with Labeled Members and Nodes .....	46
Figure 4.2: Member End Nodes and Node Coordinates .....	46
Figure 4.3: Panel List and Surrounding Members .....	47
Figure 4.4: Four Load Paths within Each Lane .....	48
Figure 4.5: Truck Load and Placement Information.....	49
Figure 4.6: Reduction Factor .....	49
Figure 4.7: Load Length for Impact Factor Calculation .....	50
Figure 4.8: RISA Model of Finite Element Analysis of Panel with 3 Inch $\times$ 3 Inch Mesh.....	52
Figure 4.9: Reaction at Each Node along Primary Diaphragm .....	52
Figure 4.10: Reaction at Each Node along Secondary Diaphragm .....	53
Figure 4.11: Reaction at Each Node along Primary Girder .....	53
Figure 4.12: Reaction at Each Node along Secondary Girder .....	54

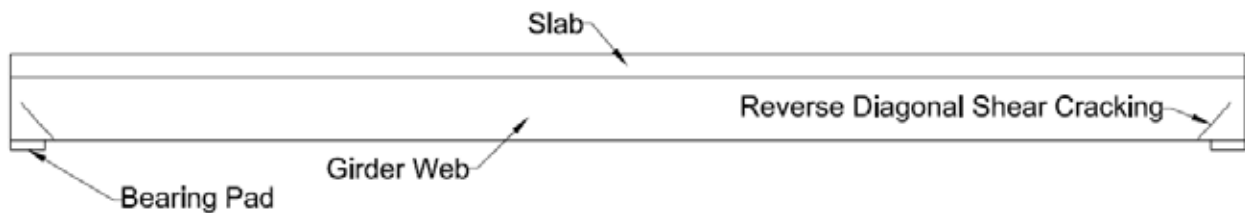


Figure 4.13: RISA Model of Rigid Slab Analysis of Panel with Pinned Girders and Free Diaphragms .....	55
Figure 4.14: RISA Model for Rigid Beam Analysis within the Panel .....	57
Figure 4.15: Load Placement on Panel .....	60
Figure 4.16: FEM for a Point Load on the Span.....	63
Figure 4.17: FEM for a Distributed Load .....	64
Figure 4.18: Snapshot of $k_{ff}$ Loads Sheet .....	65
Figure 4.19: Snapshot of $k_{sf}$ Reactions Sheet.....	65
Figure 4.20: Member Properties .....	66
Figure 4.21: Reaction and Friction Forces on the Reverse Diagonal Crack According to the Friction Load Approach .....	69
Figure 4.22: Parameters in the ABAQUS Models.....	70
Figure 4.23: Loading on ABAQUS Model Girders.....	71
Figure 4.24: Shear-To-Normal Force Ratio Tables .....	72
Figure 5.1: Support Reaction Comparison #1: RISA 3D Model.....	77
Figure 5.2: Normal Force Distribution in the Girder at the Girder-to-Bearing Pad Interface for Model 12-0.4-10-12.....	78
Figure 5.3: Shear Force Distribution in the Girder at the Girder-to-Bearing Pad Interface for Model 12-0.4-10-12.....	79
Figure 5.4: $L/h$ Ratio versus $S/N$ Ratio for Model 12-0.4-6-L.....	81
Figure 5.5: $L/h$ Ratio versus $S/N$ Ratio for Model 18-0.4-6-L .....	81
Figure B.1: Stiffness Matrix as Function Member Properties.....	92

# Chapter 1: Introduction

## 1.1 Background

The Kansas Department of Transportation (KDOT) and several Kansas counties own a large number of low-traffic bridges that were built in the early- to mid-1900s and have developed abnormal reverse diagonal shear cracking at the concrete girder supports, as shown in Figure 1.1. These cracks may cause loss of girder-bearing support. Diagonal shear cracking typically propagates from the bottom of the girder at the support toward the slab within the span of the girder, as shown in Figure 1.2. Abnormal cracking is thought to be caused by friction between the concrete girder and the rusty, locked steel-bearing pad. This friction exists because the bearing pad has corroded, preventing the girder from rotating on its rocker. Current bridges contain rubber-bearing pads that do not corrode when exposed to moisture, but steel-bearing pads also used in bridge construction corrode when exposed to decades of moisture and deicing salt, thereby turning original pinned connections into partially fixed connections.



**Figure 1.1: Reverse Diagonal Shear Cracking**

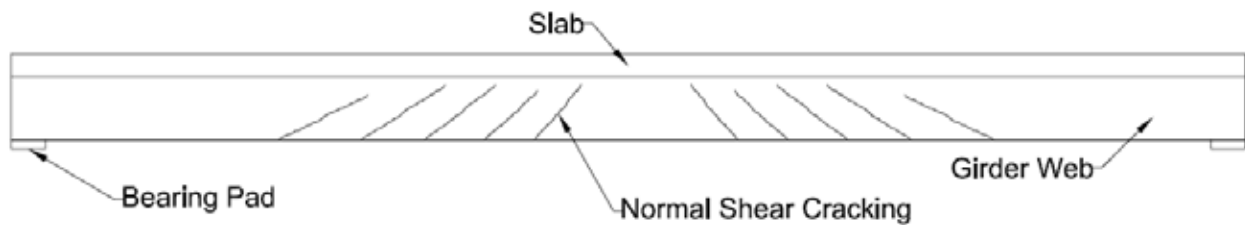


**Figure 1.2: Normal Diagonal Shear Cracking**

## 1.2 Objective

Reverse diagonal shear cracking is not addressed in the American Association of State Highway and Transportation Officials (AASHTO, 2002) *Standard Specifications for Highway Bridges* or American Concrete Institute (ACI) specifications, so the objective of this project was to determine the cause of this phenomenon. Because KDOT desires to rationally assess the safety of these bridges, this research also sought to determine an accurate method for calculating the capacity and load rating factor (RF) for girders experiencing reverse diagonal shear cracking. An Excel-based program, KSU Bridge Rating of Inclined Damage at Girder Ends (KSU BRIDGE), was developed to analyze a user-defined bridge span and determine the capacity and RF for each girder end.

## Chapter 2: Literature Review

### 2.1 Load Ratings

Bridge load rating, which determines safe live-load capacities of new and existing bridges, considers only permanent loads (dead loads) and vehicular loads (live loads and impact loads). Therefore, extreme event loads such as earthquake, wind, ice, flood, truck crashes, and fire loads were not considered in this study. This load rating was then used along with engineering judgement to determine the need for bridge strengthening or load posting. Load posting restricts truck loads on a bridge to a fraction of legal truck load limits, as discussed in Section 2.1.2.1 of Bernica (2016). The structure should be posted at a safe level that will not shorten the life of the structure (KDOT, 2016). The *Manual for Bridge Evaluation* (AASHTO, 2011) state that any bridge that cannot carry a minimum gross live load of 6 kips must be closed. Article 6 in the *Manual for Bridge Evaluation* outlines three methods to determine load rating: the load and resistance factor rating (LRFR) method, the allowable stress design (ASD) method, and the load factor (LF) method. However, AASHTO (2011) does not distinguish a preferred method, allowing bridge owners to choose which method to use.

Because KDOT uses the LF method to load rate bridges (KDOT, 2016), that method was used in this study. According to AASHTO (2011), the LF method analyzes actual loads on the structure multiplied by load factors ( $A_1$  and  $A_2$  defined in Equation 2.2 below), and factors are applied to dead and live loads based on uncertainty in load calculations. For example, dead loads are typically calculated with more accuracy than live loads, so the dead-load multiplication factor is smaller than the live-load multiplication factor. These factored loads are used in Equation 2.2 below to determine the bridge rating to ensure that bridge member strength is not exceeded. Bridges under investigation displayed unusual reverse diagonal shear cracking at the supports, so this work focused on shear strength capacity at girder ends.

The LF method utilizes two rating levels: inventory rating and operating rating. Inventory rating describes the load a bridge can sustain for an indefinite period of time. This rating is similar to the design load level, but it also incorporates bridge deterioration. Operating rating describes the absolute maximum live load to which a bridge may be subjected (AASHTO, 2011); frequent loads at the operating level cause bridge deterioration. Each bridge member is rated, and

the lowest rating becomes the governing load rating for that bridge. A bridge's rating, as defined by AASHTO (2011) Equation 6B.4.1-2, is the RF multiplied by the rating vehicle (Equation 2.1):

$$\mathbf{Load\ Rating = RF \times Rating\ Vehicle\ Weight} \qquad \mathbf{Equation\ 2.1}$$

The rating vehicle weight is the maximum legal load for a particular type of vehicle. According to the KDOT (2016) *Design Manual*, Kansas statutes allow for a gross vehicle weight of 80,000 pound (lbs) on interstate highways and 85,000 lbs on other highways without a special permit. The KSU BRIDGE program provides 13 standard trucks (Bernica, 2016, Section 2.1.2) for the end users to load rate a bridge. Each standard truck produces a unique live-load effect on a bridge, resulting in a different RFs and ratings for each truck. Any truck that causes a rating less than the legal limit will be used for posting (KDOT, 2016). AASHTO (2011) Equation 6B.4.1-1 defines the RF using Equation 2.2:

$$\mathbf{RF = \frac{Capacity - A_1 DL}{A_2 (LL + I)}} \qquad \mathbf{Equation\ 2.2}$$

Where:

*Capacity* = capacity of girder

*DL* = dead-load reaction at girder support

*LL* = live-load reaction at girder support

*I* = impact factor of live load

*A<sub>1</sub>* = factor for dead loads (1.3)

*A<sub>2</sub>* = factor for live loads (1.3 for operating rating level, 2.17 for inventory rating level)

When load rating a bridge, the girders are usually assumed to be fixed or a pinned support. Girders with integral abutments, however, may need to be analyzed as partially fixed (KDOT, 2016).

## 2.2 Dead Load

The dead load of a bridge is based on existing conditions, geometry, and material properties at the time of analysis (AASHTO, 2011). Overlay thickness, which is typically measured at the time of inspection, should also be considered in the dead load.

## 2.3 Live Load

Truck loads, axle configurations, and truck placement for load rating bridges are discussed in this section. A discussion of live load reductions and when these reductions are applicable is also included.

### 2.3.1 Truck Types

AASHTO (2011) Article 6B.6.2 states that extreme live load used in Equation 2.2 is governed by AASHTO (2002) Standard Specifications. AASHTO (2011) Article 6B.7.2 states that eight standard trucks (Type 3, Type 3S2, Type 3-3, SU4, SU5, SU6, SU7, and notional rating load [NRL]) and any truck configurations specified by bridge owners should be analyzed to load rate a bridge. AASHTO (2002) Article 3.7.5 specifies two classes of loading: H and HS truck loadings. KDOT asserts that any legal truck configuration that causes increased stress on a bridge should be used for rating (KDOT, 2016). In addition to the eight standard trucks specified by AASHTO (2002) or AASHTO (2011), the KDOT (2016) *Design Manual* specifies that T130, T170, and heavy equipment transport (HET) trucks should be used to load rate bridges, for a total of 13 standard trucks. Appendix A lists these vehicles, their axle spacings, and weights. The maximum load allowed for one axle on Kansas highways is 20 kips and 34 kips for a dual axle, with a maximum total truck weight of 85.5 kips. Some truck axle loads in Appendix A exceed the maximum allowable load, so when those trucks are posted their axles are posted at the legal limit while the other axles on the truck are posted for proportionately reduced loads (KDOT, 2016).

### 2.3.1.1 Truck Placement

AASHTO (2002) should be followed when determining the number of loaded lanes and placement of wheel lines (AASHTO, 2011). AASHTO (2011) Article C6B.6.2.2 recommends consideration of multiple trucks in the same lane when necessary and adherence to a minimum of 30 feet (ft) of clear space between trucks in the same lane when the loading per truck is less than 12 tons. Truck loads should be placed within their respective load lanes so as to produce maximum stress in the member being analyzed (AASHTO, 2002). Figure 2.1 shows standard truck axles spaced 6 ft apart with the truck occupying a 10-ft-wide load lane (AASHTO, 2002), meaning that the truck will occupy 2 ft of space to either side of the wheel loads.

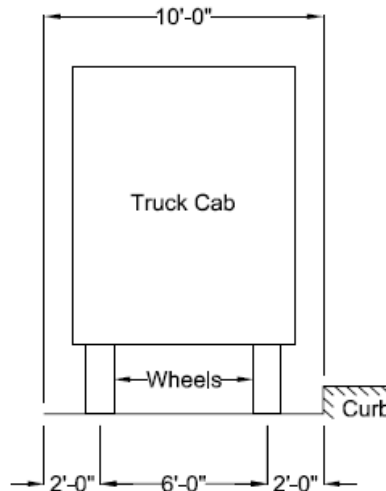


**Figure 2.1: Clearance and Load Lane Width**

### 2.3.1.2 Live Load Reduction

A reduction in live load if multiple lanes are loaded simultaneously is allowed due to the improbability of coincident maximum loading in multiple lanes (AASHTO, 2002). These live-load reduction factors are described in Table 2.1.

**Table 2.1: Multiple Presence Factor**

Number of Loaded Lanes	Multiple Presence Factor
1 or 2	1
3	0.9
4 or more	0.75

Adapted from AASHTO (2002)

### 2.3.2 Impact Factor

AASHTO (2011) specifies that AASHTO (2002) Equation 3.1 be used for the impact factor in Equation 2.2, as shown in Equation 2.3. The impact factor accounts for dynamic effects caused by a truck, such as the bounce, sway, and momentum of the vehicle. Dynamic effects also include the response of wheels impacting pavement surface discontinuities, such as joints, cracks, and potholes.  $L$  is limited to the smallest truck length or bridge length in order to conservatively allow a higher impact load coefficient.

$$I = \frac{50}{125+L} < 0.3 \quad \text{Equation 2.3}$$

Where:

$$L = \text{length of loaded part of bridge (ft)} \\ = \min \begin{cases} \text{Truck Length} \\ \text{Bridge Length} \end{cases}$$

### 2.3.3 Capacity

Field investigations are the basis of older bridge rating for load-carrying capacity. Any feature of a bridge that affects its capacity should be carefully evaluated, and any damage, deterioration, or loss of cross-sectional area should be noted (AASHTO, 2011). AASHTO (2011) also specifies that certain bridges are subject to unique geometry, loadings, and deterioration, so the load rating procedure for these bridges should be augmented to suit those unique characteristics. The KSU BRIDGE program developed in this study analyzes bridges that are experiencing unusual reverse diagonal shear cracking at the supports. Girder capacity at the supports is governed by the shear capacity of the girder at these cracks. This girder capacity is a function of two parameters: material shear strength of the girder and friction force between the two faces of the crack caused by clamping forces on either side of the crack.



### 2.3.3.1 Material Capacity

Figure 2.2 is a photograph from an inspection report of Kansas Bridge No. 54-104-317.27 taken in 2011. As shown in the photo, the claw of a hammer is wedged into a shear crack at a girder support, demonstrating that parts of the girder have spalled off at the crack interface and not all of the girder width provides shear resistance.



**Figure 2.2: Crack Width at Girder C, Left Side, Pier 1 of Bridge No. 54-104-317.27**

Source: KDOT (2011)

AASHTO (2011) Article 6B.5.3 states that capacity calculations should account for observable effects of deterioration in the girder, while Article C6.1.2 explicitly states that the member cross section used to determine capacity is the gross cross section less the deteriorated section of the member. In order to account for the deterioration shown in Figure 2.2, the KSU BRIDGE program allows a user to decrease girder width used in material shear capacity calculations by a certain percentage to be estimated during inspection.

Ultimate shear strength  $V_u$  of a shear cracked section is described by AASHTO (2002) Equation 8-46, rewritten here as Equation 2.4:

$$V_u = \phi V_n \quad \text{Equation 2.4}$$

Where:

$V_u$  = ultimate shear strength of the beam (lbs)

$V_n$  = nominal shear strength of the beam (lbs)

$\phi$  = shear strength reduction factor

= 0.85 for reinforced concrete (AASHTO, 2002)

Nominal shear capacity  $V_n$  is given by Equation 2.5 (AASHTO, 2002):

$$V_n = V_c + V_s \quad \text{Equation 2.5}$$

Where:

$V_c$  = shear capacity provided by concrete (lbs)

$V_s$  = steel shear strength (kips per square inch [ksi])

The simplified modified compression field theory (SMCFT), developed by Bentz, Vecchio, and Collins (2006) as an abbreviated, simple form of the modified compression field theory (MCFT) proposed in the 1980s, was used to find the shear capacity of the girder provided by concrete,  $V_c$ . The MCFT reliably determines the shear capacity of reinforced concrete sections. Prior to the MCFT, shear capacity calculations in various codes, including ACI codes, were extremely inconsistent and inaccurate. The ACI code found the shear strength as the load causing diagonal shear cracking at a 45° angle plus the axial load effect (subtracted capacity if member was in axial-tension and added strength if member was in axial-compression). Bentz et al. (2006) asserted that, on average, ACI-calculated capacity was 40% more conservative than experimental shear capacities and that the coefficient of variation (COV) was 46.7%.

The MCFT was introduced as a more effective method for calculating the shear capacity of a section. Bentz et al. (2006) and Abouelleil (2015) explained the assumptions made by Vecchio and Collins (1982) in order to derive the MCFT. First, the MCFT calculates the diagonal crack angle based on strain conditions in the section instead of assuming an angle of 45° (with respect to the bottom of the beam). It also accounts for the fact that tensile stresses exist in the concrete between the cracks and uses average stresses and strains over large areas (covering multiple cracks) in the beam. In addition, each strain state is assumed to correspond to one stress

state, the longitudinal and transverse steel is assumed to be distributed uniformly across the element, and a perfect bond is assumed to exist between the steel and concrete. Shear capacity calculated by the MCFT is, on average, only 1% greater than experimental shear failures, with a COV of only 12.2%. Although the MCFT is a much more accurate predictor of shear capacity than previous methods, this model is mathematically very complex, requiring 15 equations shown in Bentz et al. (2006) to be solved iteratively via computer modeling. Bentz et al. (2006) simplified the MCFT to allow increased understanding of the calculations so ‘back of the napkin’ calculations could be made.

The SMCFT assumes that the direction of principal compressive stress remains constant, on average, over the effective shear depth  $d_v$  and that shear stresses are uniformly distributed over the width of the web and  $d_v$ . It also assumes that shear strength of the section is calculated by considering biaxial stress conditions at one location in the section web (AASHTO, 2014). According to Bentz et al. (2006), SMCFT predicts shear capacities only 11% larger than experimental shear capacities, with a reasonably accurate COV of 13%. AASHTO (2014) incorporates SMCFT into their procedure to find the nominal shear capacity of a section, as shown in the following equations (Equations 5.8.3.3-1 through 5.8.3.4.2-5 of AASHTO, 2014):

$$V_c = \beta \sqrt{f'_c} b_v d_v \quad \text{Equation 2.6}$$

$$V_s = \frac{A_v f_y d_v (\cot \theta + \cot \alpha) \sin \alpha}{s} \quad \text{Equation 2.7}$$

$$\beta = \begin{cases} \frac{4.8}{(1+750\varepsilon_s)} & \text{contains } \geq \text{ min. shear reinf.} \\ \frac{4.8}{(1+750\varepsilon_s)} \frac{51}{(39+s_{xe})} & \text{contains } < \text{ min. shear reinf.} \end{cases} \quad \text{Equation 2.8}$$

$$\theta = 29 + 3500\varepsilon_s \quad \text{Equation 2.9}$$

$$\varepsilon_s = \frac{\frac{M}{d_v} + 0.5N + V_n}{A_s E_s} \quad \text{Equation 2.10}$$

$$s_{xe} = s_x \frac{1.38}{a_g + 0.63} \quad \text{Equation 2.11}$$

Where:

$\beta$  = factor indicating ability of diagonally cracked concrete to transmit tension and shear

$b_v$  = effective web width (inches) (minimum web width within depth  $d_v$ )

$d_v$  = effective shear depth, measured perpendicular to the neutral axis between the tensile resultant and compressive flexure forces (maximum depth defined as  $0.9d$  and  $0.72h$  [inches])

$s$  = spacing of transverse steel (inches)

$A_v$  = area of shear reinforcement within distance  $s$  (inches<sup>2</sup>)

$\alpha$  = angle of transverse reinforcement to longitudinal axis (degrees)

= angle of inclination of diagonal compressive stresses (degrees)

$\epsilon_s$  = strain in longitudinal steel

$N$  = axial force (positive if tensile, negative if compressive) (kips)

$M$  = absolute value of moment (kips)

$A_s$  = area of longitudinal steel on flexural tension side of member (inches<sup>2</sup>)

$s_{xe}$  = crack spacing parameter

$s_x$  = minimum of  $d_v$  and maximum distance between layers of longitudinal crack control reinforcement (inches)

$a_g$  = maximum aggregate size (inches)

Shear strength  $V_n$  is initially assumed, and Equation 2.10 is used to determine steel strain  $\epsilon_s$ . Equation 2.11 determines  $s_{xe}$ , and  $s_{xe}$  and  $\epsilon_s$  are used in Equation 2.8 and Equation 2.9 to determine  $\beta$  and  $\theta$ , respectively.  $\beta$  and  $\theta$  are used in Equation 2.6 and Equation 2.7 to find  $V_c$  and  $V_s$ , respectively. Equation 2.5 is then used to find a new  $V_n$ . The process is repeated until convergence of  $V_n$ . Shear at this convergence is the final shear capacity of the section.

## 2.4 Friction Coefficients

### 2.4.1 Steel-to-Concrete

Steel-bearing pads were used to build the bridges analyzed in the present study because rubber was not yet used for bearing pads when these bridges were built in the 1920s to 1940s. As shown in Figure 2.3 from the inspection report for Kansas Bridge No. 54-104-317.27 (KDOT,

2011), steel rockers can become heavily corroded, limiting the ability of the rockers to rotate and preventing the girders from rotating at the supports as designed. The girder consequently locks on the plate, producing a friction force at the girder-steel boundary. Therefore, a coefficient of friction must be used for this interface in order to estimate friction forces at the girder supports.

Rabbat and Russell (1985) conducted tests to determine the static coefficient of friction between concrete and steel for dry and wet interface conditions. The superstructure of bridges is assumed to shelter the girder-bearing pad interface from most rain water, so dry interface conditions were assumed in the present study. Rabbat and Russell also tested a set of concrete specimens with dry interfaces at a normal stress of 60 pounds per square inch (psi). Test results led to a recommended static coefficient of friction of 0.57 for normal compressive stresses between 20 and 100 psi. This value was implemented in the current study.



**Figure 2.3: Support Rockers at Pier 4, Left Side, Span 5 of Bridge No. 54-104-317.27**

Source: KDOT (2011)

#### *2.4.2 Cracked Concrete-To-Cracked Concrete*

ACI 318-14 Table 22.9.4.2 recommends a coefficient of friction,  $\mu_c$ , of  $1.4\lambda$  for concrete placed monolithically, where  $\lambda$  is 1 for normal-weight concrete, which was assumed in this project. ACI 318-14 Section 22.9 utilizes the shear-friction concept to determine shear capacity of the beam, with the assumption that shear reinforcement crosses the crack and friction between crack faces produces all the shear resistance. Therefore, ACI 318-14 recommends artificially

high values of the coefficient of friction so that calculated shear strengths agree with test results (ACI 318-14, Section R22.9.4.2). AASHTO (2002) Article 8.16.6.4, which outlines the shear-friction process, reflects the values of  $\mu_c$  referenced in ACI 318-14.

Shear reinforcing steel, however, was not shown to traverse reverse diagonal cracks in girders analyzed by BRIDGE. Although reinforcing tension steel may or may not traverse the crack, the conservative and likely accurate assumption was made that it does not contribute to shear capacity. The shear-friction value assumes that tension forces develop in the steel traversing the crack, thereby causing compressive forces in the concrete surrounding the steel at the crack interface and creating a clamping force between the two faces of the crack, which causes friction between the crack faces. Since cracked faces are clamped together, as explained in Section 4.3.9, the  $\mu_c$  value of 1.4 is still applicable although no reinforcement was assumed to cross the crack.

## 2.5 Transformation of Stress

Stresses on a finite cube of an element, centered at  $Q$ , are described by six stress components shown in Figure 2.4. In the figure,  $\sigma_x$ ,  $\sigma_y$ , and  $\sigma_z$  represent normal stresses on the faces of the cube, while  $\tau_{xy}$ ,  $\tau_{yz}$ , and  $\tau_{zx}$  represent shear stress on the element faces. When two faces of the cubic element do not experience any stresses, as on the surface of a structural element not subject to external forces, the remaining stresses are called plane stresses. Figure 2.5 shows resulting plane stresses when faces are perpendicular to the z-axis in Figure 2.4.

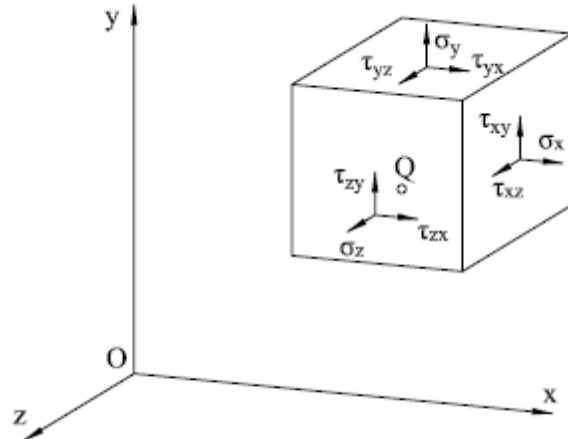


Figure 2.4: General State of Stress at a Point

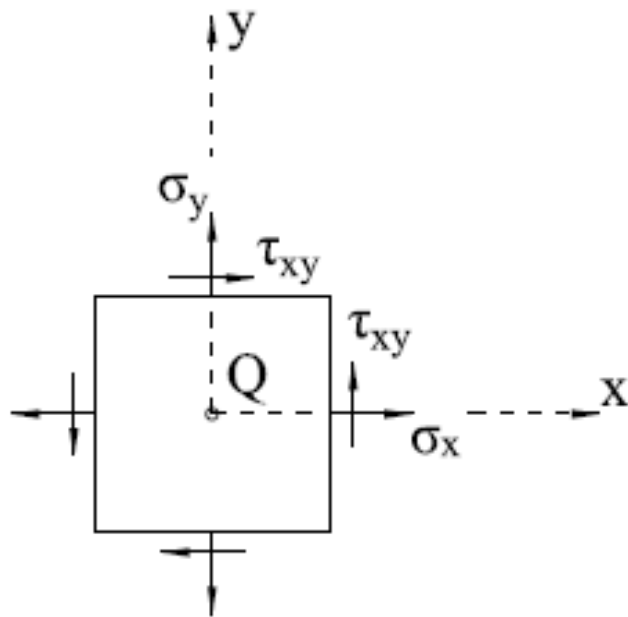
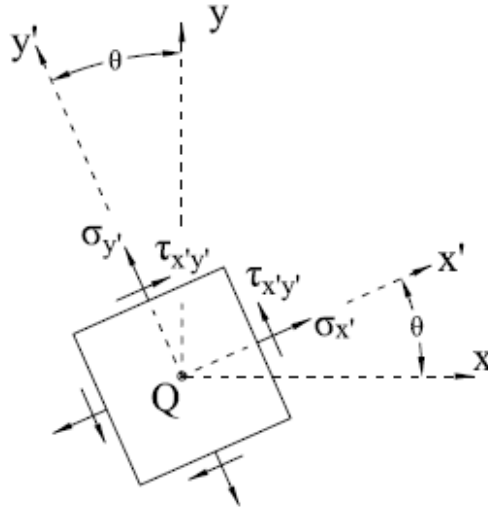


Figure 2.5: Plane Stresses

### 2.5.1 Transformation of Stress Block

If Figure 2.5 is rotated about its z-axis by angle  $\theta$ , then stresses at the cube faces change to  $\sigma_{x'}$ ,  $\sigma_{y'}$ , and  $\tau_{x'y'}$ , as shown in Figure 2.6. Beer, Johnston, DeWolf, and Mazurek (2012) derived Equation 2.12, Equation 2.13, and Equation 2.14 to define these transformed stresses.



**Figure 2.6: Transformed Plane Stresses**

$$\sigma_{x'} = \frac{\sigma_x + \sigma_y}{2} + \frac{\sigma_x - \sigma_y}{2} \cos 2\theta + \tau_{xy} \sin 2\theta \quad \text{Equation 2.12}$$

$$\sigma_{y'} = \frac{\sigma_x + \sigma_y}{2} - \frac{\sigma_x - \sigma_y}{2} \cos 2\theta - \tau_{xy} \sin 2\theta \quad \text{Equation 2.13}$$

$$\tau_{x'y'} = -\frac{\sigma_x - \sigma_y}{2} \sin 2\theta + \tau_{xy} \cos 2\theta \quad \text{Equation 2.14}$$

Where:

$\sigma_x$  = normal stress normal to x-axis (psi)

$\sigma_y$  = normal stress normal to y-axis (psi)

$\tau_{xy}$  = shear stress perpendicular to z-axis and parallel to x- or y- axis (psi)

$\theta$  = angle of transformation ( $^\circ$ )

$\sigma_{x'}$  = normal stress normal to x'-axis (psi)

$\sigma_{y'}$  = normal stress normal to y'-axis (psi)

$\tau_{x'y'}$  = shear stress perpendicular to z'-axis and parallel to x'- or y'- axis (psi)

### 2.5.2 Formulation of Mohr's Circle

Mohr's circle of plane stress, displayed in Figure 2.7, was introduced by German engineer Otto Mohr. Mohr's circle is derived from Equation 2.12 and Equation 2.14, which are the parametric equations of a circle (Beer et al., 2012). For any given value of  $\theta$  the point of abscissa  $\sigma_{x'}$  and ordinate  $\tau_{x'y'}$  defines a point  $F$  that lies on a circle, as displayed in Figure



2.7. When  $(\sigma_x + \sigma_y)/2$  is subtracted from each side of Equation 2.12, both sides of Equation 2.12 and Equation 2.14 are squared, and when Equation 2.12 and Equation 2.14 are added together, Equation 2.15 is formed.

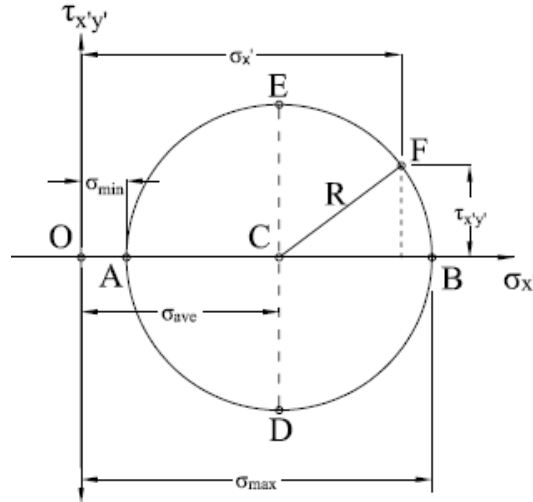


**Figure 2.7: Mohr's Circle of Plane Stresses**

$$\left(\sigma_{x'} - \frac{\sigma_x + \sigma_y}{2}\right)^2 + \tau_{x'y'}^2 = \left(\frac{\sigma_x - \sigma_y}{2}\right)^2 + \tau_{xy}^2 \quad \text{Equation 2.15}$$

Substituting Equation 2.16 and Equation 2.17 into Equation 2.15 yields Equation 2.18, which is the equation of a circle with radius  $R$  and center point  $C$ . Figure 2.7 shows that  $C$  is at abscissa  $\sigma_{ave}$  and ordinate 0.

$$\sigma_{ave} = \frac{\sigma_x + \sigma_y}{2} \quad \text{Equation 2.16}$$

$$R = \sqrt{\left(\frac{\sigma_x - \sigma_y}{2}\right)^2 + \tau_{xy}^2} \quad \text{Equation 2.17}$$

$$(\sigma_{x'} - \sigma_{ave})^2 + \tau_{x'y'}^2 = R^2 \quad \text{Equation 2.18}$$

Where:

$\sigma_{ave}$  = stress at center of Mohr's circle (psi)

$R$  = radius of Mohr's circle (psi)

### 2.5.3 Principal Stresses and Maximum Shearing Stress

Points  $A$  and  $B$  of Figure 2.7 represent the minimum,  $\sigma_{max}$ , and maximum,  $\sigma_{min}$ , value of normal stress  $\sigma_{x'}$ , respectively. As shown in Figure 2.7,  $\tau_{x'y'}$  equals 0 at these points. Substituting  $\tau_{x'y'} = 0$  into Equation 2.14 and rearranging yields Equation 2.19, which finds angle  $\theta_p$  of the principal planes of stress at point  $Q$ . Maximum and minimum normal stresses,  $\sigma_{max}$  and  $\sigma_{min}$ , are the principal stresses at point  $Q$ , and they act normal to the principal planes of stress. Equation 2.19 defines two values of  $\theta_p$  that are  $90^\circ$  apart. As shown in Figure 2.8, one value is the angle from the  $x$ -axis to the  $x'$ -axis, which is perpendicular to the maximum principal plane. The other value is the angle from the  $x$ -axis to the  $y'$ -axis, which is perpendicular to the minimum principal plane. No shear stresses are present on the principal planes.

$$\theta_{p \max, \min} = \frac{\tan^{-1} \left[ \frac{2\tau_{xy}}{\sigma_x - \sigma_y} \right]}{2} \quad \text{Equation 2.19}$$

Where:

$\theta_{p \max, \min}$  = transformed angles to the principal planes of stress ( $^\circ$ )

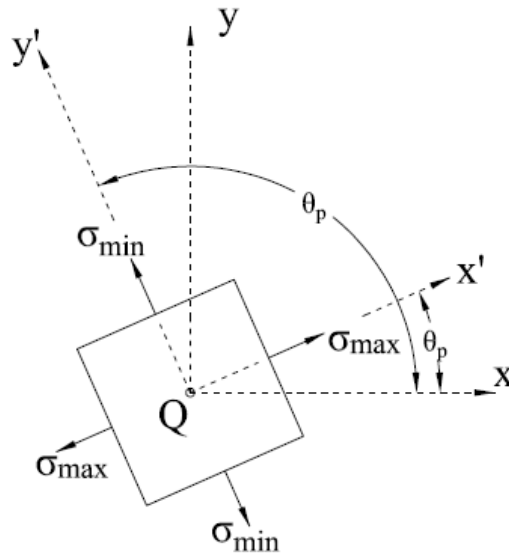


Figure 2.8: Principal Stresses

Figure 2.7 shows that  $\sigma_{max,min} = \sigma_{ave} \pm R$ , so substituting Equation 2.16 and Equation 2.17 yields Equation 2.20, which defines maximum and minimum stresses. However,  $\sigma_p$  values must be substituted from Equation 2.19 into Equation 2.12 in order to determine which  $\sigma_p$  corresponds to which principal stress.

$$\sigma_{max,min} = \frac{\sigma_x + \sigma_y}{2} \pm \sqrt{\left(\frac{\sigma_x - \sigma_y}{2}\right)^2 + \tau_{xy}^2} \quad \text{Equation 2.20}$$

Where:

$\sigma_{max,min}$  = maximum and minimum principle stresses (psi)

Points *D* and *E* in Figure 2.7 correspond to the points of maximum shearing stress,  $\tau_{max}$ . The abscissa of these points is  $\sigma_{ave}$ . Substituting  $\sigma_{ave}$  from Equation 2.16 as  $\sigma_x$ , in Equation 2.12 and rearranging yields Equation 2.21, which defines two angles,  $\theta_s$ , that are 90° apart. As shown in Figure 2.9, either of the  $\theta_s$  values correspond to the orientation of the cubic element that yields the maximum shearing stress at point *Q*. The angles  $\theta_s$  are 45° less than their corresponding  $\theta_p$  values.

$$\theta_s = \frac{\tan^{-1}\left(-\frac{\sigma_x - \sigma_y}{2\tau_{xy}}\right)}{2} \quad \text{Equation 2.21}$$

Where:

$\theta_s$  = transformed angles to the planes of maximum shear stress (°)

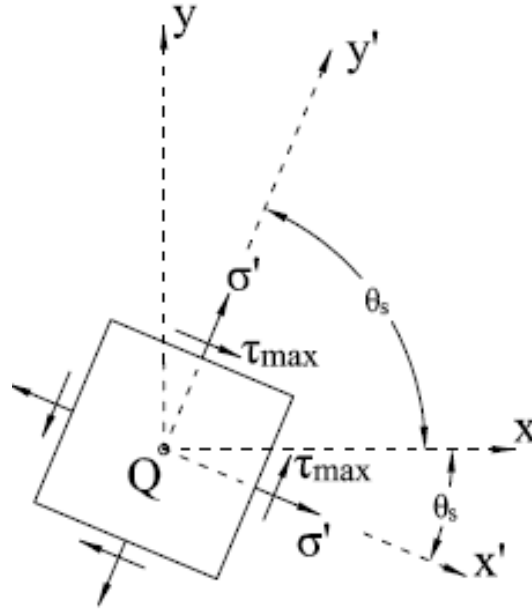


**Figure 2.9: Maximum Shearing Stress**

The planes of maximum shear stress, as defined by the angles  $\theta_s$  and displayed in Figure 2.9, are subject to shear stress  $\tau_{max}$ . As shown in Figure 2.7,  $\tau_{max}$  is equal to the radius of Mohr's circle,  $R$ . Thus, Equation 2.17 also yields maximum shear stress redefined as Equation 2.22.

$$\tau_{max} = \sqrt{\left(\frac{\sigma_x - \sigma_y}{2}\right)^2 + \tau_{xy}^2} \quad \text{Equation 2.22}$$

## 2.6 Effective Flange Width

AASHTO (2014) Article C4.6.2.6.1 defines effective flange width as the “width of the deck over which the assumed uniformly distributed longitudinal stresses result approximately in the same deck force and member moments calculated from elementary beam theory assuming plane sections remain plane, as are produced by the non-uniform stress distribution.” AASHTO (2002) Article 8.10 specifies that the total effective flange width for a T-girder should not exceed one-quarter of the span length of the girder and that the effective flange width overhang on each side of the web should not be more than 6 times the slab thickness or half the clear distance to the adjacent girder web. Effective overhanging flange width for exterior girders with a slab only

on one side of the web should be less than  $1/12$  of the span length, 6 times the slab thickness, or one-half the clear distance to the adjacent girder web.

## 2.7 Poisson's Ratio

When stress is applied on a material in one direction, the material typically deforms in the other two orthogonal directions, as described by Poisson's ratio of the material. When an axial load is applied to a material, Poisson's ratio,  $\nu$ , is described by Equation 2.23. AASHTO (2002) Article 8.7.3 defines Poisson's ratio as 0.2 for reinforced concrete.

$$\nu = - \frac{\textit{Lateral Strain}}{\textit{Axial Strain}} \qquad \text{Equation 2.23}$$

Where:

$\nu$  = Poisson's ratio

## Chapter 3: KSU BRIDGE Input/Output Interface

The Excel-based program KSU BRIDGE allows a user to model a simply supported bridge span composed of concrete girders, diaphragms, and a deck slab. The user then loads the bridge with the desired truck loading, and BRIDGE uses the user-input data to analyze the bridge and loading to determine the RF for each girder support.

### 3.1 Mesh & Alignment Sheet

The Mesh & Alignment sheet displays the bridge mesh and lane alignment options in in Figure 3.1. User input data is provided in the white boxes next to the respective parameters.

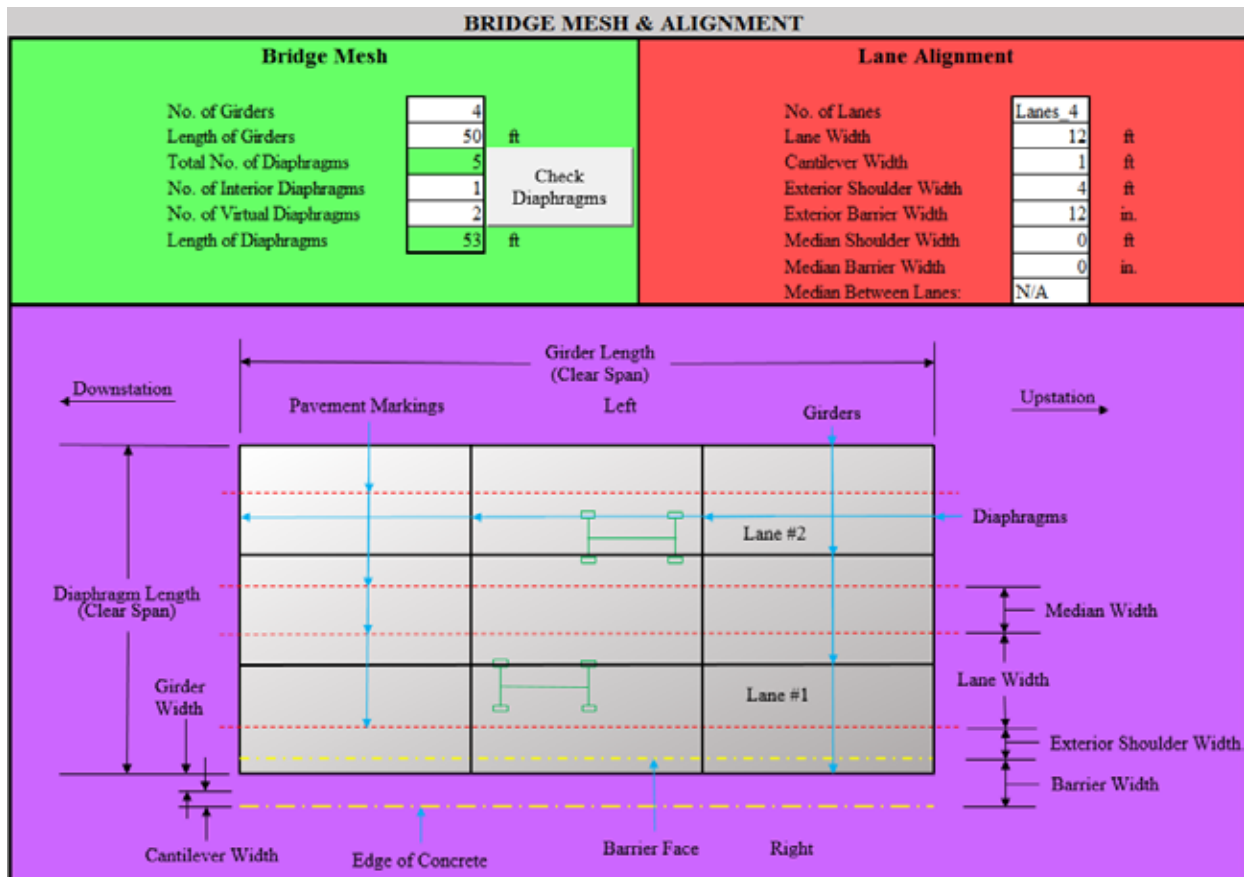


Figure 3.1: Bridge Mesh and Alignment User Interface

### 3.1.1 Lane Alignment

In the Lane Alignment section, shown in Figure 3.1, the user selects the number of lanes from a drop-down menu, shown in Figure 3.2, which ranges from ‘Lanes\_1’ to ‘Lanes\_4.’ Lane width is assumed to be equal for all lanes. The cantilever width is the distance from the outside face of the exterior girder to the edge of the slab, as displayed in Figure 3.1. The cantilever width, exterior shoulder width, and exterior barrier width are assumed to be equal for both sides of the bridge, and the median shoulder width is assumed to be equal on both sides of the median barrier if median barriers and shoulders are present. When one or two lanes are selected, the Median between Lanes drop-down menu is disabled, displaying “N/A” in this field because BRIDGE assumes that no medians exist on bridges with only one lane and any existing median on a two-lane bridge is between the two lanes. For three lanes, the Median between Lanes drop-down menu, shown in Figure 3.3, allows the user to place the median between Lanes 1 and 2 or between Lanes 2 and 3. When four lanes are selected, the Median between Lanes drop-down menu is again disabled, and “N/A” is displayed as the program assumes that an existing median is between Lanes 2 and 3. As shown in Figure 3.1, the program assumes that Lane #1 is nearest to the bottommost girder. The number of lanes increases until the last lane is closest to the topmost girder.

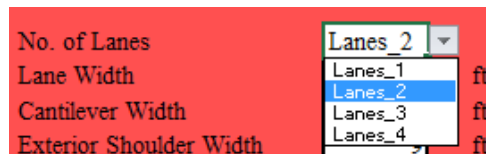


Figure 3.2: Drop-Down Menu for Number of Lanes

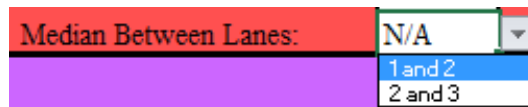


Figure 3.3: Drop-Down Menu for Median between Lanes

### 3.1.2 Bridge Mesh

The girders shown in Figure 3.1 refer to bridge beams that run parallel to the bridge span. Girder length input is defined as the clear span between exterior diaphragms, or the distance from inside face to inside face of the exterior diaphragms (NOT the center-to-center distance between exterior diaphragms). In accordance with KDOT's request, clear span length is utilized for user convenience. Because a majority of bridge plans call out the clear-span spacing of the diaphragms, users can conveniently input the clear-span girder length, as described in the bridge plans.

Diaphragms are bridge beams that run perpendicular to the span length and the girders. Exterior diaphragms are located on the outside edges of the analyzed bridge span. BRIDGE automatically assumes two exterior diaphragms: one on either side of the span. Interior diaphragms, real diaphragms between two exterior diaphragms, are an optional user input. BRIDGE assumes that these interior diaphragms are uniformly spaced between exterior diaphragms.

Virtual diaphragms, which can also be optional user input, are illusory diaphragms within the bridge that have total depth equal to the depth of the slab; thus, virtual diaphragms have no web. BRIDGE automatically spaces any virtual diaphragms uniformly between the real end diaphragms and interior diaphragms. The inclusion of virtual diaphragms increases the number of nodes and members used in the analysis, increasing analysis accuracy, especially when the distance between real diaphragms is large. Proper operation of KSU BRIDGE requires the same number of virtual diaphragms between each pair of real diaphragms. For example, if one interior diaphragm is present, an even number of virtual diaphragms must be used; if two interior diaphragms are present, the number of virtual diaphragms must be divisible by three. If no interior diaphragms are used, the number of virtual diaphragms is unlimited.

The Check Diaphragms button runs the `Verify_Deck_Width` macro, which ensures that the number of virtual diaphragms is compatible with the number of real diaphragms. If the number of virtual diaphragms is incompatible, an error message will appear, as shown in Figure 3.4. The user must then select "OK" on the error message box, adjust the number of virtual diaphragms until Equation 3.1 is satisfied, and then reselect the Check Diaphragms button. If



Equation 3.1 is satisfied, the message box shown in Figure 3.5 appears, and the user can then select “OK” and continue with the BRIDGE program.

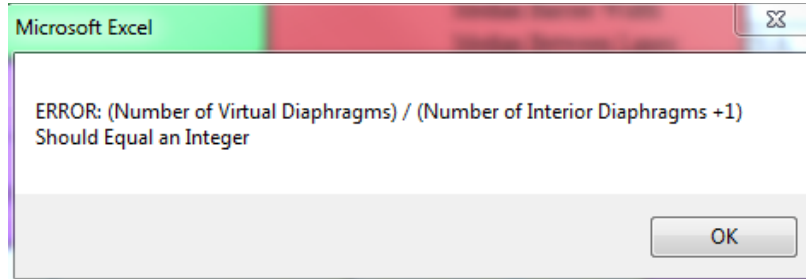


**Figure 3.4: “Check Diaphragms” Error Message**

$$\# \textit{Virtual Diaphragms} = n(\# \textit{Interior Diaphragms} + 1)$$

**Equation 3.1**

Where:

$n$  = any integer

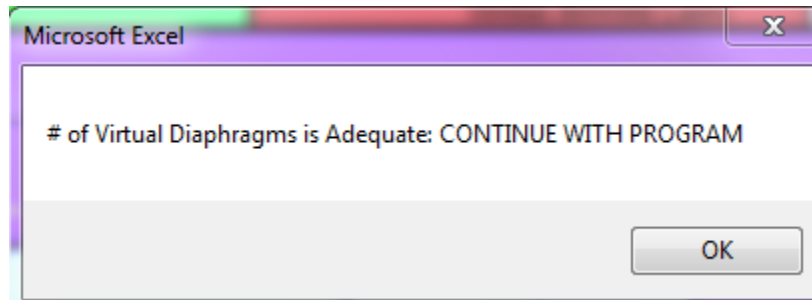


**Figure 3.5: “Check Diaphragms” Virtual Diaphragm Adequacy Message**

The total number of diaphragms and diaphragm length, which are automatically calculated within BRIDGE, are dependent upon user inputs. The total number of diaphragms is two (exterior diaphragms are automatically assumed as part of the bridge) plus the number of interior and virtual diaphragms. The diaphragm length, displayed in BRIDGE and shown in Figure 3.1, is the clear distance between the interior faces of the two exterior girders. Similar to girder length, the use of clear span length is in accordance with KDOT’s request. Diaphragm length is defined by Equation 3.2.

$$DL = (NL \times LW) + (2 \times ESW) + (2 \times MSW) + \left(\frac{MBW}{12}\right) + \left(\frac{2 \times EBW}{12}\right) - (2 \times CW) - \left(\frac{2 \times GW}{12}\right)$$

**Equation 3.2**

Where:

$DL$  = diaphragm length (ft)

$GW$  = girder width (inches) (described in Section 3.2.1)

### 3.1.3 Background Functions of the Mesh & Alignment Sheet

A table outside of the user input screen view shown in Figure 3.1 calculates actual and effective slab flange widths for each interior and exterior girder and diaphragm. The actual slab width of girders is the slab portion that is tributary to a girder and consists of the girder web width plus half the distance to the adjacent girder web on either side of the web. This actual slab width is used to calculate the dead load of the structure. Because dead load calculations account for the entire slab in the actual tributary widths of the girders, the actual tributary width of the diaphragms is unnecessary and is not calculated. The effective slab width of the girders is in accordance with AASHTO (2002) Article 8.10 and follows guidelines outlined in Section 2.4. AASHTO (2002) Article 8.10, however, does not specify an effective flange width for diaphragms, so the actual tributary width of the diaphragms is the effective slab width. The tributary width of each diaphragm consists of the diaphragm web width plus half the distance to adjacent diaphragm webs on either side of the web. These effective slab widths are used in the Section Properties sheet to determine girder and diaphragm section properties. Figure 3.6 displays actual and effective slab widths.

	Effective Width of Slab	Actual Width of Slab	
Interior Girder	83.75	83.75	in.
Exterior Girder	60.875	60.875	in.
Interior Diaphragm	612		in.
End Diaphragm	310.5		in.

**Figure 3.6: Effective and Actual Slab Widths**

BRIDGE also determines and prints the number of user-specified lanes. Since the Median between Lanes drop-down menu is dependent upon the Number of Lanes menu, Excel will not

allow only numbers to populate the Number of Lanes menu, so this cell, shown in Figure 3.7, determines the numerical number of lanes from available drop-down menu options.

# of Lanes:
4

**Figure 3.7: Numerical Value for User-Specified Number of Lanes**

The table in Figure 3.8 facilitates the drop-down menu for the Median between Lanes user input since it is dependent upon the selected number of lanes. Number of Lanes options are shown in the first row of the table, while Median between Lanes options for each Number of Lanes option, as discussed in Section 3.1.1, are included in the columns.

Facilitates Drop-Down Menus			
Lanes_1	Lanes_2	Lanes_3	Lanes_4
N/A	N/A	1 and 2	N/A
N/A	N/A	2 and 3	N/A

**Figure 3.8: Median Placement Drop-Down Menu Facilitation**

Figure 3.9 displays the box that reads user selections for Median between Lanes and shows a numerical value in accordance with the selection. If the user selects “1 and 2,” then the box will display the number 1; if the user selects “2 and 3,” then this box will display the number 2. If the user selects “N/A” for the median location, then this box will display a 0. BRIDGE uses the number displayed in this box and the number of lanes to correctly place a median.

Median Placement:
0

**Figure 3.9: Numerical Representation of Median Placement**

### 3.2 Section Geometry and Material Properties Sheet

The Section Geometry and Material Properties user interface, shown in Figure 3.10, allows a user to input girder, diaphragm, slab, and wearing surface geometry. The user can also input concrete material properties and crack width properties. All user-input boxes are displayed with a white background.

**SECTION GEOMETRY AND MATERIAL PROPERTIES**

Component	Parameter	Value	Unit
Girder	Height (through deck) (h)	41	in.
	Width (web) (b)	15	in.
Diaphragms	Exterior:		
	Height (through deck) (h)	21	in.
	Width (web) (b)	9	in.
	Interior:		
	Height (through deck) (h)	0	in.
	Width (web) (b)	0	in.
Deck Slab	Thickness (t)	6.5	in.
Wearing Surface	Thickness	2	in.
	Unit Weight	150	pcf
Material Properties	Concrete Strength ( $f'_c$ )	3000	psi
	Concrete Unit Weight ( $\gamma_c$ )	150	pcf
Crack Properties	% Cracked Girder Width Used	100	%
	Angle of Crack Propagation ( $\theta$ )	50	$^\circ$
	Use Input or Calculated Angle?	Calculated	
	Aggregate Diameter	1	in.

Figure 3.10: Section Geometry and Material Properties User Interface

#### 3.2.1 Section Geometry

The Section Geometry sheet allows a user to input the height (inches) and width (inches) of girders and diaphragms, as well as deck slab thickness (inches). Per KDOT request, BRIDGE defines girder height and diaphragms as the distance from the bottom of the element through the top of the slab. This height definition should allow a user to conveniently input girder and diaphragm properties directly from bridge design plans. If a web section is not desired for the girder or diaphragm, a user can make the girder height or diaphragm equal to the deck slab

thickness and make the web width equal to any number. BRIDGE will assume that no web exists for the member.

In accordance with KDOT, girders and diaphragms are assumed to be rectangular since this is the only beam shape used in bridges targeted by this program. Although BRIDGE allows a user to specify various dimensions for interior and exterior diaphragms, the program assumes that all exterior diaphragms have identical dimensions and that all interior real diaphragms have identical dimensions. If a user specifies no interior diaphragms, then the interior diaphragm user-input cells in the Section Geometry and Material Properties sheet can be set to any value because BRIDGE will ignore these inputs. No user input for virtual diaphragms is necessary since the program assumes that virtual diaphragms, as discussed in Section 3.1.2, have heights equal to the deck slab thickness and have tributary widths equal to the interior diaphragm effective slab width, as displayed in Figure 3.6.

A user also may input the wearing surface thickness (inches) and the wearing surface unit weight (pcf). Wearing surface properties are only used for bridge dead-load calculations and do not contribute to girder or diaphragm cross-sectional properties or bridge stiffness.

### *3.2.2 Material Properties*

Per KDOT request, a user can specify concrete compressive strength,  $f'_c$  (psi), and concrete unit weight,  $\gamma_c$  (pcf), in order to determine a bridge's dead-load weight. Although concrete strength is a user input, if the user does not know the specified design concrete strength, a value of 3000 psi is recommended, the common compressive strength for concrete in the early 1900s when most bridges affected by reverse diagonal cracking were built.

### *3.2.3 Crack Properties*

In this sheet, a user specifies crack properties and the condition of girders near the supports. As discussed in Section 2.1.4.1 of Bernica (2016) and shown in Figure 2.2, the crack width of reverse diagonal shear cracks are sometimes so severe that a portion of the crack faces are no longer in contact with each other and thus do not provide any shear capacity. Based on inspection reports and engineering judgment, a user should determine the percentage of girder width that maintains full contact between crack faces and consequently transfers shear across the

crack. This percentage is entered in the “% Cracked Girder Width Used” cell. A small girder width results in decreased shear capacity and conservative load rating.

A user may also specify the angle of crack propagation,  $\theta$ , of the reverse diagonal crack. Orientation of this angle is shown in Figure 3.11. As discussed in Section 4.3.9, BRIDGE calculates a predicted crack angle based on the effects of friction forces at the girder-to-bearing pad interface. A user can use either a manually entered crack angle,  $\theta$ , or a program-calculated crack angle. For a manually entered angle, a user should select “Manual” from the User Input or Calculated Angle? drop-down menu shown in Figure 3.12. Otherwise, a user should select “Calculated” for a program-calculated crack angle. A user may also specify the diameter of the aggregate used in the girder concrete in the Aggregate Diameter input box. If this parameter is unknown, a user should input an aggregate diameter of 1 inch. The larger the specified aggregate diameter, the larger and less conservative the RF.

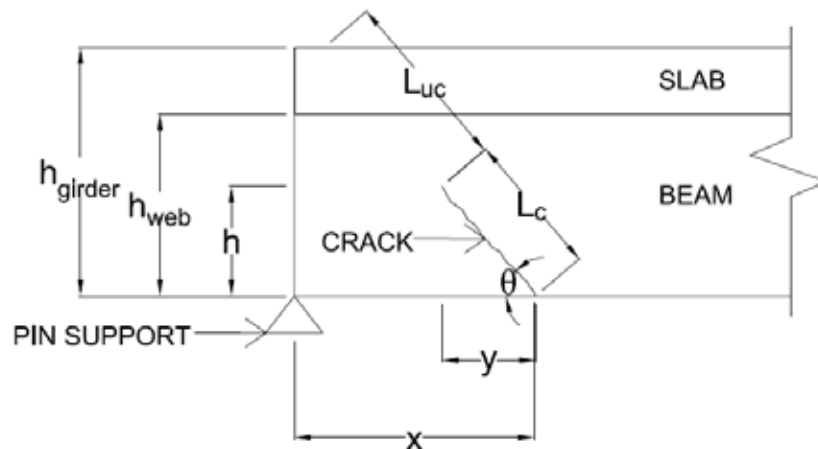


Figure 3.11: Angle of Crack Propagation

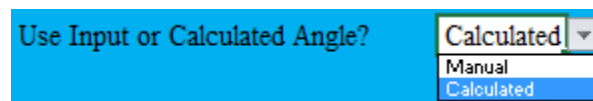


Figure 3.12: Use Input or Calculated Angle? Drop-Down Menu

### 3.2.4 Background Computations of Section Geometry Sheet

Two tables, shown in Figure 3.13, are located in the background of this sheet. The first table displays the web area of the girders and diaphragms and the distance from the top of the slab to the centroid of the girder or diaphragm web (assuming slab thickness is NOT part of the girders and diaphragms). These are used later to find other geometric properties for bridge members. The other table displays torsion constants  $J$  for each interior, exterior, real, and virtual girder and diaphragm and its corresponding effective slab. If interior or virtual diaphragms do not exist in the run, then no  $J$  is calculated for those members. The slab/girder or slab/diaphragm element is broken into simple rectangular sections in order to calculate the torsional constant. The elements can be broken using Method 1 or Method 2, as shown in Figure 3.14. For each method, the torsional constant for each cut-up section is computed using Equation 3.3. The torsional constants are then added together to find the overall torsional constant of the shape for each method. Because virtual diaphragms are composed entirely of a slab element, only the torsional constant  $J$  of a single rectangular section is calculated. BRIDGE uses the greater calculated torsional constants (using Method 1 or Method 2) in the analysis because it is most similar to the actual value.

	X-Centroid (from top of deck) (in.)				
	Area (in <sup>2</sup> )				
Girder	504	22			
Ext. Diaphragm	192	16			
Int. Diaphragm	192	16			
	Interior Girder & Deck	Exterior Girder & Deck	Interior Diaphragm & Deck	End Diaphragm & Deck	Virtual Diaphragm & Deck
J (Method 1)	69046	54027	30228	18196	25252
J (Method 2)	80467	69073	31836	20664	

Figure 3.13: Background of Section Geometry and Material Properties Sheet



Figure 3.14: Methods to Calculate the Torsional Constant

$$J = \sum b^3 h \left( \frac{1}{3} - 0.21 \frac{b}{h} \left[ 1 - \frac{1}{12} \left( \frac{b}{h} \right)^4 \right] \right) \quad \text{Equation 3.3}$$

Where:

$J$  = torsional constant (inches<sup>4</sup>)

$b$  = smaller dimension of rectangles in Figure 3.14 (inches)

$h$  = larger dimension of rectangles in Figure 3.14 (inches)

### 3.3 Section Properties Sheet

Although the Section Properties sheet is not a user input sheet, the user may view this sheet in order to gain increased understanding of KSU BRIDGE-conducted analysis or to help them perform hand checks. Areas  $A$ ,  $y$ -centroid from top of deck,  $C_y$ ,  $x$ -centroid from center of the girder/diaphragm web,  $C_x$ , and moments of inertia in the  $x$  and  $y$  directions from the section centroid are calculated for each interior, exterior, real, and virtual girder and diaphragm web and effective tributary slab width. These properties are displayed in Figure 3.15. The torsional constant  $J$  for each section is calculated in the background of the Section Geometry sheet, and the governing  $J$  is displayed in Figure 3.15. The parallel axis theorem is used to find moments of inertia about the centroid of each section. However, the moment of inertia does not include barriers, per KDOT request. Since barriers would increase section stiffness, their exclusion is conservative. A cross-sectional view of each real element, including the effective deck section, with general centroid locations, is also included in this sheet as shown in Figure 3.15. Conservative simplification asserts that steel reinforcement does not contribute to these section properties.



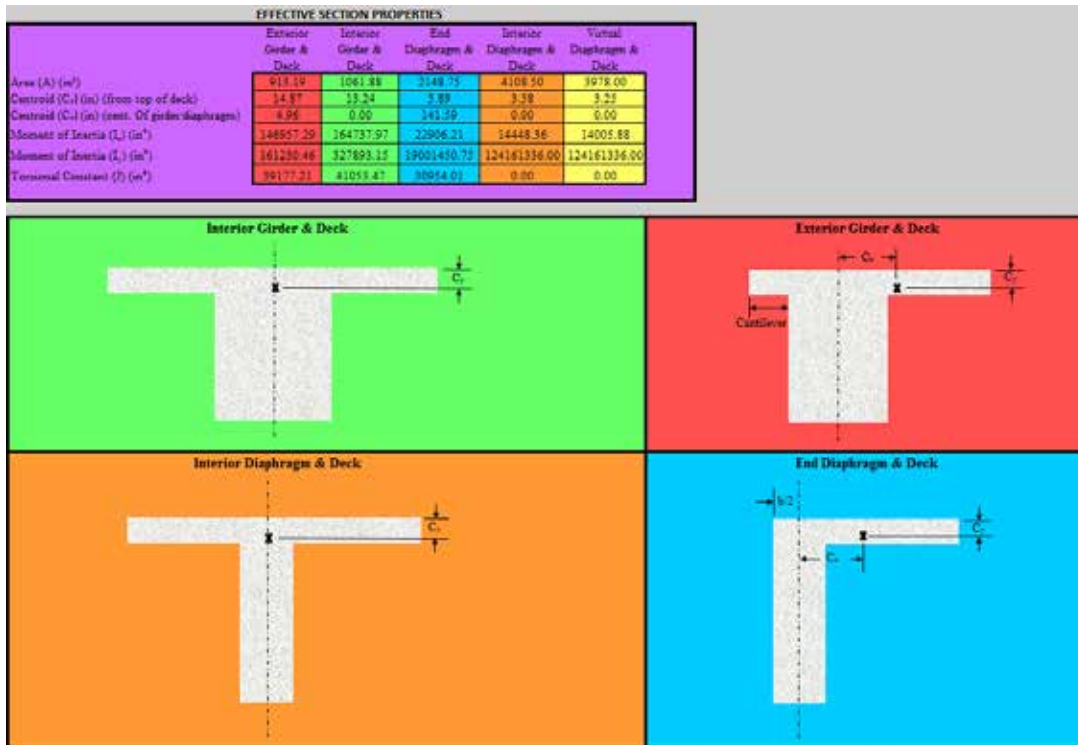


Figure 3.15: Section Properties Sheet

### 3.4 Truck Input Sheet

The Truck Input user interface shown in Figure 3.16 allows a user to place one to four trucks on a bridge. All user input boxes are displayed with a white background, and information for Truck #1 is displayed in the upper-left section, information for Truck #2 is in the upper-right section, information for Truck #3 is in the lower-left section, and information for Truck #4 is in the lower-right section. Display options are identical for each truck. If a user wants to place only one truck on the bridge, then the “Truck #1” section must be completed and the other truck sections must display “None” in the Truck Type user input box, as shown in Figure 3.16. As long as the Truck Type user input displays “None,” displays of the other user-input boxes are negligent. If a second truck is added to the bridge, it must be entered into the “Truck #2” section and so forth.

Truck #1			
Truck Type:	H Unit		
Gross Vehicle Weight (tons):	20		
Number of Axles:	2		
Lane #	2		
Direction of Travel	Up-Station		
Truck Location	Entering Bridge		
Load Length (ft)	14		
Axle #	Distance Behind Front (1st) Axle (ft):	Weight on Axle (tons):	Weight on Axle (lbs)
1	0	4	8000
2	14	16	32000

Truck #2			
Truck Type:	None		
Gross Vehicle Weight (tons):			
Number of Axles:			
Lane #			
Direction of Travel	Down-Station		
Truck Location	Exiting Bridge		
Load Length (ft)	14		
Axle #	Distance Behind Front (1st) Axle	Weight on Axle (tons):	Weight on Axle

Use Multiple Lane Presence Factor from AASHTO Standard Specifications (2002) Article 3.12?	<input type="checkbox"/> YES
--	------------------------------

Create Mesh (SELECT 1st)
Place Trucks on Bridge (SELECT 2nd)

Truck #3			
Truck Type:	None		
Gross Vehicle Weight (tons):			
Number of Axles:			
Lane #			
Direction of Travel	Up-Station		
Truck Location	Entering Bridge		
Truck Position	Rightmost		
Load Length (ft)	14		
Axle #	Distance Behind Front (1st) Axle (ft):	Weight on Axle (tons):	Weight on Axle (lbs)

Truck #4			
Truck Type:	None		
Gross Vehicle Weight (tons):			
Number of Axles:			
Lane #			
Direction of Travel	Down-Station		
Truck Location	Entering Bridge		
Truck Position	Rightmost		
Load Length (ft)	14		
Axle #	Distance Behind Front (1st) Axle	Weight on Axle (tons):	Weight on Axle

Figure 3.16: Truck Input User Interface

3.4.1 Truck Selection and Placement

Further discussion of the Truck Input user interface will focus on the “Truck #1” section, shown in Figure 3.17.

Truck #1

Truck Type:	H Unit	▼
Gross Vehicle Weight (tons):	20	
Number of Axles:	2	
Lane #	2	
Direction of Travel	Up-Station	
Truck Location	Entering Bridge	
Load Length (ft)	14	

Axle #	Distance Behind Front (1st) Axle (ft):	Weight on Axle (tons):	Weight on Axle (lbs)
1	0	4	8000
2	14	16	32000

**Figure 3.17: Truck Input and Information Section**

3.4.1.1 Truck Type

When the Truck Type user interface box is selected, a drop-down menu appears (Figure 3.18) that lists the 13 truck types a user can place on a bridge (discussed in Bernica, 2016, Section 2.1.2.1) as well as the “None” option discussed previously. For rating purposes, all trucks on a bridge should be the same type. Once a truck type is selected, the Gross Vehicle Weight (tons) and Number of Axles sections will populate automatically to display information unique to the truck type selected. The table at the bottom of the Truck #1 section will also populate automatically. The Axle # column lists the number of axles for each truck type: Axle #1 is always the axle closest to the front of the truck. The Distance Behind Front (1<sup>st</sup>) Axle column displays the location (ft) of each axle relative to the truck’s front axle. For example, as shown in Figure 3.17, the second axle of an H Unit truck is 14 ft behind the frontmost axle. As shown in the figures in Appendix A, the third axle of the HS Unit truck varies from 14 to 30 ft behind the second axle, while the second axle of the notional rating load (NRL) varies from 6 to 14 ft behind the first axle. For simplicity, a user is not given an option to choose axle location.

BRIDGE assumes the smallest axle spacing permitted (i.e., 14 ft for the HS Unit truck and 6 ft for the NRL) because this configuration leads to less-distributed truck loads across the length of the bridge. This conservative approach to establish concentrated load pattern leads to larger live-load reactions at supports close to the truck, thereby lowering the RF. The Weight on Axle (tons) and Weight on Axle (lbs) columns display the gross weight on each axle in the corresponding units in order to confirm that the program is using correct data taken from the AASHTO (2002), AASHTO (2011), and KDOT (2016) figures displayed in Appendix A.

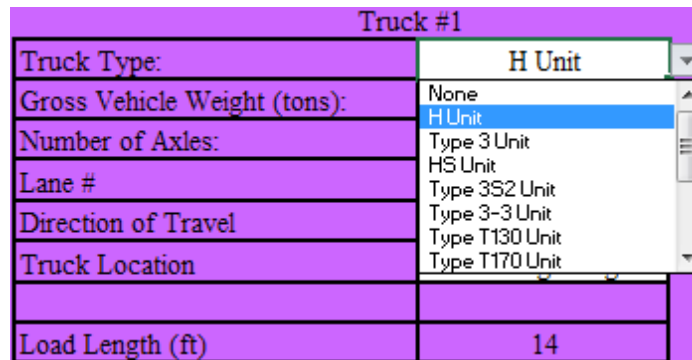


**Figure 3.18: Truck Type Drop-Down Menu**

BRIDGE, however, contains a glitch that occurs when a new truck type is selected for Truck #1: the Gross Vehicle Weight box, Number of Axles box, and Truck #1 table do not repopulate to display information for the new truck selection. Fortunately, the problem is entirely cosmetic since a user-selected truck is placed on the bridge and analyzed if the Create Mesh and Place Trucks on Bridge buttons are selected. In order to adjust for this malfunction, a user should reset Truck #2 to the desired truck type after adjusting Truck #1. Once Truck #2 is reset, the page refreshes to display the correct information for Truck #1.

### 3.4.1.2 Lane Number Assignment

A drop-down menu appears when the Lane # user interface box is selected, as shown in Figure 3.19. The menu displays only the number of lanes a user defined in the Mesh & Alignment sheet. As stated in Section 3.1 and shown in Figure 3.1, Lane #1 is closest to the bottom girder. The lane numbers progressively increase toward the top girder, as shown in Figure

3.1. BRIDGE allows a user to place multiple trucks in one lane if necessary to load rate bridges, as stated in Section 2.1.2.2 of Bernica (2016) and specified in AASHTO (2011). If a user specifies that two trucks are occupying one lane, the Lane # user-interface boxes turn red and a warning message with red text appears, as shown in Figure 3.20. Although the program allows a user to place multiple trucks in one lane, a user must place the trucks so that they do not occupy the same space or overlap in accordance with the following criteria:

1. Both trucks must be traveling in the up-station direction or in the down-station direction.
2. One truck must be at the Entering Bridge location and the other truck must be in the Exiting Bridge location.
3. The sum of extreme axle spacing (last number in the Distance Behind Front [1<sup>st</sup>] Axle column) of the two trucks must not exceed the user-specified girder length in the Mesh & Alignment sheet. (AASHTO [2011] recommends an additional 30 ft of clearance.)

Truck #1	
Truck Type:	H Unit
Gross Vehicle Weight (tons):	20
Number of Axles:	2
Lane #	2
Direction of Travel	1
Truck Location	Entering Bridge
Load Length (ft)	14

Figure 3.19: Lane Number Drop-Down Menu

Multiple trucks are in the same lane! Ensure they do not overlap! Trucks in the same lane should have same 'Direction of Travel' and opposite 'Truck Location'!

Create Mesh (SELECT 1st)

Place Trucks on Bridge (SELECT 2nd)

Figure 3.20: Warning Message for Multiple Trucks in a Lane

### 3.4.1.3 Direction of Travel

When the Direction of Travel user-interface box is selected, a user can choose Up-Station or Down-Station, as shown in Figure 3.21. Up-Station refers to the direction right of the bridge; therefore, all trucks heading toward the right of the bridge should be specified as traveling in the Up-Station direction, while all trucks heading toward the left of the bridge should be specified as traveling in the Down-Station direction. The direction of travel must be identical for all trucks placed in one lane because trucks in the same lane should travel in the same direction. BRIDGE uses this connotation because most bridge design sheets are orientated so that roadway stationing increases from left to right on the sheet. Thus, Up-Station is in the direction of increasing station numbers, while Down-Station is in the direction of decreasing station numbers.

Truck #1	
Truck Type:	H Unit
Gross Vehicle Weight (tons):	20
Number of Axles:	2
Lane #	2
Direction of Travel	Up-Station
Truck Location	Up-Station Down-Station
Load Length (ft)	14

**Figure 3.21: Direction of Travel Drop-Down Menu**

### 3.4.1.4 Truck Location

When the Truck Location user-interface box is selected, a user can choose Entering Bridge or Exiting Bridge, as shown in Figure 3.22. BRIDGE conservatively places the entire truck on the bridge in order to increase the live load at the girder supports (compared to the same truck on only one-half of the bridge), thus producing a smaller RF. The Entering Bridge option places the truck's last axle on the center of the end diaphragm and the rest of the truck on the bridge. The Exiting Bridge option places the truck's first axle on the center of the end diaphragm (the opposite end diaphragm referenced for the Entering Bridge option) and the rest of the truck on the bridge. When two trucks are placed in the same lane and given the same truck location,

the program assumes that the user places these trucks directly on top of each other, which is not realistic and should be avoided.

Truck #1	
Truck Type:	H Unit
Gross Vehicle Weight (tons):	20
Number of Axles:	2
Lane #	2
Direction of Travel	Up-Station
Truck Location	Entering Bridge
	<div style="border: 1px solid black; padding: 2px;">           Entering Bridge            Exiting Bridge         </div>
Load Length (ft)	14

**Figure 3.22: Truck Location Drop-Down Menu**

### 3.4.2 Multiple Lane Presence Factor

AASHTO (2002) Article 3.12 allows reduction of live loads by the factors specified in Table 2.1, and BRIDGE allows a user to choose whether or not to use this reduction. A drop-down menu appears when the Use Multiple Lane Presence Factor user-interface box is selected, as shown in Figure 3.23. If a user selects “YES,” the program applies reduction factors to all truck loads placed on the bridge. (When only one or two lanes contain trucks, the reduction factor is 1, and the load is not reduced.) If a user selects “NO,” the program will not apply reduction factors to any trucks, and the bridge is analyzed for the full gross weight of all trucks placed on the bridge. The “NO” selection is conservative because it increases the live-load reaction at the girder supports, causing a small RF at those supports.

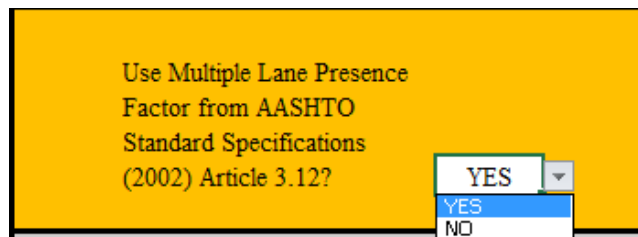


**Figure 3.23: Multiple Lane Presence Factor Drop-Down Menu**

### 3.4.3 Background of the Truck Input Sheet

The Truck Input sheet contains many tables used within the program in order to properly assign a magnitude and location to each truck load. The first table, shown in Figure 3.24, calculates and displays the number of user-specified trucks used in the analysis.

# of Trucks:
2

**Figure 3.24: Number of Trucks**

The second table, shown in Figure 3.25, gives numerical values to user inputs. For the direction of each truck, a 1 signifies Up-Station, and a 2 signifies Down-Station. For the Entering or Exiting row, a 1 signifies that the truck is entering the bridge, while a 2 signifies that the truck is exiting the bridge. The Direction and Entering or Exiting rows may contain a value for a truck that is not placed on the bridge. The Lane # row indicates the lane for each truck; a blank value indicates no selected truck.

	Truck #1	Truck #2	Truck #3	Truck #4
Direction:	1	2	1	2
Entering or Exiting:	1	2	1	1
Lane #:	1	2		

**Figure 3.25: Numerical Representation of Truck Placement User Inputs**

The third table, shown in Figure 3.26, identifies which trucks share a lane with another truck. A 0 indicates that a truck is sharing a lane with another truck, while a 1 indicates that the truck is not sharing a lane.

	Multiple Truck in Lane?			
Truck #	Truck #1	Truck #2	Truck #3	Truck #4
YES/NO	1	1	1	1

**Figure 3.26: Trucks that Share a Lane**

The table in Figure 3.27 indicates lanes that contain a truck. A 1 indicates that the specified lane contains a truck, while a 0 indicates that the lane is empty or that there is no



corresponding lane. The table in Figure 3.28 displays the number of lanes that contain a truck, which is the sum of values in Figure 3.27.

Lane 1	Lane 2	Lane 3	Lane 4
1	1	0	0

**Figure 3.27: Lanes Occupied by a Truck**

# Loaded Lanes
2

**Figure 3.28: Number of Loaded Lanes**

The box in Figure 3.29 shows the number of lanes the user specified in the Mesh & Alignment sheet. This box and the table in Figure 3.30 facilitate the Lane # drop-down menu.

#Lanes
Two Lanes

**Figure 3.29: User-Specified Number of Lanes**

Lane # List
1
2
3
4

**Figure 3.30: Possible Lane Numbers**

The background of this sheet contains a list of axle spacings and the weight on each axle for every truck. This list (sample shown in Figure 3.31) displays the automatically generated information in this sheet to use within the program in order to place truck loads on the bridge.

	Distance Behind Front (1st) Axle (ft):	Weight on Axle (tons):
H Unit	0	4
	14	16
Type 3 Unit	0	8
	15	8.5
	19	8.5
HS Unit	0	4
	14	16
	28	16
Type 3S2 Unit	0	5
	11	7.75
	15	7.75
	37	7.75
	41	7.75

**Figure 3.31: Spacing and Loads on Each Truck Axle**

#### *3.4.4 Bridge Creation and Placement of Trucks on the Bridge*

Once user inputs in the Mesh & Alignment, Section Geometry, and Truck Input sheets are completed, the program can create the bridge and place truck loads on the bridge when the user selects the Create Mesh and Place Trucks on Bridge buttons in Figure 3.32. A user must select the Create Mesh button before the Place Trucks on Bridge button. Although these buttons require no more than a few seconds to perform their respective functions, numerous and large trucks on the bridge require additional time to run the Place Trucks on Bridge function. Because the amount of data needed to perform tasks completed by these two buttons is too big to fit into one module, they are divided into two modules with two buttons to run the two modules. Functions performed by these buttons are described in Sections 4.1 and 4.2.

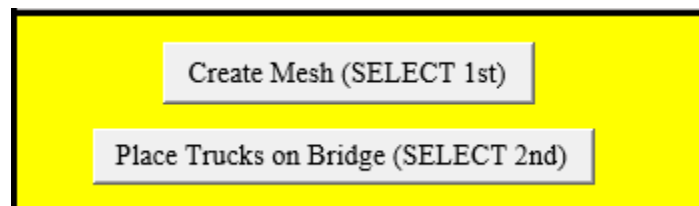


**Figure 3.32: First Two Buttons that Run BRIDGE**

### 3.5 Reaction Input Sheet

The Reaction Input user interface, shown in Figure 3.33, allows a user to choose girder support reactions calculated by BRIDGE or their own reactions calculated externally by any other software in order to determine the RF for a bridge. In order to enter a reaction, a user inputs dead- and live-load reactions (kips) in the appropriate columns and rows (Figure 3.33). Each Support Node # represents a girder support. Figure 3.36 shows the support that corresponds to each Support Node # shown in the Results sheet.

Support Node #:	Reaction at Support Caused By:	
	Dead Load (kips):	Live Load (kips):
1	5.00	16.00
3	5.00	8.00
4	7.00	16.00
6	7.00	8.00
7	7.00	16.00
9	7.00	8.00
10	5.00	16.00
12	5.00	8.00

Use Calculated or Input Reactions: CALCULATED

Load Rate Bridge

Figure 3.33: Reaction Input User Interface

Selection of the Use Calculated or Input Reactions user-input box activates a drop-down menu with two options: CALCULATED and INPUT, as shown in Figure 3.34. The CALCULATED option bases the RF on program-calculated reactions, and the INPUT option bases the RF on user-input reactions.

Use Calculated or Input Reactions:

CALCULATED

CALCULATED

INPUT

Figure 3.34: Use Calculated or Input Reactions Drop-Down Menu

The load rating is calculated and displayed in the Results sheet when the Load Rate Bridge button is selected. The functionality of this button is described in Section 4.3.

### **3.6 Results Sheet**

The Results sheet shown in Figure 3.35 displays the operating (left column) and inventory (right column) minimum load ratings at each support caused by the truck-load placement combination that caused the largest live load at each support. However, the Results sheet is not a user-input sheet; it displays only program results. Similar to the Reaction Input sheet, each Support Node # represents a girder support, as shown in Figure 3.36. When “N/A” is the RF at a support, minimal or no live-load reaction is noted at that support, resulting in an RF that is either very large or undefined because the RF equation is divided by 0. If this is the case, the RF at this support will not govern the RF of the bridge; therefore, it is noted as inconsequential and “N/A” is printed. The Governing Load Rating table displays absolute minimum operating and inventory load ratings for the bridge.

This tab also contains a graphical representation of the bridge mesh, as shown in Figure 3.36, which is created when the Create Mesh button is selected. This graphic illustrates the number of girders (horizontal members) and diaphragms (vertical members) and shows how the program labels each member and node. When the Show Node Numbers circle is selected, the graph only displays node labels that, in Figure 3.36, are the numbers by the member intersections that are not boxed. When Show Member Numbers is selected, the graph only displays member labels that, in Figure 3.36, are boxed numbers adjacent to their respective members. When Show Node & Member Numbers is selected, node and member labels are displayed on the graphic. The graphic can illustrate up to 12 girders and any number of diaphragms, as well as end, real interior, and virtual interior diaphragms.

Support Node #:	Minimum Load Rating		Governing Load Rating:	
	Operating	Inventory	Operating	Inventory
1	1.26	0.76	1.10	0.66
3	N/A	N/A		
4	1.10	0.66		
6	2.13	1.28		
7	1.12	0.67		
9	1.44	0.86		
10	1.17	0.70		
12	1.42	0.85		

Figure 3.35: Results Sheet

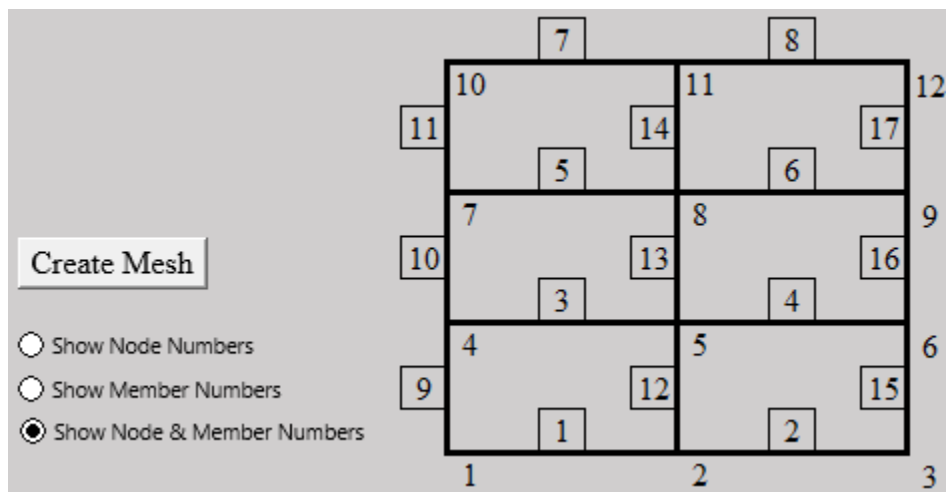


Figure 3.36: Bridge Mesh Graphic

## Chapter 4: KSU BRIDGE Functionality

### 4.1 Mesh Creation

The Create Mesh button initializes the Load\_Path\_Locations module within the BRIDGE program. The following sections describe the tasks BRIDGE performs when this module is run.

#### *4.1.1 Creating Grid and Assigning Member and Node Numbers*

This module creates a grid composed of bridge girders and diaphragms and assigns a number to each member and node (member ends) within the grid. The grid of a bridge with four girders and three diaphragms is shown in Figure 4.1. The numbers in boxes represent member numbers, and the numbers not in boxes represent node numbers.

If the number of girders is greater than or equal to the number of diaphragms, node numbering begins at the bottom left corner of the bridge and increases along the bottom girder until all diaphragm-girder connecting points are assigned a number. When the end of the first girder is reached, the successive node is on the far left end of the adjacent girder, and the node numbering then increases along the girder until all nodes on this girder are assigned. This continues with each successive girder until all diaphragm-girder connecting nodes are assigned, and then the members are numbered, starting at the bottom leftmost girder and increasing across the girder before moving to the girder above, as shown in Figure 4.1. After all girder members are labeled, the diaphragm members are numbered starting at the bottom leftmost diaphragm member and increasing along the left diaphragm before beginning at the next diaphragm, as shown in Figure 4.1.

When the number of diaphragms is greater than the number of girders, the numbering of nodes and members is similar to when the number of girders is greater than the number of diaphragms except the numbering initially increases along the diaphragms beginning at the leftmost diaphragm before progressing to the girders.

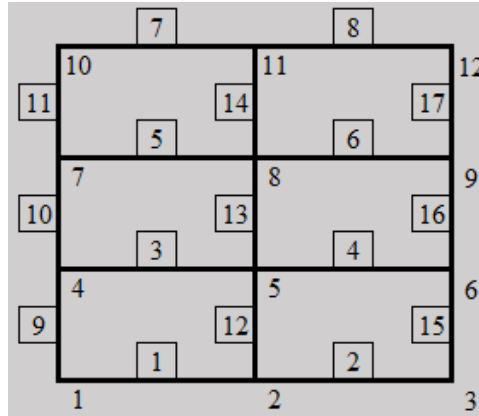


**Figure 4.1: Bridge Mesh with Labeled Members and Nodes**

#### 4.1.2 Assigning Coordinates to Nodes and End Nodes to Members

Coordinates (in inches) are assigned to each node based on user input from the Mesh & Alignment sheet, and nodes are assigned to the ends of each member, as displayed in the Node and Member Assignment sheet shown in Figure 4.2. The x-axis is parallel to the bridge span and girders for node coordinates, and the y-axis is parallel to the diaphragms. End node  $i$  is the node to the left of a girder member or bottom of a diaphragm member, while the  $j$  node is on the opposite end of the member.

Node	Node Coordinates		Member	End Nodes	
	x	y		i	j
1	0	0	1	1	2
2	306	0	2	2	3
3	612	0	3	4	5
4	0	171.333	4	5	6
5	306	171.333	5	7	8
6	612	171.333	6	8	9
7	0	342.667	7	10	11
8	306	342.667	8	11	12
9	612	342.667	9	1	4
10	0	514	10	4	7
11	306	514	11	7	10
12	612	514	12	2	5
			13	5	8
			14	8	11
			15	3	6
			16	6	9
			17	9	12

**Figure 4.2: Member End Nodes and Node Coordinates**

### 4.1.3 Identifying Boundary Members for Panels

The grid creates panels, or rectangles, that are surrounded above and below by girders and surrounded on the left and right by diaphragms. BRIDGE numbers these panels beginning with 1 for the bottom leftmost panel in Figure 4.1 and increasing numerically first to the right and then to the top. The panel numbers and number of each surrounding member are displayed in a table in the Node and Member Assignments sheet, as shown in Figure 4.3.

Panel #	Member # Above	Member # Below	Member # Left	Member # Right
1	3	1	9	12
2	4	2	12	15
3	5	3	10	13
4	6	4	13	16
5	7	5	11	14
6	8	6	14	17

**Figure 4.3: Panel List and Surrounding Members**

### 4.1.4 Determining Truck-Load Paths

BRIDGE determines the truck paths in each lane. Standard truck axles are spaced 6 ft apart, and the truck encroaches an additional 2 ft past the centerline of each wheel load, making the entire truck clearance 10 ft, as illustrated in Figure 2.1. AASHTO (2002) asserts that a truck should be placed in its lane so as to produce the maximum live-load reaction at the girder supports, thereby requiring the creation of influence lines to determine the exact truck placement combination that creates maximum live load for each girder support. However, this type of analysis is computationally expensive because it requires much longer run times for the program. As a simplified alternative, the program places each truck in four load paths across their respective lanes. The exterior wheels in the first and fourth load paths are placed 2 ft from the edge of the barrier or lane-dividing line, as demonstrated by the exterior trucks in Figure 4.4. The other two truck-load paths (interior trucks in Figure 4.4) are spaced uniformly between the two exterior loading paths at Load Path Spacing in Figure 4.4. Load Path Spacing is unique for each lane depending on the lane width and shoulder widths adjacent to that lane. Shoulder widths are



considered part of the adjacent lane, so a truck is allowed to encroach upon the shoulder width. Truck-load paths are assumed to extend straight across the length of the bridge.

In order to determine the extreme live load at each girder support, the BRIDGE program places Truck #1 in its first load path and incrementally moves all the other trucks throughout their load paths. Truck #1 is then moved to its second load path, and the process is repeated until all possible truck placement combinations and girder support reactions caused by each combination are analyzed. For example, the placement of two trucks on the bridge results in 16 load combinations that the program must analyze. Three trucks results in 64 total load combinations.

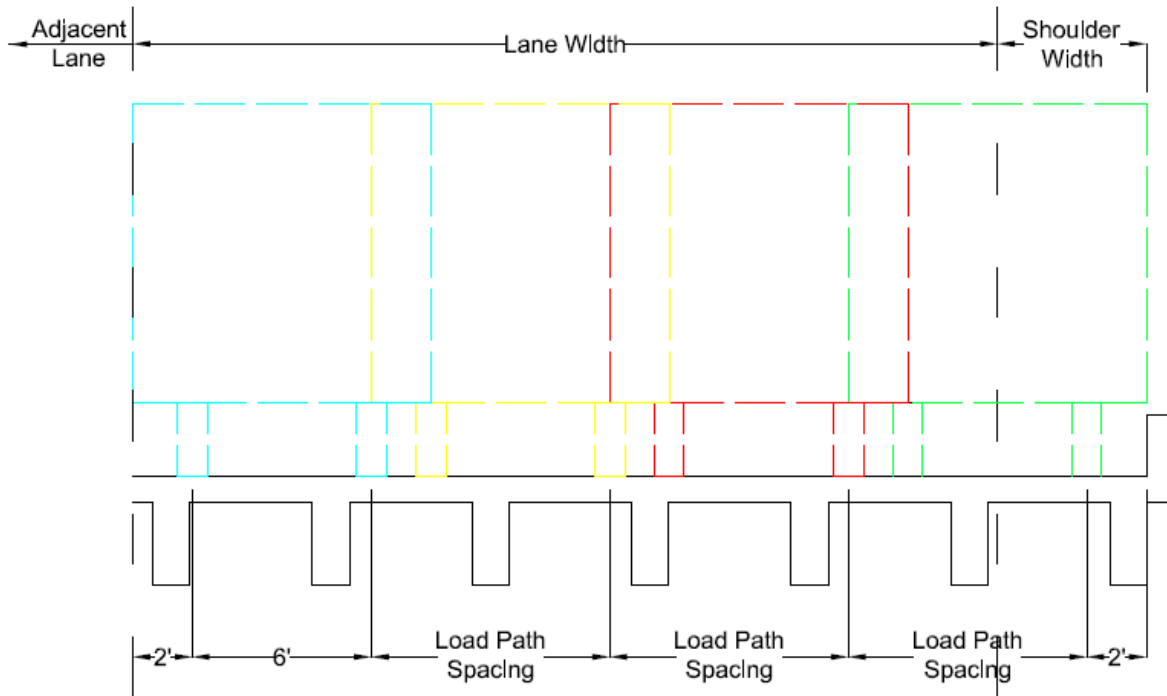


**Figure 4.4: Four Load Paths within Each Lane**

#### *4.1.5 Placing Trucks on Bridge*

The BRIDGE program uses tables in the background of the Truck Input sheet to place truck loads in appropriate user-specified locations. Each wheel load is assigned a number: loads from Truck #1 are labeled first, followed by Truck #2, and so on. The location of each wheel load is then identified. The  $x$  coordinate of each load is measured from the center of the far left

diaphragm, and the y coordinate of each load is measured from the center of the bottom exterior girder. Four y coordinates that correspond to each load represent positions of the four truck-load paths discussed in the previous section. The “Rightmost” load path refers to the load path closest to the bottom girder; the “Leftmost” load path refers to the load path furthest from the bottom girder. The load magnitude and location of each load is displayed in the Node and Member Assignments sheet, as shown in Figure 4.5.

Load #	Load on Wheel (tons)	x-dist from cent. far left diaphragm (in.)	y-dist from cent. of bottom girder for each "load path" (in.)			
			"Rightmost"	"Right"	"Left"	"Leftmost"
1	4	168	17	65	113	161
2	4	168	89	137	185	233
3	16	0	17	65	113	161
4	16	0	89	137	185	233
5	4	0	281	329	377	425
6	4	0	353	401	449	497
7	16	168	281	329	377	425
8	16	168	353	401	449	497
9	16	336	281	329	377	425
10	16	336	353	401	449	497

**Figure 4.5: Truck Load and Placement Information**

#### *4.1.6 Determining Multiple Presence Factor*

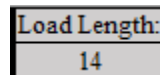
BRIDGE reads whether or not a user chooses to use the live-load reduction factor for loads in multiple lanes in accordance with AASHTO (2002) Article 3.12. If the user chooses not to use the reduction factors, the program sets the reduction factor to 1; if the user utilizes the reduction factors, however, the program reads the background of the Truck Input sheet to determine how many lanes are loaded and assigns a reduction factor based on Table 2.1. The program then prints the reduction factor into the background of the Truck Input sheet, as shown in Figure 4.6.

Reduction Factor
1

**Figure 4.6: Reduction Factor**

#### 4.1.7 Determining Load Length

The BRIDGE program determines the length of each truck, which is defined as the distance between the first and last axles. This length (ft) is then printed in Load Length in the user-input section of the Truck Input sheet shown in Figure 3.17. The overall load length used to determine the impact factor in Equation 2.3 is then found and printed in the background of the Truck Input sheet, as shown in Figure 4.7. This length is the smallest of the shortest truck length on the bridge or bridge length in order to conservatively provide the highest impact load coefficient.



Load Length:
14

**Figure 4.7: Load Length for Impact Factor Calculation**

## 4.2 Placement of Trucks on Bridge

The Place Trucks on Bridge button initializes the Truck\_Placement module. The following sections describe the tasks BRIDGE performs when this module is run.

### 4.2.1 Identifying Panels under Each Load and Location of Load on the Panel

This module reads the location of each load and determines the panel that contains the load. The relative location of each load on the panel is then determined. The  $x$  distance of the load is measured from the center of the diaphragm on the left edge of the panel, and the  $y$  distance is measured from the center of the girder on the bottom edge of the panel.

### 4.2.2 Distributing Each Load to Members Surrounding the Panel

Each load is then distributed to the girders and diaphragms on the edges of each panel. The portion of each load distributed to various edge members is dependent upon the length of the edge diaphragms and girders, as well as the location of the load on the panel. Three methods were investigated to find the most appropriate method of distributing truck wheel point loads from the panels to the surrounding girders and diaphragms. The three methods included Finite

Element Analysis of Panel, Rigid Slab Analysis of Panel, and Rigid Beam Analysis within the Panel.

#### 4.2.2.1 Finite Element Analysis of Panel

In order to investigate the Finite Element Analysis of Panel method, a RISA model was created to represent a panel surrounded by 8-ft-long diaphragms and 12-ft-long girders, as shown in Figure 4.8 (RISA Technologies, Inc., 2012). The panel, which was assumed to be flexible, consisted of an 8-inch-thick plate of 4 ksi normal weight concrete, thereby representing bridge deck slab thicknesses and material strength. In order to improve model accuracy, the plate was divided using a 1 ft  $\times$  1 ft mesh. A 10-kip load was placed 3 ft from the origin along the girder and 2 ft from the origin along the diaphragm. If the origin was located at the bottom-left corner of the plate and the entire plate lies in the first quadrant with the bottom girder along the x-axis, then the load was placed at the coordinates (3 ft, 2 ft), as shown in Figure 4.8. Each node along the boundary girders and diaphragms was set as a pinned reaction, and the model was run. The reaction at each node of the boundary elements was recorded; the sum of the reactions equaled 10.242 kips, which differed from the 10 kip original point load more significantly than desired, so the plate's mesh was further refined to a 3 inch  $\times$  3 inch mesh. The model was run again while maintaining the load location, resulting in a sum of reactions at the boundary elements of 9.997 kips, which is very close to the original 10 kip point load. Therefore, the 3 inch  $\times$  3 inch mesh was deemed to produce adequately accurate results. Reactions along each boundary member are shown in Figure 4.9, Figure 4.10, Figure 4.11, and Figure 4.12. The primary diaphragm is the diaphragm closest to the point load, while the secondary diaphragm is the diaphragm furthest from the point load. The same description applies for the girders. The total load on each edge member is shown in Table 4.1.

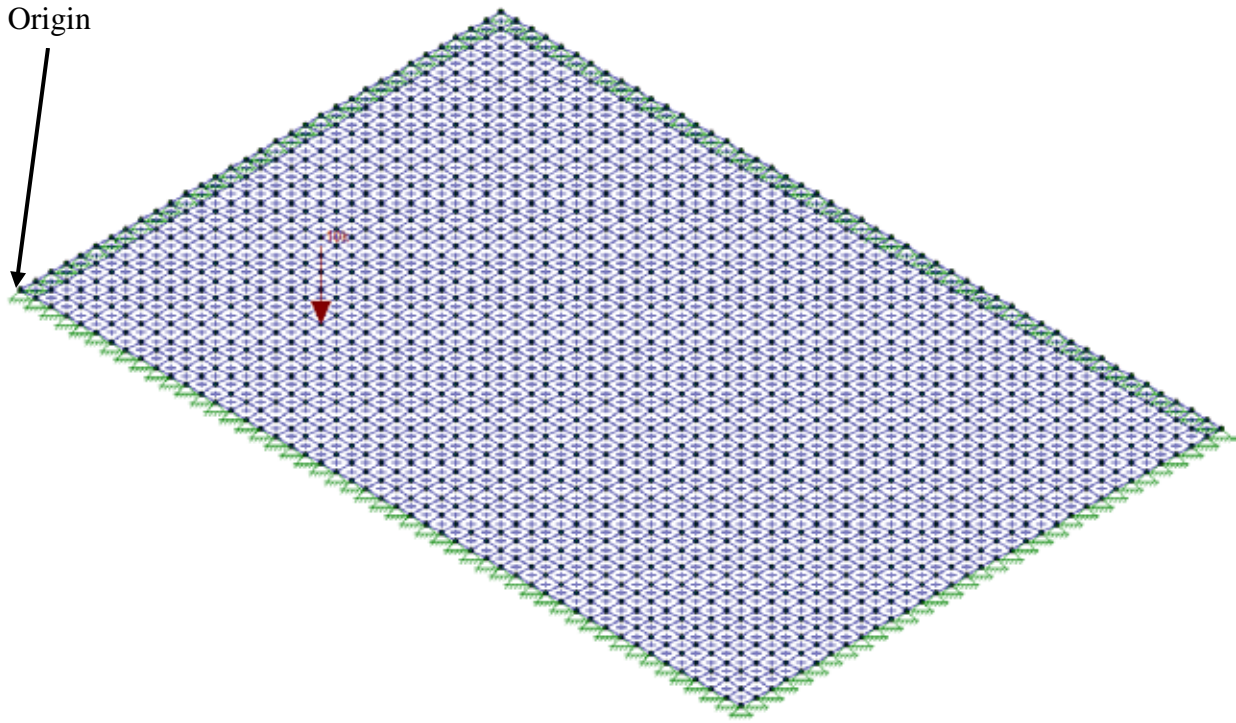


**Figure 4.8: RISA Model of Finite Element Analysis of Panel with 3 Inch x 3 Inch Mesh**

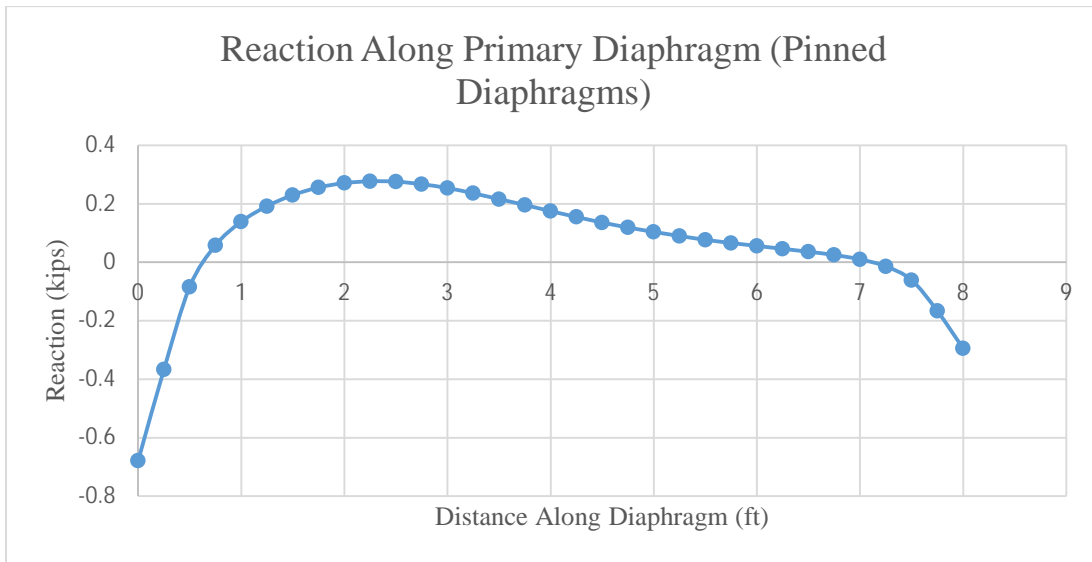


**Figure 4.9: Reaction at Each Node along Primary Diaphragm**

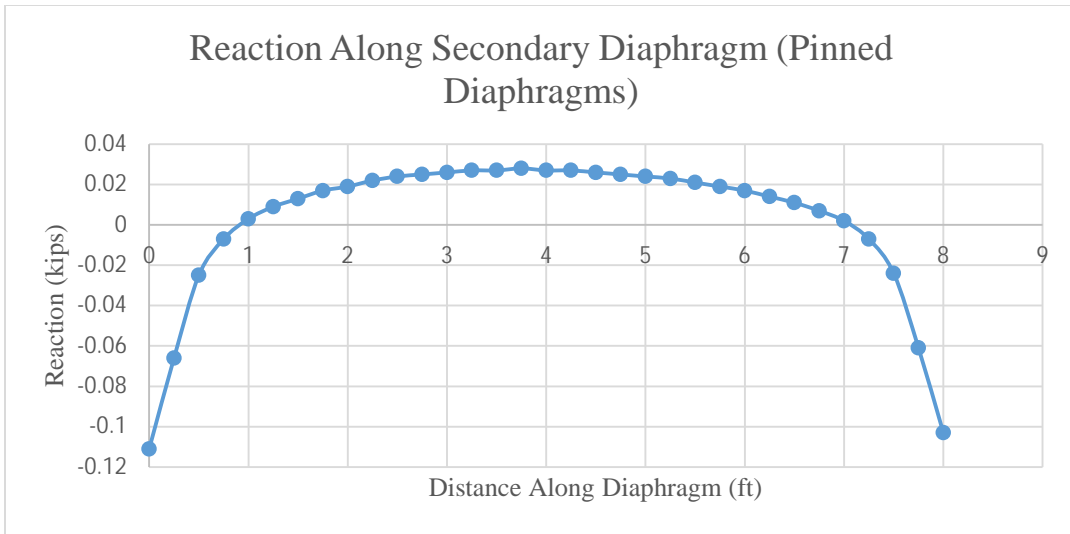


**Figure 4.10: Reaction at Each Node along Secondary Diaphragm**

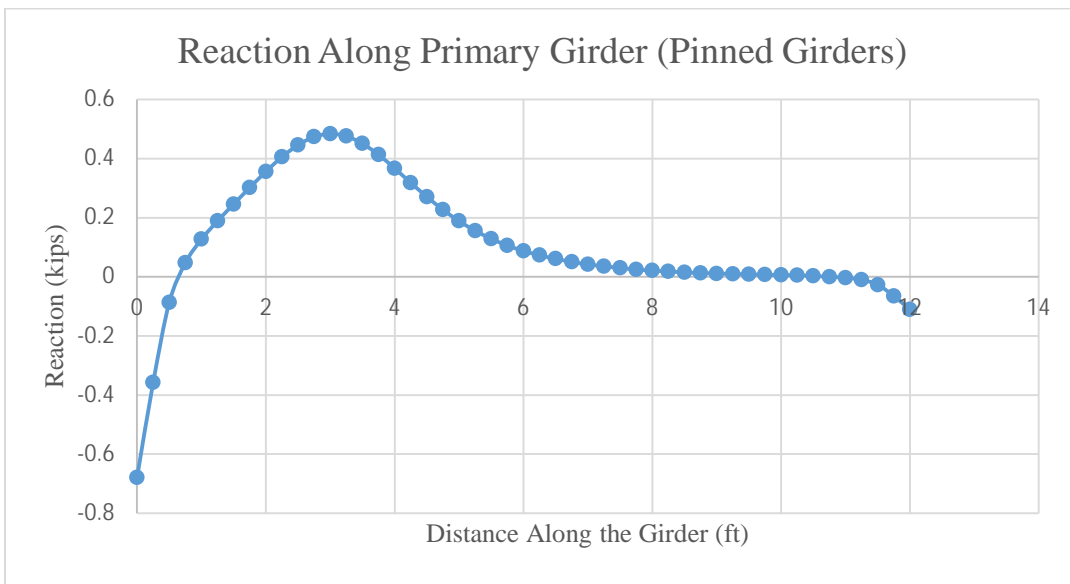


**Figure 4.11: Reaction at Each Node along Primary Girder**

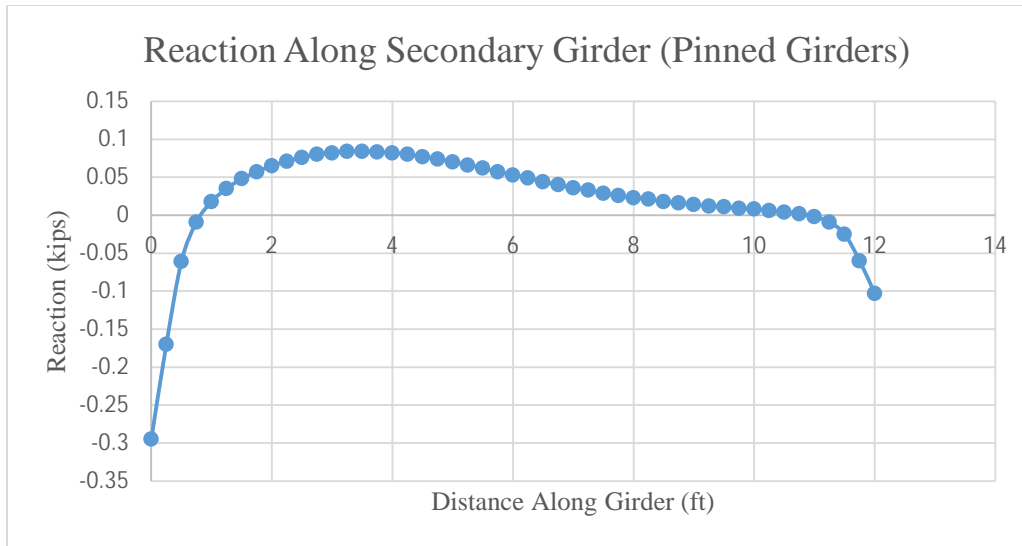


**Figure 4.12: Reaction at Each Node along Secondary Girder**

Because loads along each girder and diaphragm were centered near the location of the load, determination had to be made as to whether or not the portion of load distributed to each member could act as a single-point load along the member at the load location. Utilization of this method in the program would require complicated, time-consuming finite element analysis for each panel on the bridge in order to find loads on each surrounding girder and diaphragm. Consequently, other distribution methods were investigated to determine if they would yield reasonable results.

#### 4.2.2.2 Rigid Slab Analysis of Panel

A RISA model of the same panel from Section 4.2.2.1 was analyzed for the Rigid Slab Analysis of Panel method, with the exceptions that the diaphragms' end nodes were freed so that only the girder nodes were pinned, and the slab acted in one way action between the girders, as shown in Figure 4.13. The load and load location remained the same, and deflection of the slab at the location of the load ( $\Delta_d$ ) was found. The girder nodes were then freed, and the diaphragm nodes were pinned so that the slab acted in one way action between the diaphragms. The load and load location remained the same, and the deflection at the location of the load ( $\Delta_g$ ) was found. These deflections and the applied load were used to determine how the load distributed to each of the end diaphragms and girders. For these calculations, the slab was assumed to be rigid.

Calculations to distribute the load are derived below. Equation 4.1 was substituted to create Equation 4.2, Equation 4.3 was substituted into Equation 4.4 to yield Equation 4.5 and Equation 4.6, and Equation 4.1 and Equation 4.2 were substituted into Equation 4.6 to yield Equation 4.7.

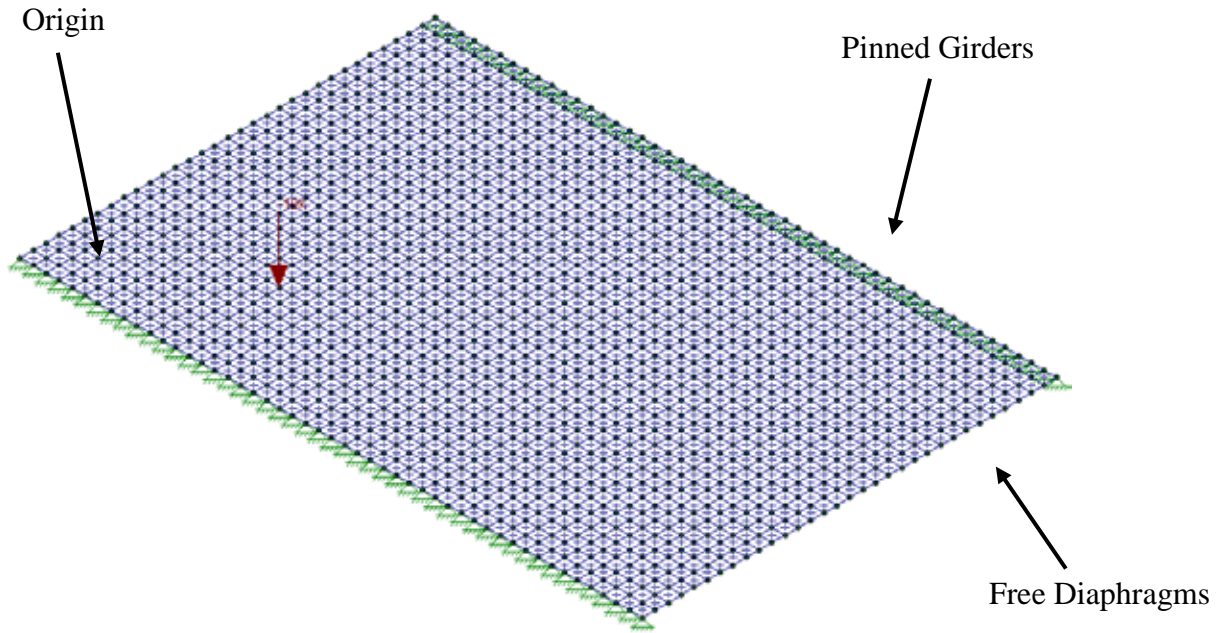


**Figure 4.13: RISA Model of Rigid Slab Analysis of Panel with Pinned Girders and Free Diaphragms**

Derivation:

$$K_G = \frac{P}{\Delta_G} \text{ \& \ } K_D = \frac{P}{\Delta_D} \quad \text{Equation 4.1}$$

$$K_{sum} = K_G + K_D = \frac{P}{\Delta_G} + \frac{P}{\Delta_D} \quad \text{Equation 4.2}$$

$$\Delta = \frac{P_G}{K_G} = \frac{P_D}{K_D} \quad \text{Equation 4.3}$$

$$K_{sum} = \frac{P}{\Delta} \rightarrow \Delta = \frac{P}{K_{sum}} \quad \text{Equation 4.4}$$

$$\frac{P_G}{K_G} = \frac{P}{K_{sum}} \text{ \& \ } \frac{P_D}{K_D} = \frac{P}{K_{sum}} \rightarrow \quad \text{Equation 4.5}$$



$$P_G = K_G \frac{P}{K_{sum}} \quad \& \quad P_D = K_D \frac{P}{K_{sum}} \rightarrow \quad \text{Equation 4.6}$$

$$P_G = \frac{P}{\Delta_G} \left( \frac{P}{\left( \frac{P}{\Delta_G} + \frac{P}{\Delta_D} \right)} \right) \quad \& \quad P_D = \frac{P}{\Delta_D} \left( \frac{P}{\left( \frac{P}{\Delta_G} + \frac{P}{\Delta_D} \right)} \right) \quad \text{Equation 4.7}$$

Where:

$P$  = load applied to the slab

$K_G$  = stiffness of the slab when acting as a girder (kip/inches)

$K_D$  = stiffness of the slab when acting as a diaphragm (kip/inches)

$c$  = deflection of the slab when acting as a girder (inches)

$d$  = deflection of the slab when acting as a diaphragm (inches)

$K_{sum}$  = sum of slab stiffness when acting as girder and diaphragm (kip/inches)

$P_G$  = total load transferred to diaphragms (slab acts as girder) (kips)

$P_D$  = total load transferred to girders (slab acts as diaphragm) (kips)

For this analysis the  $c$  and  $d$  were 0.029 and 0.009 inches, respectively, while the applied load  $P$  was 10 kips. Therefore,  $P_G$  and  $P_D$  were 2.39 and 7.63 kips, respectively, as shown in Equation 4.8 and Equation 4.9.

$$P_G = \frac{10}{0.029} \left( \frac{10}{\left( \frac{10}{0.029} + \frac{10}{0.009} \right)} \right) = 2.39 \text{ kip} \quad \text{Equation 4.8}$$

$$P_D = \frac{10}{0.009} \left( \frac{10}{\left( \frac{10}{0.029} + \frac{10}{0.009} \right)} \right) = 7.63 \text{ kip} \quad \text{Equation 4.9}$$

Loads on each girder and diaphragm were then determined in a similar method as used to determine the reactions of a simply supported beam caused by a point load on the beam, as shown in Equation 4.10 and Equation 4.11. Point loads transferred to each member using Rigid Slab Analysis are displayed in Table 4.1.

$$P_{\text{distributed to diaphragm}} = P_G \frac{a}{L_G} \quad \text{Equation 4.10}$$

$$P_{\text{distributed to girder}} = P_D \frac{a}{L_D} \quad \text{Equation 4.11}$$

Where:

$P_{\text{distributed to diaphragm}}$  = point load on each diaphragm

$P_{\text{distributed to girder}}$  = point load on each girder

$a$  = distance between point load and girder/diaphragm analyzed

$L_G$  = length of girders

$L_D$  = length of diaphragms

#### 4.2.2.3 Rigid Beam Analysis within the Panel

The modeling accuracy of the slab as two beams was also tested. A RISA model consisting of two beams (each 1 ft wide and 8 inches thick) was created in the Rigid Beam Analysis. The girder beam was 2 ft from the origin, and the diaphragm beam was 3 ft from the origin so that the intersection of the two beams was at the coordinates (3 ft, 2 ft). The 10 kip point load was applied at this location as in previous models (Figure 4.14). The girder beam was deleted, leaving the diaphragm beam with both ends pinned. Deflection of the beam,  $\Delta_D$ , at the location of the load was determined, and then the girder beam was added and the diaphragm beam was deleted. Deflection of the girder beam,  $\Delta_G$ , at the location of the load was then found, and Equation 4.7 and Equation 4.10 were used to find the load transferred to each diaphragm and girder. For this analysis the  $\delta_G$  and  $\delta_D$  were 0.19 and 0.057 inches, respectively, while applied load  $P$  was 10 kips. Therefore,  $P_G$  and  $P_D$  were 2.308 and 7.69 kips, respectively. The load transferred to each girder and diaphragm is shown in Table 4.1.

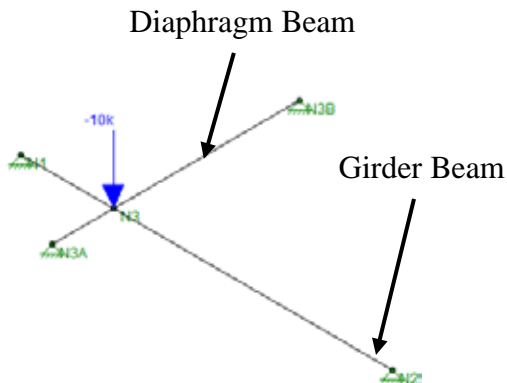


Figure 4.14: RISA Model for Rigid Beam Analysis within the Panel

#### 4.2.2.4 Analysis Results and Conclusions

As seen in Table 4.1, Rigid Slab Analysis of Panel and Rigid Beam Analysis within the Panel distribute loads similarly to the more accurate Finite Element Analysis of Panel, especially for the primary girder that receives a majority of the load. Therefore, the conclusion was made that the Rigid Beam Analysis of Panel can distribute loads to girders and diaphragms with reasonable accuracy.

The centroid of reaction along each girder and diaphragm for each method are shown in Table 4.2. The areas under the curves of Figures 4.9 through 4.12 were analyzed to find the reaction location for Finite Element Analysis; a similar process was used for Rigid Slab Analysis. For Rigid Beam Analysis, the load was assumed to transfer to the girders and diaphragms at the point along the member corresponding to the location of the concentrated load. The centroid of the reaction for Rigid Slab Analysis was extremely close to the location along the girders and diaphragms of the concentrated load. The centroid of reactions along the girders and diaphragms for Finite Element Analysis was further away from the location of the concentrated load; however, for the primary girder that carries a majority of the load, the centroid of reaction was 3.7 ft from the origin, which is close to the center of reaction for the Rigid Beam Analysis. For the other diaphragms and girders, the centroid of reaction was 1.25 to 2 ft from the reactions of the Rigid Beam Analysis, which was considered insignificant since less load was transferred to these members. Therefore, the conclusion was made that Rigid Beam Analysis transfers the load to girders and diaphragms with reasonable accuracy. Therefore, this load distribution method was incorporated into BRIDGE.

**Table 4.1: Comparison of Load Distribution to Girders and Diaphragms using Various Analysis Methods**

ANALYSIS METHOD	Load Transferred to:			
	Diaphragm		Girder	
	Primary	Secondary	Primary	Secondary
Finite Element	2.783	0.186	5.758	1.27
Rigid Slab	1.776	0.592	5.723	1.908
Rigid Beam	1.731	0.577	5.769	1.923

**Table 4.2: Comparison of the Centroid of Reaction along Girders and Diaphragms using Various Analysis Methods**

ANALYSIS METHOD	Centroid of Reaction from Origin (ft)			
	Diaphragm		Girder	
	Primary	Secondary	Primary	Secondary
Finite Element	3.25	3.99	3.70	4.99
Rigid Slab	2.27	2.35	3.10	3.28
Rigid Beam	2	2	3	3

#### 4.2.2.5 Aspect Ratio Tables

The Rigid Beam Analysis method was run for a series of girder-to-diaphragm length aspect ratios. In the analysis, each diaphragm beam was 1 ft wide, 8 inches thick, and 10 ft long, and each girder beam was 1 ft wide and 8 inches deep; the length of the beam varied. For an aspect ratio of 1, the beam length was 10 ft, and for each incremental 0.1 increase of the aspect ratio, the length of the girder beam increased by 1 ft. Therefore, for an aspect ratio of 1.5, the girder length was 15 ft. The aspect ratio is the girder-length-to-diaphragm-length ratio of a panel.

The  $f_D/f_{Dmax}$  and  $f_G/f_{Gmax}$  values, which were calculated for various  $x/a$  and  $y/b$  load locations for each aspect ratio combination, were used to find the flexibility of the panel in each bending direction, as described by Equations 4.12 through 4.15. These values were multiplied by the  $f_{Dmax}$  and  $f_{Gmax}$  for the actual program-analyzed panel in order to obtain the flexibility of the diaphragm and girder panel beams,  $f_D$  and  $f_G$ , respectively, in which  $f_D$  is the flexibility of the panel beam acting as a diaphragm (spanning between the girders and parallel to the diaphragms), while  $f_G$  is the flexibility of the panel beam acting as a girder (spanning between the diaphragms and parallel to the girders). These flexibilities were inverted to find the stiffness of each beam,  $K_D$  and  $K_G$ , and these values were used in Equation 4.7 and Equation 4.10 to distribute the load to girders and diaphragms. The  $x/a$  and  $y/b$  ratios describe the location of the load on the panel. As shown in Figure 4.15,  $a$  represents the girder length along the panel edge,  $b$  is the diaphragm length along the panel edge,  $x$  is the position of the load along the girder, and  $y$  is the position of the load along the diaphragm.

$$f_{Dmax} = \frac{L_D^3}{48EI_D} \quad \text{Equation 4.12}$$

$$f_{Gmax} = \frac{L_G^3}{48EI_G} \quad \text{Equation 4.13}$$

$$f_D = \frac{\Delta_D}{P} \quad \text{Equation 4.14}$$

$$f_G = \frac{\Delta_G}{P} \quad \text{Equation 4.15}$$

Where:

$f_{Dmax}$  = maximum flexibility of the diaphragm beam (inches/kip)

$f_{Gmax}$  = maximum flexibility of the girder beam (inches/kip)

$L_D$  = length of diaphragm (inches)

$L_G$  = length of girder (inches)

$E$  = modulus of elasticity for concrete

$I_D$  = moment of inertia of diaphragm beam (inches<sup>4</sup>)

$I_G$  = moment of inertia of girder beam (inches<sup>4</sup>)

$f_D$  = actual flexibility of the diaphragm beam (inches/kip)

$f_G$  = actual flexibility of the girder beam (inches/kip)

$P$  = point load placed on beams (kips)

$\Delta_D$  = deflection of the diaphragm beam at location of point load (inches)

$\Delta_G$  = deflection of the girder beam at location of point load (inches)

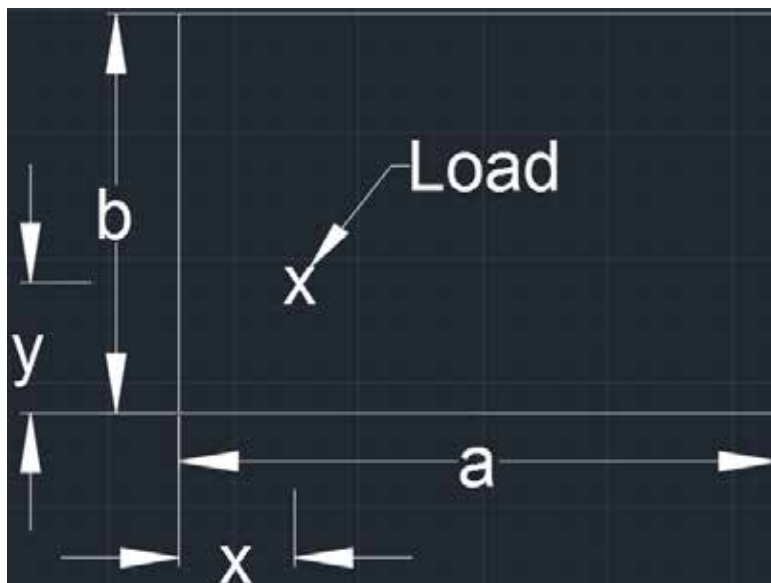


Figure 4.15: Load Placement on Panel

The  $f_D/f_{Dmax}$  and  $f_G/f_{Gmax}$  values were calculated for aspect ratios ranging from 1 to 2 by 0.1 increments. Aspect ratios from 0.5 to 1 use the same values calculated from aspect ratios 1 to 2, with the exception that the load distribution is switched from the girders to the diaphragms and vice versa. For example, the  $f_D/f_{Dmax}$  value for an aspect ratio of 0.6 is the same as the  $f_G/f_{Gmax}$  value for an aspect ratio of 1.2. When the aspect ratio is below 0.5, the program assumes that the entire load is transferred to the diaphragms, but when the ratio is over 2, the program assumes that the entire load is transferred to the girders. If a wheel load is on the cantilever portion of the deck, the program automatically transfers the full load to the adjacent girder.

The  $f_G/f_{Gmax}$  and  $f_D/f_{Dmax}$  values for various  $x/a$  and  $y/b$  values at different aspect ratios are displayed in Table 4.3 and Table 4.4, respectively.

**Table 4.3:  $f_G/f_{Gmax}$  Values for  $x/a$  Locations and Aspect Ratios**

$f_G/f_{Gmax}$		Aspect Ratio										
		1	1.1	1.2	1.3	1.4	1.5	1.6	1.7	1.8	1.9	2
$x/a$	0	0.0	0.0	0.0	0.0	0.0	0.0	0.0	0.0	0.0	0.0	0.0
	0.2	0.4153	0.4122	0.4095	0.4107	0.4092	0.4086	0.4081	0.4080	0.4079	0.4074	0.4070
	0.4	0.9229	0.9206	0.9198	0.9195	0.9174	0.9176	0.9163	0.9152	0.9152	0.9149	0.9145
	0.6	0.9229	0.9206	0.9198	0.9195	0.9174	0.9176	0.9163	0.9152	0.9152	0.9149	0.9145
	0.8	0.4153	0.4122	0.4095	0.4107	0.4092	0.4086	0.4081	0.4080	0.4079	0.4074	0.4070
	1	0.0	0.0	0.0	0.0	0.0	0.0	0.0	0.0	0.0	0.0	0.0

**Table 4.4:  $f_D/f_{Dmax}$  Values for  $y/b$  Locations and Aspect Ratios**

$f_D/f_{Dmax}$		Aspect Ratios:
$y/b$	0	0
	0.2	0.415295601
	0.4	0.922879112
	0.6	0.922879112
	0.8	0.415295601
	1	0

Table 4.3 shows  $f_G/f_{Gmax}$  values for various  $x/a$  load locations. Although the values changed for varying aspect ratios as the girder became longer, for a given  $x/a$  the  $f_G/f_{Gmax}$  value was extremely close for all aspect ratios. Therefore, for simplicity, an aspect ratio of 1 was used regardless of the actual aspect ratio of the panel, similar to the  $f_D/f_{Dmax}$  values for various  $y/b$  ratios. Table 4.4 shows  $f_D/f_{Dmax}$  values for varying  $y/b$  load locations. The diaphragm beam length was kept constant, so the  $f_D/f_{Dmax}$  value was constant for every aspect ratio.

Table 4.3 and Table 4.4 were combined into Table 4.5, and additional  $x/a$  and  $y/b$  values were included to increase interpolation accuracy within the table. The BRIDGE program uses  $x/a$  and  $y/b$  locations of the wheel load on the panel to interpolate within Table 4.3 to determine appropriate  $f_G/f_{Gmax}$  and  $f_D/f_{Dmax}$  values for each load. Table 4.5 is displayed in the program's Tables sheet.

**Table 4.5:  $f_G/f_{Gmax}$  and  $f_D/f_{Dmax}$  Values for Load Location on Panel**

$x/a$ and $y/b$		$f_G/f_{Gmax}$ and $f_D/f_{Dmax}$
<b>Aspect Ratios</b>	0	0
	0.1	0.133304761
	0.2	0.415295601
	0.3	0.707540653
	0.4	0.922879112
	0.5	0.999785705
	0.6	0.922879112
	0.7	0.707540653
	0.8	0.415295601
	0.9	0.133304761
	1	0

#### *4.2.3 Determining Fixed End Reactions at Each Node Caused by Live Loads*

BRIDGE also applies the redistributed load as a point load on the edge girders and diaphragms at a distance along the diaphragm member equal to the load's  $y$  distance on the panel and along the girder member equal to the load's  $x$  distance on the panel. These loads are then

converted into fixed-end forces at the member end nodes. The fixed-end moments (FEMs) are defined by Equation 4.16 and Equation 4.17, while Equation 4.18 and Equation 4.19, with reference to Figure 4.16, define the fixed-end shear forces, which are always in the positive upward direction. The FEMs and shears at each end nodes of the member are then summed.

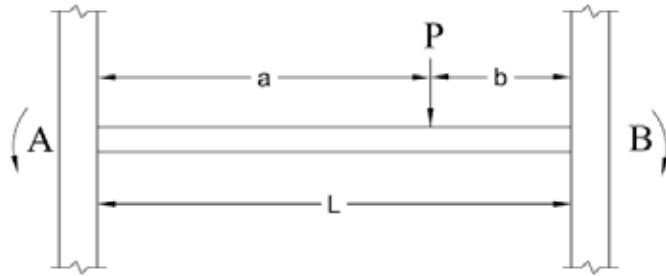


**Figure 4.16: FEM for a Point Load on the Span**

$$FEM_{AB} = \frac{Pb^2a}{L^2} \quad \text{Equation 4.16}$$

$$FEM_{BA} = \frac{Pa^2b}{L^2} \quad \text{Equation 4.17}$$

$$V_a = \frac{Pb^2}{L^3} [L + 2a] \quad \text{Equation 4.18}$$

$$V_b = \frac{Pa^2}{L^3} [L + 2b] \quad \text{Equation 4.19}$$

Where:

$FEM_{AB}$  = fixed-end moment at point A in Figure 4.16

$FEM_{BA}$  = fixed-end moment at point B in Figure 4.16

$V_a$  = vertical reaction at point A in Figure 4.16

$V_b$  = vertical reaction at point B in Figure 4.16

#### 4.2.4 Determining Reactions at Nodes Caused by Dead Loads

BRIDGE utilizes the cross-sectional properties and material properties for the girders, slab, and wearing surface, as well as the actual effective slab width from the background of the Mesh & Alignment sheet to calculate the uniform dead load  $w$  along each girder. The weight of



the diaphragms and barriers is neglected as insignificant because their inclusion would add significant unnecessary complication to the user input section and dead load calculations. The dead load is transferred to the girders because the girders typically are closer together than the diaphragms. Greater proximity between diaphragms is impractical, however, so the program always transfers dead load to the girders. The FEMs are defined by Equation 4.20, while Equation 4.21, with reference to Figure 4.17, defines the fixed-end shear forces, which are always in the positive upward direction.

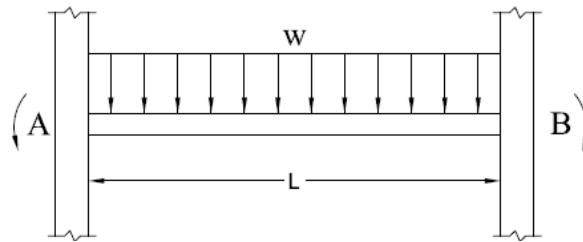


**Figure 4.17: FEM for a Distributed Load**

$$FEM_{AB} = FEM_{BA} = \frac{wL^2}{12} \quad \text{Equation 4.20}$$

$$V_A = V_B = \frac{wL}{2} \quad \text{Equation 4.21}$$

#### 4.2.5 Printing $k_{ff}$ and $k_{sf}$ Reactions for the Bridge Matrix

BRIDGE sorts dead- and live-load fixed-end forces into  $k_{ff}$  loads and  $k_{sf}$  reactions for the bridge mesh. The live  $k_{ff}$  loads and  $k_{sf}$  reactions for each truck placement combination, discussed in Section 4.1.4, are calculated and printed. The dead  $k_{ff}$  loads and  $k_{sf}$  reactions are kept separate from the live loads because the governing live load combination for each girder is not yet determined. A sample of these reactions is displayed in  $k_{ff}$  Loads and  $k_{sf}$  Reactions sheets, respectively, in Figure 4.18 and Figure 4.19.

		<b><math>k_{ff}</math> Dead Loads:</b>					
		0.00	-953.14	-37.38	0.00	0.00	0.00
<b>Combination #</b>	<b><math>k_{ff}</math> Live Loads</b>						
1	-555.77	-175.89	-3.16	-7.59	214.12	0.00	
2	-555.77	-175.89	-3.16	-7.59	214.12	0.00	
3	-555.77	-175.89	-3.16	-7.59	214.12	0.00	
4	-555.77	-175.89	-3.16	-7.59	214.12	0.00	
5	-495.54	-98.56	-1.88	-8.45	119.99	0.00	
6	-495.54	-98.56	-1.88	-8.45	119.99	0.00	

Figure 4.18: Snapshot of  $k_{ff}$  Loads Sheet

		<b><math>k_{sf}</math> Dead Reactions:</b>						
		-6.5876	-6.58759	-7.5649	-7.5649	-7.5649	-7.5649	-7.5649
<b>Combination #</b>	<b><math>k_{sf}</math> Live Reactions:</b>							
1	-12.423	0	-16.39	0	-3.8862	0	-4.0976	
2	-12.423	0	-16.39	0	-3.187	0	-3.3984	
3	-12.423	0	-16.39	0	-3.187	0	-2.0976	
4	-12.423	0	-16.39	0	-3.187	0	-0.7967	
5	-7.2195	0	-16.39	0	-9.0894	0	-4.0976	
6	-7.2195	0	-16.39	0	-8.3902	0	-3.3984	

Figure 4.19: Snapshot of  $k_{sf}$  Reactions Sheet

### 4.3 Load Rate Bridge

User selection of the Load Rate Bridge button activates the Stiffness module, which performs the following tasks.

#### 4.3.1 Assigning Properties to Each Member

BRIDGE uses the information displayed in the Section Properties sheet, shown in Figure 3.15, along with the concrete strength user-input and the coordinates of each node to determine the area, length, moment of inertia ( $I_x$ ), torsional constant ( $J$ ), shear modulus ( $G$ ), elastic modulus ( $E$ ), and angle of rotation ( $\alpha = 0$  or  $90$ ) for each member in the bridge mesh. These properties are displayed in the Member Properties sheet, as shown in Figure 4.20. Equation 4.22 and Equation

4.23 are used to find the elastic modulus and shear modulus, respectively. A Poisson's ratio ( $\nu$ ) of 0.2 is also used. The girders are oriented at an angle of  $0^\circ$ , while the diaphragms are oriented at  $-90^\circ$ . The theta column in Figure 4.20 displays these angles in radians.

$$E = 57\sqrt{f'_c} \quad \text{Equation 4.22}$$

$$G = \frac{E}{2(1+\nu)} \quad \text{Equation 4.23}$$

Member	Area (in <sup>2</sup> )	Length (in)	I (in <sup>4</sup> )	J (in <sup>4</sup> )	G (ksi)	E (ksi)	theta
1	943.25	306	150991	39601	1301	3122.019	0
2	943.25	306	150991	39601	1301	3122.019	0
3	1122	306	170629	41900	1301	3122.019	0
4	1122	306	170629	41900	1301	3122.019	0
5	1122	306	170629	41900	1301	3122.019	0
6	1122	306	170629	41900	1301	3122.019	0
7	943.25	306	150991	39601	1301	3122.019	0
8	943.25	306	150991	39601	1301	3122.019	0
9	1154.25	171.333333	18652	16948	1301	3122.019	-1.5708
10	1154.25	171.333333	18652	16948	1301	3122.019	-1.5708
11	1154.25	171.333333	18652	16948	1301	3122.019	-1.5708
12	2119.5	171.333333	7834	0	1301	3122.019	-1.5708
13	2119.5	171.333333	7834	0	1301	3122.019	-1.5708
14	2119.5	171.333333	7834	0	1301	3122.019	-1.5708
15	1154.25	171.333333	18652	16948	1301	3122.019	-1.5708
16	1154.25	171.333333	18652	16948	1301	3122.019	-1.5708
17	1154.25	171.333333	18652	16948	1301	3122.019	-1.5708

Figure 4.20: Member Properties

### 4.3.2 Creating Assembled Stiffness Matrix for Bridge

The BRIDGE program uses member properties to create the  $6 \times 6$  stiffness matrix for each member, as shown in Appendix B. The member end nodes are then used to combine the

member stiffness matrices into one large assembled stiffness matrix that encompasses the entire bridge.

#### *4.3.3 Creating $k_{ff}$ and $k_{sf}$ Matrices*

BRIDGE separates the assembled stiffness matrix into  $k_{ff}$  and  $k_{sf}$  matrices. The  $k_{ff}$  matrix is square and consists of matrix elements corresponding to unknown nodal displacements and known nodal forces. In this program, unknown nodal displacements are translational displacements and rotations at all non-support nodes as well as rotations at the support nodes (nodes on the end diaphragms). Translational displacements at each support are zero and are known. Known nodal forces are all forces and moments at non-support nodes and moments at support nodes. The  $k_{sf}$  matrix consists of matrix elements corresponding to unknown nodal displacements and unknown nodal forces. Unknown nodal forces consist of all vertical forces at the support nodes.

#### *4.3.4 Creating $k_{ff}^{-1}$ Matrix*

BRIDGE utilizes the Gauss-Jordan elimination method to find the  $k_{ff}^{-1}$  matrix by creating an identity matrix and the half-bandwidth  $k_{ff}$  matrix. The identity matrix is the same size as the  $k_{ff}$  matrix, and its elements are all 0s except for the diagonal, which are 1s. Because the  $k_{ff}$  matrix is symmetric, to save memory only the half-bandwidth matrix is used to solve for the  $k_{ff}^{-1}$  matrix. This half-bandwidth and identity matrix are manipulated using the Gauss-Jordan elimination method to find the  $k_{ff}^{-1}$  matrix, as displayed in the  $k_{ff}^{-1}$  sheet.

#### *4.3.5 Finding Displacements at Each Node*

The program finds unknown nodal displacements caused by the combination of dead loads and live loads. These displacements are found by multiplying the  $k_{ff}^{-1}$  matrix by the 'k<sub>ff</sub>' loads, as discussed in Sections 4.2.3, 4.2.4, and 4.2.5.

#### *4.3.6 Finding Reactions at Each Support*

The program also finds the reaction at each support due to the combination of dead loads and live loads by multiplying the  $k_{sf}$  matrix by displacements found in the previous section and

then subtracting the fixed-end forces at the supports ( $k_{sf}$  reactions [ $P_s$  vector], discussed in Sections 4.2.3, 4.2.4, and 4.2.5).

#### *4.3.7 Determining Governing Live Load at Each Support*

BRIDGE cycles through the reaction caused by each load combination at every support and identifies the largest live-load reaction at each support. This load contributes to the governing RF for that support.

#### *4.3.8 Calculating the Impact Factor*

The load length from Figure 4.7 is used in Equation 2.3 to find the impact factor used in Equation 2.2.

#### *4.3.9 Determining Girder Capacity*

As shown in Equation 2.2, the capacity of each girder at its supports must be known in order to determine the RF of the bridge. The approach used to calculate girder capacity assumes that the friction force between the girder and bearing pad is significant and actually causes the crack to propagate in the reverse diagonal direction. The dead- and live-load reaction  $R$  and friction force  $F$  act at the crack interface, as shown in Figure 4.21. Corrosion of the bearing pad and rocker prevents the end of the girders from rotating, leading to friction force, which was not considered in the girder design. As the girder is loaded it deflects downward, creating tension in the bottom of the girder and causing the girder, at the supports, to try to slide further away from the center of the girder. This movement, however, is prevented by the friction force at the beam-to-pad interface. The friction force in the girder, thus, acts toward the center of the girder, as shown in Figure 4.21, and the crack-driving force component of the two forces, shown parallel to the crack in Figure 4.21, act against each other. The crack-clamping forces, shown perpendicular to the crack in Figure 4.21, are additive. The driving and clamping forces are shown as Equation 4.24 and Equation 4.25.

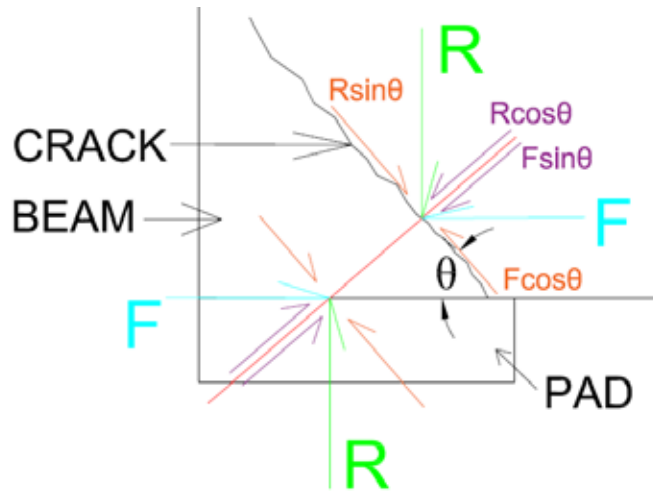


Figure 4.21: Reaction and Friction Forces on the Reverse Diagonal Crack According to the Friction Load Approach

$$\text{Driving Force} = R \sin \theta - F \cos \theta \quad \text{Equation 4.24}$$

$$\text{Clamping Force} = R \cos \theta + F \sin \theta \quad \text{Equation 4.25}$$

#### 4.3.9.1 ABAQUS Study

A parametric study using ABAQUS (Dassault Systèmes, 2013) was conducted to test the validity of this approach. Various girder models were created with different geometric and loading parameters in order to investigate the reaction-to-friction force relationship at the beam-to-bearing pad interface.

#### Parameters

Various T-shape girders were created in ABAQUS. The web width  $b_w$ , web width-to-height ratio  $b_w/h$ , slab (flange) thickness  $h_s$ , and beam length-to-girder height ratio  $L/h$  were varied in each model, as displayed in Figure 4.22. The figure also shows that the slab extends past the girder web at a distance equal to the girder web height ( $h-h_s$ ) on either side of the web, forming a  $45^\circ$  angle with the bottom of the girder web. Table 4.4 displays the variations for each parameter. One variation was changed, but the others were held constant until a model was created for every possible combination.

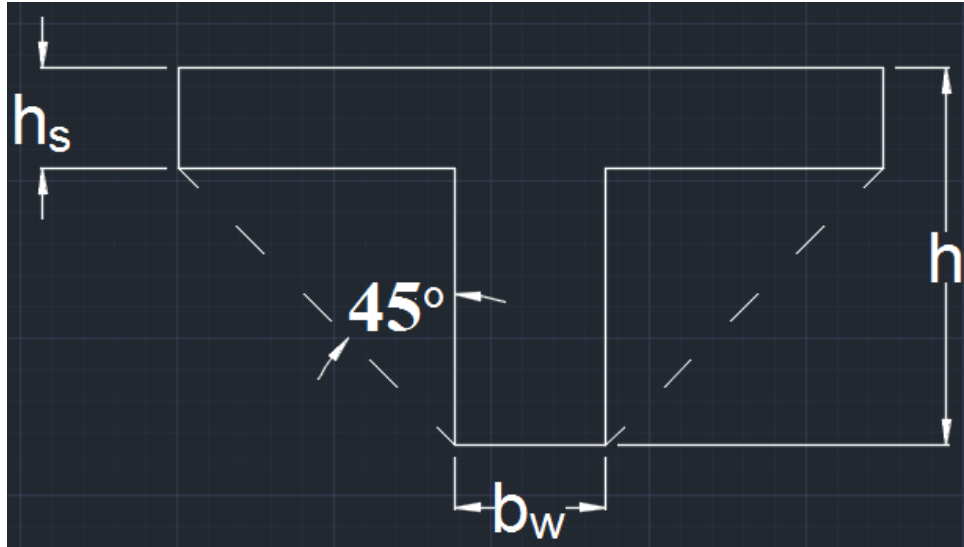


Figure 4.22: Parameters in the ABAQUS Models

Table 4.6: ABAQUS Parameter Variation

Variable Parameter:	Variation:		
$b_w$ (inches)	12	15	18
$b_w/h$	0.4	0.5	0.6
$h_s$ (inches)	6	8	10
$L/h$	7	12	17

### Model Creation

A Poisson's ratio of 0.2 was used for the concrete beams, along with a Young's modulus  $E$  of 3,122,019 psi. This modulus was calculated using Equation 4.22 with an assumed compressive strength  $f'_c$  of 3000 psi. The pad sections consisted of steel with a Poisson's ratio of 0.3 and a Young's modulus of 29,000,000 psi, and the coefficient of friction between the bearing pad and beam was 0.57.

The HS20 truck was used to estimate loading on the beams, with the assumption that an entire line of wheel loads acts on the girder. This is a conservative assumption because a wheel load is typically distributed to multiple girders. The assumption was also made that if the beam is long enough, wheel loads from multiple trucks are placed on the bridge. As shown in Figure 4.23, a wheel load of 16 kips (half of the 32 kip axle load) was placed on the right end of the beam. The HS20 truck's middle wheel load of 16 kips was placed 14 ft away, while the truck's

front wheel load of 4 kips was placed 14 ft away from the middle wheel load. A 6-ft buffer region was assumed to separate two trucks, after which another truck's rear wheel load was placed. This process continued until no more wheel loads could fit within the beam span. The truck loads were then applied as a pressure load to the beam part using Equation 4.26.

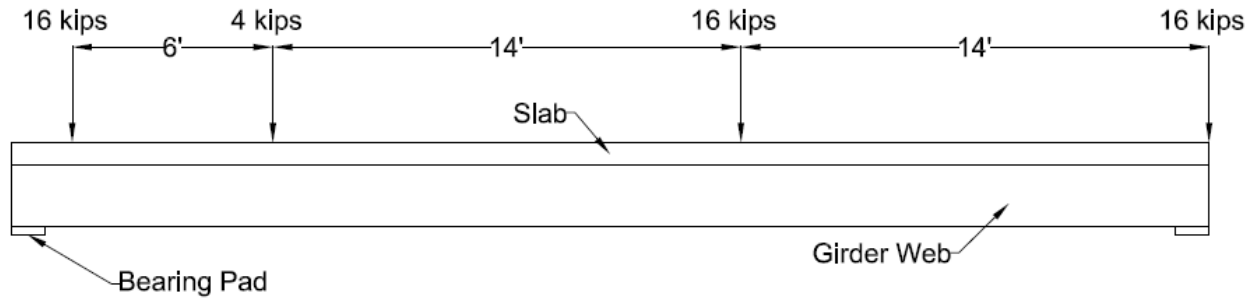


**Figure 4.23: Loading on ABAQUS Model Girders**

$$Pressure (psi) = \frac{\sum Truck\ wheel\ loads\ (lbs.)}{Length\ (inches) \times Effective\ Flange\ Width\ (inches)}$$

**Equation 4.26**

### *Model Output and Program Incorporation*

After a model was analyzed in the ABAQUS study, the normal and shear forces in the beam at the beam-to-bearing pad interface were found. Results of these models are discussed further in Section 5.3.3 of Bernica (2016). Using the results, shear-to-normal force ratios  $S/N$  were found for each parametric variation. These ratios are displayed in the Tables sheet shown in Figure 4.24.

BRIDGE used girder length  $L$ , girder height  $h$ , slab thickness  $h_s$ , and girder web width  $b_w$  of user-defined girders to interpolate within the tables in Figure 4.24 in order to find the  $S/N$  ratio corresponding to girders in the program. This  $S/N$  ratio is the predicted ratio of the friction force to normal force between the girder and bearing pad. If the interpolation yields a ratio larger than 0.57, then the program will limit the coefficient of friction to 0.57 since this is the theoretical point at which the girder starts slipping on the pad, which does not occur. The program then finds



the friction (shear) force due to live load, dead load, and combined dead and live load at each girder support by multiplying the  $S/N$  ratio by the reaction at the support caused by live load, dead load, and combined dead and live load, respectively, as shown in Equations 4.27 through 4.29.

%S/N				
bw: 12				
L/h: 7				
$b_w/h:$	$h_s$	6	8	10
0.4		14.9%	15.1%	15.1%
0.5		14.5%	14.6%	14.7%
0.6		7.4%	7.5%	7.5%
L/h: 12				
$b_w/h:$	$h_s$	6	8	10
0.4		46.9%	47.4%	48.0%
0.5		42.8%	43.5%	44.0%
0.6		42.7%	43.6%	43.9%
bw: 15				
L/h: 7				
$b_w/h:$	$h_s$	6	8	10
0.4		12.9%	12.9%	13.0%
0.5		12.6%	12.7%	12.8%
0.6		12.3%	12.4%	12.5%
L/h: 12				
$b_w/h:$	$h_s$	6	8	10
0.4		53.4%	53.6%	54.2%
0.5		40.3%	40.7%	41.2%
0.6		36.7%	37.2%	37.7%
bw: 18				
L/h: 7				
$b_w/h:$	$h_s$	6	8	10
0.4		11.4%	11.3%	11.3%
0.5		11.2%	11.2%	11.2%
0.6		11.0%	11.0%	11.1%
L/h: 12				
$b_w/h:$	$h_s$	6	8	10
0.4		47.4%	47.2%	47.4%
0.5		47.6%	47.7%	48.2%
0.6		35.4%	35.8%	36.2%

Figure 4.24: Shear-To-Normal Force Ratio Tables

$$F_{LL} = \frac{S}{N} \times R_{LL} \quad \text{Equation 4.27}$$

$$F_{DL} = \frac{S}{N} \times R_{DL} \quad \text{Equation 4.28}$$

$$F_{LL+DL} = \frac{S}{N} \times R_{LL+DL} \quad \text{Equation 4.29}$$

BRIDGE then divides the friction and reaction forces at each support caused by the total live and dead loads by the area of the girder-to-bearing pad interface in order to obtain the stresses at this location. The program arbitrarily uses an area of 10 inches<sup>2</sup>. All forces in the

analysis are divided by the same area to find stresses; thus, the actual magnitude of the area is inconsequential. The *R/Area* and *F/Area* stresses are  $\sigma_y$  and  $\tau_{xy}$ , respectively;  $\sigma_x$  is 0 at the interface.

The method outlined in Section 2.3 was used to find the maximum shear stress  $\tau_{max}$  and the angle of rotation to the plane of maximum shear stress  $\theta_s$  for each support. This  $\theta_s$ , which is the calculated crack propagation ( $\theta$  from Figure 4.21), is the same at every girder support for a user-defined bridge because, in the BRIDGE, the geometry of every girder is identical, so every *S/N* ratio is identical. This leads to identical  $\theta_s$  at every girder even if the reactions are dissimilar. In the Section Geometry and Material Properties sheet, a user has the option to use this calculated angle or a manually entered crack angle. The chosen angle, along with the friction force calculated in Equation 4.27 and the reaction force calculated within BRIDGE, are used in Equation 4.24 and Equation 4.25 to find the clamping and driving forces on the crack at each girder support. These forces are then used to find the RF for each girder support, as described by Equation 4.30.

$$RF = \frac{[Capacity\ w/o\ Clamping\ Force + \mu_c(Clamping_{DL+LL})] - A_1 Driving_{DL}}{A_2 Driving_{LL+IL}}$$

**Equation 4.30**

Where:

$\mu_c$  = concrete-to-concrete coefficient of friction (1.4)

$Clamping_{DL+LL} = \cos\theta R_{DL+LL} + \sin\theta F_{DL+LL}$

$Driving_{DL} = \sin\theta R_{DL} - \cos\theta F_{DL}$

$Driving_{DL+IL} = \sin\theta(1+I)R_{LL} - \cos\theta(1+I)F_{LL}$

$I$  = impact load (Equation 2.3)

$\theta$  = angle of crack propagation chosen by user

### *Capacity without Clamping Force*

Equation 2.4 describes shear capacity in which the SMCFT Equation 2.6, described in Section 2.1.4.1 of Bernica (2016), is used to find the  $V_n$  used in KSU BRIDGE to determine girder capacity. This method was chosen because it is consistent with AASHTO shear design specifications and it produces a conservative RF. In addition, many studies have proven the

accuracy and validity of the SMCFT. This project assumed that steel reinforcement does not cross the crack, so steel strain  $\varepsilon_s$  and steel shear capacity  $V_s$  in the SMCFT equations are assumed to equal zero.

#### *4.3.10 Calculating the Rating Factor at Each Support*

The RF is calculated using Equation 4.30.

# Chapter 5: Analysis and Results

## 5.1 Support Reactions: BRIDGE versus RISA 3D

Eighteen program and RISA 3D models were created with various combinations of parameters shown in Table 5.1 in order to test the accuracy of BRIDGE’s calculated live-load reactions at the support of each girder. The remainder of the bridge parameters, displayed in Table 5.2 and Appendix C, were varied randomly within reasonable and realistic bounds in order to obtain bridge diversity for the support reaction comparison. At the time of this analysis, the dead load of the bridge was not calculated, the program did not simultaneously calculate the inventory and operating levels, and the user specified the location of each truck in its respective lane with “South,” referring to the position in the lane closest to the bottommost girder. None of these changes, however, affected calculations of the live-load reaction at the supports.

Figure 5.1 shows the RISA model for Comparison #1 with truck wheel loads distributed to each surrounding girder and diaphragm using Rigid Beam Analysis within the Panel discussed in Section 4.2.2.3, which is the method used by BRIDGE to distribute wheel loads. The program and RISA 3D models were run, and results for Comparison #1 are displayed in Table 5.3. The BRIDGE input and results tables for the other 17 comparisons are displayed in Appendix C. As shown in the results tables, the live-load reactions calculated by BRIDGE and RISA 3D were extremely close, with less than 0.3% error between results. A larger error between the two models typically occurred at supports with very small reactions, demonstrating that even very small differences result in large percentage errors. These comparisons show that the program calculates live-load reactions with high accuracy, indicating that the stiffness matrix creation and manipulation within the program is accurate.

**Table 5.1: BRIDGE versus RISA 3D Model Parameter Variations**

	Parameter Variations:		
<b># of Lanes:</b>	---	2	4
<b># of Girders:</b>	3	4	5
<b>Diaphragm Configuration:</b>	4 Real	4 Real, 3 Virtual	3 Real, 4 Virtual

**Table 5.2: Support Reaction Comparison #1: BRIDGE Input**

<b>LOADING</b>				
	<b>Truck #1:</b>		<b>Truck #2:</b>	
<b>Truck Type:</b>	Type T170 Unit		Type T130 Unit	
<b>Lane #:</b>	1		2	
<b>Direction of Travel:</b>	Up-station		Down-station	
<b>Truck Location:</b>	Entering Bridge		Exiting Bridge	
<b>Position in Lane:</b>	South Edge		North Edge	
<b>Analysis Level:</b>	Inventory		Inventory	
<b>LANE ALIGNMENT:</b>			<b>SECTION GEOMETRY:</b>	
<b># of Lanes:</b>	2	<b>Girders</b>	<b>Height (in.):</b>	60
<b>Lane Width (ft.):</b>	11		<b>Width (in.):</b>	18
<b>Cantilever Width (ft.):</b>	0.083333	<b>Exterior Diaphragms</b>	<b>Height (in.):</b>	24
<b>Ext. Shld. Width (ft.):</b>	3		<b>Width (in.):</b>	18
<b>Ext. Barrier Width (in.):</b>	11	<b>Interior Diaphragms</b>	<b>Height (in.):</b>	12
<b>Median Shld. Width (ft.):</b>	0		<b>Width (in.):</b>	8
<b>Median Barrier Width (in.):</b>	0	<b>Slab Thickness (in.):</b>		6
<b>BRIDGE MESH:</b>				
<b># of Girders:</b>	3	<b># of Interior Diaphragms:</b>		1
<b>Length of Girders (ft.):</b>	60	<b># of Virtual Diaphragms</b>		4
<b>Tot. # of Diaphragms:</b>	7	<b>Diaphragm Length (ft.):</b>		36
<b>MATERIAL PROPERTIES:</b>			<b>Concrete Strength (psi)</b>	4000

**Table 5.3: Support Reaction Comparison #1: Results**

<b>Reactions at Supporting Nodes: Program vs RISA</b>			
<b>Node:</b>	<b>Program (k)</b>	<b>RISA (k)</b>	<b>% Difference:</b>
1	87.595	87.721	-0.1434%
2	122.985	122.735	0.2039%
3	64.621	64.746	-0.1923%
19	73.373	73.457	-0.1149%
20	101.957	101.786	0.1676%
21	55.469	55.555	-0.1550%

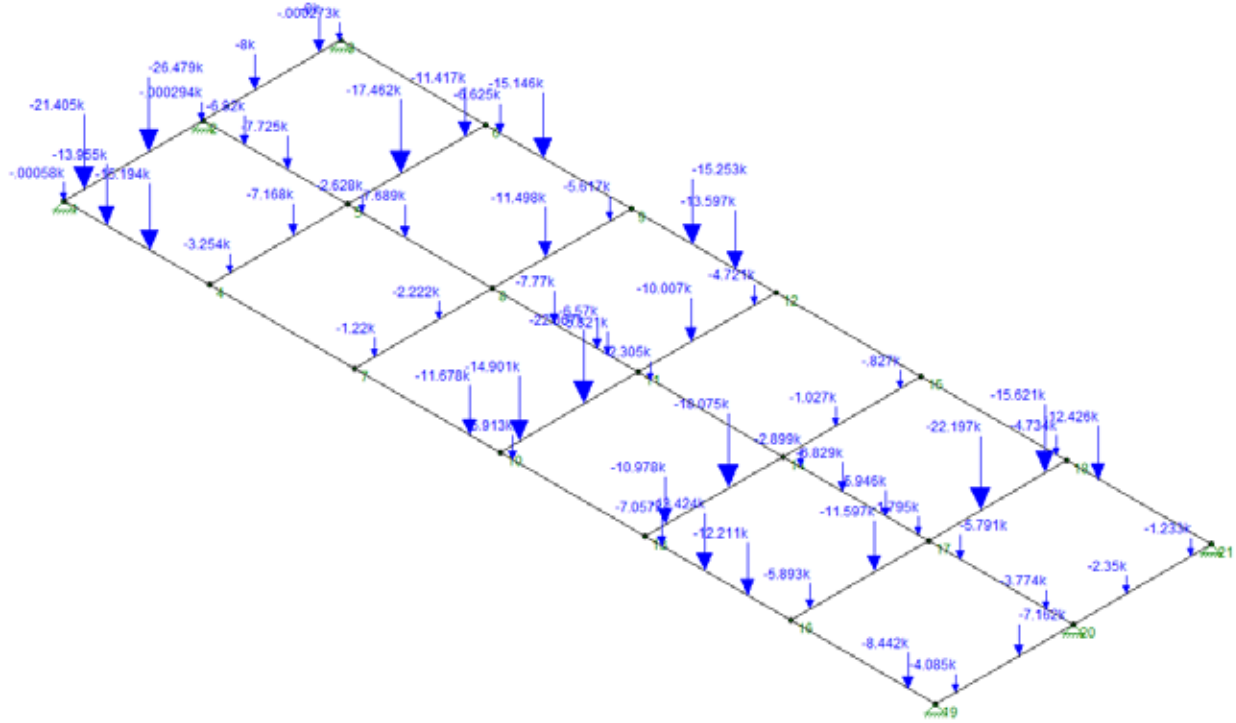


**Figure 5.1: Support Reaction Comparison #1: RISA 3D Model**

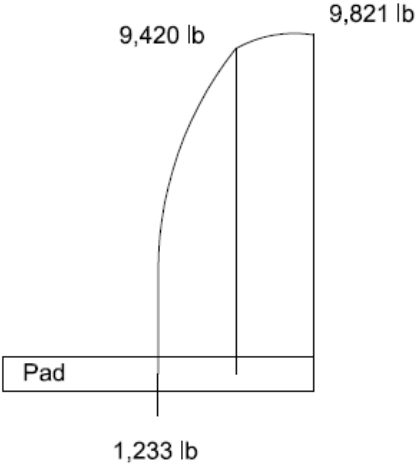
## 5.2 Capacity

### 5.2.1 ABAQUS Setup Confirmation

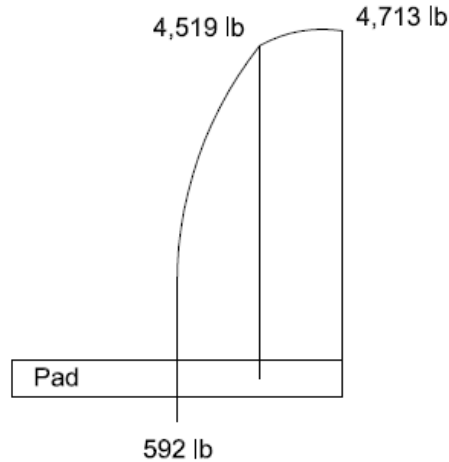
The ABAQUS models described in Section 4.3.9.1 were analyzed to obtain normal and shear forces at the girder-to-bearing pad interface. The  $12 - 0.4 - 10 - 12$  model was selected for initial testing to ensure that the ABAQUS setup yielded accurate results. In this model, the first number refers to the girder width (inches)  $b_w$ , the second number refers to the web width-to-girder height ratio  $b_w/h$ , the third number refers to the height (thickness) of the slab (inches)  $h_s$ , and the fourth number refers to the  $L/h$  ratio.

Figure 5.2 and Figure 5.3 display the normal and shear force distribution, respectively, in the girder at the girder-to-bearing pad interface for *Model 12 - 0.4 - 10 - 12*. The left edge of the pads represent the outside face of the pad and girder, while the right edge of the pads represent the inside face of the pad, which is oriented toward the center of the girder. In Figure 5.2, the numbers and lines above the pad midpoint surface represent compressive forces at the interface, and the numbers and lines below the midpoint surface represent tensile forces. In Figure 5.3, the

numbers and lines above the pad midpoint surface represent shear forces in the girder acting toward the center of the girder, and the number and lines below the midpoint surface represent shear forces in the girder acting toward the girder ends. These results show that the bottom of the girder lifts off the pad at the ends of the girder, causing the girder and bearing pad to lose contact so no forces are transferred in this area, leaving a majority of force transfer to occur at the girder-to-bearing pad interface closest to the midpoint of the girder. The uniform load on this girder was 1.92308 psi or 36 kips total. If the load is split evenly between the bearing pads on either end of the girder, then the total normal force at one bearing pad should equal 18 kips. Figure 5.2 shows that the ABAQUS model predicted a total normal force of 18.0008 kips on one pad, which was within 0.039% of the theoretical value.



**Figure 5.2: Normal Force Distribution in the Girder at the Girder-to-Bearing Pad Interface for Model 12-0.4-10-12**



**Figure 5.3: Shear Force Distribution in the Girder at the Girder-to-Bearing Pad Interface for Model 12-0.4-10-12**

The deflection at the midspan of *Model 12 – 0.4 – 10 – 12* at the bottom face of the web was 0.105162 inches. Because the girder supports in ABAQUS were modeled to act as a partially fixed support, the midspan deflection was expected to range between the values obtained from Equation 5.1 and Equation 5.2, which describe the theoretical maximum deflection for a beam with fully fixed supports and fully pinned supports, respectively.  $\Delta_F$  equaled 0.023156 inches, and  $\Delta_P$  equaled 0.115779 inches, so the measured deflection lies between these extreme values. Based on these deflection results and the normal force at the supports, the ABAQUS setup was accurate and the models were expected to generate accurate data.

$$\Delta_F = \frac{wL^4}{384(57000\sqrt{f'_c})(I)} = \mathbf{0.028429 \text{ inches}} \quad \text{Equation 5.1}$$

$$\Delta_P = \frac{5wL^4}{384(57000\sqrt{f'_c})(I)} = \mathbf{0.142147 \text{ inches}} \quad \text{Equation 5.2}$$

Where:

$\Delta_F$  = displacement at midspan for fixed girder supports (inches), 0.0232 inches

$\Delta_P$  = displacement at midspan for pinned girder supports (inches), 0.116 inches

$w$  = uniform linear load on girder (psi), 100 lb/inches

$L$  = length of girder (clear span between bearing pads) (inches), 342 inches

$I$  = moment of inertia of girder (inches<sup>4</sup>), 49280.7 inches<sup>4</sup>

$f'_c$  = concrete strength (psi), 3000 psi



### 5.2.2 Girder Length versus S/N ratio

The girder length-to-height ratio ( $L/h$ ) was recognized as the most crucial parameter varied in the ABAQUS models, so its effect on the shear-to-normal force ratio ( $S/N$ ) at the girder-to-bearing pad interface was investigated first. Two parameter combinations from Table 4.4 were selected: *Model 12 - 0.4 - 6 - L* and *Model 18 - 0.4 - 6 - L*. ABAQUS models for these two parameter combinations were created for various  $L/h$  ratios ranging from 7 to 17, and the resulting  $S/N$  (%) ratios are shown in Table 5.4. As shown, the  $S/N$  ratio increased for increasing  $L/h$  ratios until the  $S/N$  ratio reached 0.57 (57%), at which point the  $S/N$  ratio remained constant. The coefficient of friction was 0.57 at the girder-to-bearing pad interface, which is the limiting value before movement of the girder on the bearing pad. Correlation between the  $L/h$  and  $S/N$  ratios was also investigated: The values in Table 5.4 were plotted in Figure 5.4 and Figure 5.5 for *Model 12 - 0.4 - 6 - L* and *Model 18 - 0.4 - 6 - L*, respectively. The  $L/h$  ratios corresponding to an  $S/N$  ratio of 0.57 were excluded. A line of best fit was created for each graph, and the coefficient of determination  $R^2$  was calculated for the lines. The  $R^2$  values for *Model 12 - 0.4 - 6 - L* and *Model 18 - 0.4 - 6 - L* were 0.9789 and 0.9752, respectively, as shown in Figure 5.4 and Figure 5.5, indicating that the  $L/h$ -to- $S/N$  relationship can be accurately approximated as a linear function. Therefore, throughout the remainder of the parametric analysis, only  $L/h$  values of 7 and 12 were modeled. The assumption was made that the  $S/N$  relationship between these two values is linear until an  $S/N$  ratio of 0.57 is reached, at which point the  $S/N$  ratio is constant for every increasing  $L/h$  ratio.

**Table 5.4: S/N Ratios at Bearing Pad for L/h Ratios for ABAQUS Models 12-0.4-6-L and 18-0.4-6-L**

L/h ratio	S/N ratio (%)	
	12 - 0.4 - 6 - L	18 - 0.4 - 6 - L
7	14.9	11.4
8	19.5	16.3
9	27	20.4
10	30.1	34
11	36.2	40.4
12	46.9	47.4
13	54.4	57
14	57	57
17	57	57

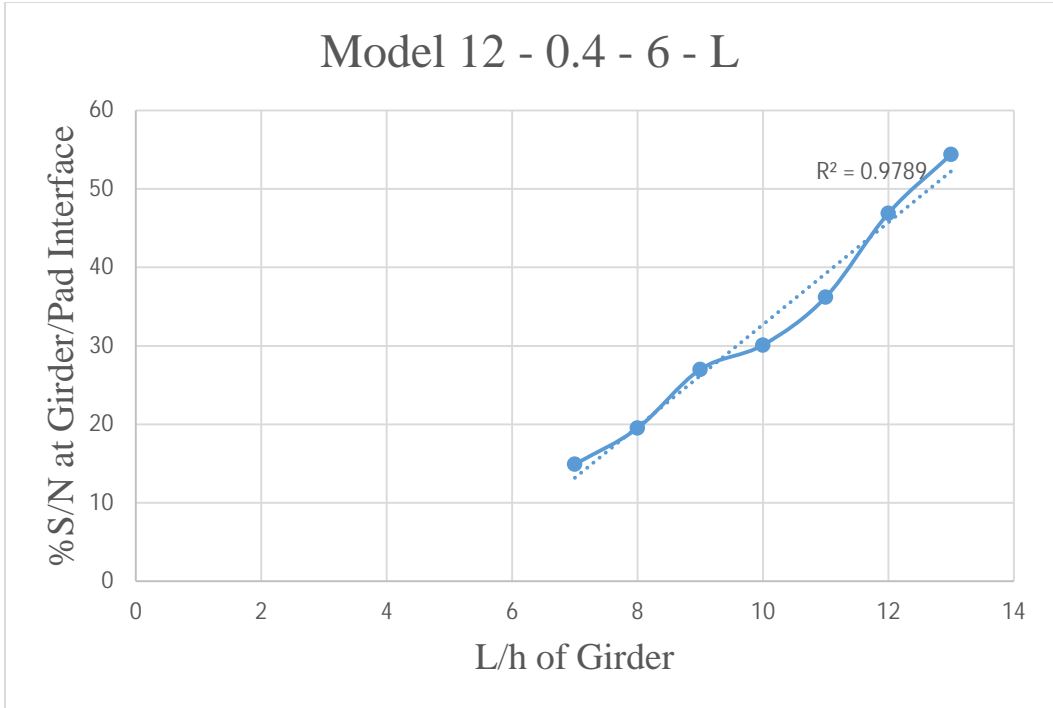


Figure 5.4: *L/h* Ratio versus *S/N* Ratio for Model 12-0.4-6-L

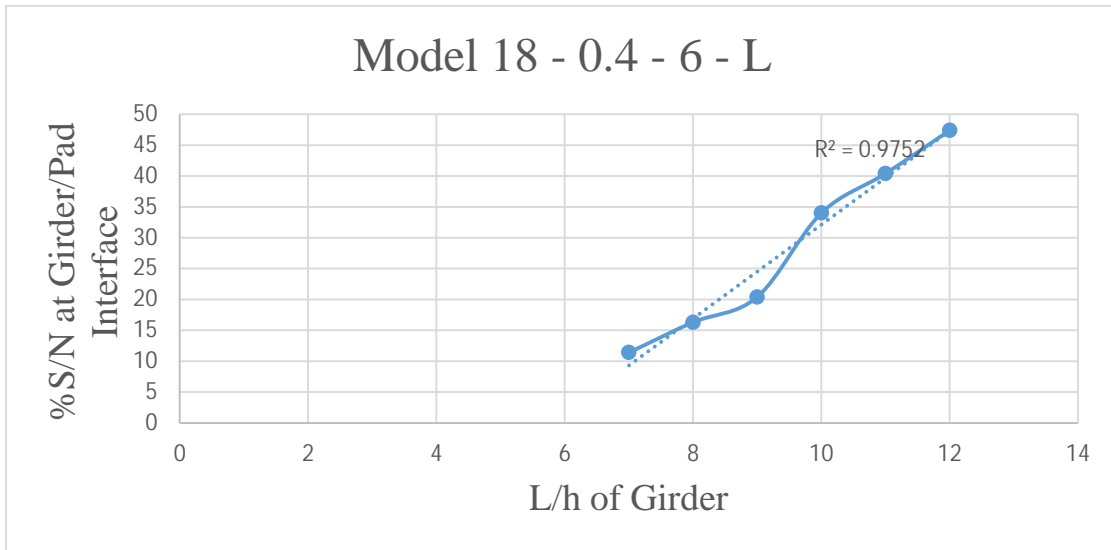


Figure 5.5: *L/h* Ratio versus *S/N* Ratio for Model 18-0.4-6-L

### 5.2.3 *S/N* Relationships

Every combination of parameters in Table 4.4, except  $L/h = 17$ , was modeled in ABAQUS, and the shear and normal forces in the girder at the girder-to-bearing pad interface were recorded at one of the supports. The forces for each model are shown in Appendix D.

Tables 5.6 through 5.11 display the resulting  $S/N$  ratio for every combination. These tables are color-coded and labeled similar to Table 5.5 based on total load applied to the model. As mentioned, the amount of load applied to a girder is dependent upon the length of the girder.

**Table 5.5: Load on Corresponding ABAQUS Models as Shown in Tables 5.6 through 5.11**

Load on Beam (kips)
<sup>1</sup> 16
<sup>2</sup> 32
<sup>3</sup> 36
<sup>4</sup> 52
<sup>5</sup> 68

**Table 5.6:  $S/N$  Ratio Tables for ABAQUS Models with  $b_w = 12$  inches and  $L/h = 7$**

	$h_s$	6	8	10
$b_w/h$				
0.4		14.9% <sup>2*</sup>	15.1% <sup>2</sup>	15.1% <sup>2</sup>
0.5		14.5% <sup>2</sup>	14.6% <sup>2</sup>	14.7% <sup>2</sup>
0.6		7.4% <sup>1</sup>	7.5% <sup>1</sup>	7.5% <sup>1</sup>

**Table 5.7:  $S/N$  Ratio Tables for ABAQUS Models with  $b_w = 12$  inches and  $L/h = 12$**

	$h_s$	6	8	10
$b_w/h$				
0.4		46.9% <sup>3</sup>	47.4% <sup>3*</sup>	48.0% <sup>3</sup>
0.5		42.8% <sup>2</sup>	43.5% <sup>2</sup>	44.0% <sup>2</sup>
0.6		42.7% <sup>2</sup>	43.6% <sup>2</sup>	43.9% <sup>2</sup>

**Table 5.8:  $S/N$  Ratio Tables for ABAQUS Models with  $b_w = 15$  inches and  $L/h = 7$**

	$h_s$	6	8	10
$b_w/h$				
0.4		12.9% <sup>2</sup>	12.9% <sup>2</sup>	13.0% <sup>2</sup>
0.5		12.6% <sup>2</sup>	12.7% <sup>2</sup>	12.8% <sup>2</sup>
0.6		12.3% <sup>2</sup>	12.4% <sup>2</sup>	12.5% <sup>2</sup>

**Table 5.9: S/N Ratio Tables for ABAQUS Models with  $b_w = 15$  inches and  $L/h = 12$**

$h_s$	6	8	10
$b_w/h$			
0.4	53.4% <sup>4</sup>	53.6% <sup>4</sup>	54.2% <sup>4*</sup>
0.5	40.3% <sup>3*</sup>	40.7% <sup>3</sup>	41.2% <sup>3</sup>
0.6	36.7% <sup>2</sup>	37.2% <sup>2</sup>	37.7% <sup>2</sup>

**Table 5.10: S/N Ratio Tables for ABAQUS Models with  $b_w = 18$  inches and  $L/h = 7$**

$h_s$	6	8	10
$b_w/h$			
0.4	11.4% <sup>2</sup>	11.3% <sup>2</sup>	11.3% <sup>2</sup>
0.5	11.2% <sup>2</sup>	11.2% <sup>2*</sup>	11.2% <sup>2</sup>
0.6	11.0% <sup>2</sup>	11.0% <sup>2</sup>	11.1% <sup>2</sup>

**Table 5.11: S/N Ratio Tables for ABAQUS Models with  $b_w = 18$  inches and  $L/h = 12$**

$h_s$	6	8	10
$b_w/h$			
0.4	47.4% <sup>4</sup>	47.2% <sup>4</sup>	47.4% <sup>4</sup>
0.5	47.6% <sup>4</sup>	47.7% <sup>4</sup>	48.2% <sup>4</sup>
0.6	35.4% <sup>3</sup>	35.8% <sup>3</sup>	36.2% <sup>3*</sup>

#### 5.2.4 Estimation of Crack Propagation Angle

Principal stresses  $\sigma_{max}$  and  $\sigma_{min}$ , maximum shearing stress  $\tau_{xy max}$ , and the angle of the maximum shear plane  $\theta_s$  were found for seven of the ABAQUS models (marked with an asterisk [\*] in Tables 5.6 through 5.11) using the transformation of stresses method discussed in Section 2.3. These values are displayed in Table 5.12. The maximum shear plane angle is, theoretically, the plane on which the crack should propagate. Angles shown in Table 5.12 were measured clockwise from the bottom of the girder, as shown in Figure 2.9, so the magnitude of these angles is the predicted crack propagation angle. All of these models predicted relatively steep angles, which coincided with the observed steep propagation angles for the reverse diagonal cracking shown in inspection report photographs.

**Table 5.12: Principal Stresses, Maximum Shear Stress, and Angle of Maximum Shear Plan for Seven ABAQUS Models**

	Model						
	12-0.4-6-7	12-0.6-6-7	12-0.4-8-12	15-0.4-10-12	15-0.5-6-12	18-0.5-8-7	18-0.6-10-12
$\sigma_{\max}$ (psi)	3.24	0.41	31.53	45.68	18.96	1.22	13.04
$\sigma_{\min}$ (psi)	-151.39	-74.48	-198.19	-238.28	-152.29	-99.98	-124.15
$\theta_{s, \max}$ (°)	-53.32	-49.22	-66.74	-68.65	-64.43	-51.29	-62.96
$\tau_{xy, \max}$ (psi)	77.31	37.44	114.86	141.98	85.62	50.60	68.59

### *5.2.5 Predicted Crack Propagation Angle versus Actual Propagation Angle*

In order to test how accurately Method #6 predicts the crack angle, seven girder supports were chosen from Bridge No. 54-104-317.27-(0005). Their location and geometry properties are displayed in Table 5.13. Interpolation was performed within Tables 5.6 through 5.11 for each girder to determine an estimated interface  $S/N$  ratio. Each girder exceeded the limits in the tables, so an  $S/N$  ratio of 0.57 was used for each girder. This coefficient, along with a reaction force of 26 kips at each support, was used to find the friction force at each support. This friction force was 14.82 kips for each girder. These forces were converted into stresses and transformed to find the predicted crack propagation angle, which was  $69.4^\circ$  for each girder. Inspection report photos (KDOT, 2011) were utilized to determine an approximate reverse diagonal crack propagation angle. These angles, as shown in Table 5.14, were close to the predicted angle of  $69.4^\circ$ . Thus, Method #6 was determined to accurately estimate the crack propagating angle for use in Equation 4.30.

**Table 5.13: Location and Geometry of Seven Girder Supports for Bridge No. 54-104-317.27-(0005)**

Support #	1	2	3	4	5	6	7
Span #	1	1	2	2	2	4	5
Girder #	F	F	E	E	F	D	G
Abutment/Pier #	P1	P1	P2	P2	P2	P4	P4
$b_w$ (inches)	15	15	15	15	15	15	15
$h$ (inches)	33	33	36	36	36	36	33
$h_s$ (inches)	6.5	6.5	6.5	6.5	6.5	6.5	6.5
$L$ (inches)	510	510	570	570	570	570	510
$b_w/h$	0.45	0.45	0.42	0.42	0.42	0.42	0.45
$L/h$	15.45	15.45	15.83	15.83	15.83	15.83	15.45

**Table 5.14: Observed Propagation Angles of Reverse Diagonal Crack for Seven Supports for Bridge No. 54-104-317-27-(0005)**

Support #	1	2	3	4	5	6	7
Observed Crack Angle	73.3	53.4	65.6	66.8	75.1	76.8	68.6

### 5.3 Analysis of Bridge No. 54-104-15.45

KDOT's Bridge No. 54-104-15.45, which displays reverse diagonal shear cracking, was analyzed by BRIDGE to demonstrate the program's output and results. This bridge consists of five spans. Spans #1 and #5 are identical, and Spans #2 and #4 are identical. Results for Spans #1 and #5 are discussed herein; results for the other three spans are similar and are included in Appendix E. Two of each truck type were placed on the bridge, one in each lane on the same side of the bridge span. Table 5.15 and Table 5.16 display the operating and inventory RFs and truck ratings, respectively, for each standard truck option available within the program. The program used Equation 4.30 and the described procedure to calculate the RFs in Table 5.15. Equation 2.1 was used to determine the truck ratings shown in Table 5.16. Each truck was analyzed twice: once assuming the entire girder width provided shear resistance and once assuming that the girder end had deteriorated to the point where only 50% of the girder width resists shear. As shown in Table 5.15 and Table 5.16, girders contributing 100% of their girder width had larger shear capacities and expected larger RFs. With few exceptions, the operating RF was larger than

1 and the inventory RF was less than 1, indicating that an engineer's judgment is required to determine whether or not to load rate this bridge.

**Table 5.15: Rating Factors for Spans #1 and #5 for 50% and 100% Girder Width**

Rating	Operating		Inventory		
	$b_w$ used	100%	50%	100%	50%
H Unit		1.22	1.07	0.73	0.64
T 3		1.17	1.04	0.7	0.62
HS		1.11	1.01	0.67	0.6
3S2		1.19	1.06	0.72	0.63
Type 3-3		1.25	1.09	0.75	0.65
T-130		1.17	1.05	0.7	0.63
T-170		1.14	1.04	0.68	0.62
HET		1.03	0.97	0.62	0.58
SU4		1.14	1.03	0.68	0.61
SU5		1.12	1.01	0.67	0.61
SU6		1.11	1.01	0.66	0.6
SU7		1.1	1	0.66	0.6
NRL		1.09	1	0.65	0.6

**Table 5.16: Truck Ratings for Spans #1 and #5 for 50% and 100% Girder Width**

Rating	Operating		Inventory		
	$b_w$ used	100%	50%	100%	50%
H Unit		15.25	13.375	9.125	8
Type 3		29.25	26	17.5	15.5
HS		24.975	22.725	15.075	13.5
3S2		42.84	38.16	25.92	22.68
Type 3-3		50	43.6	30	26
T-130		76.05	68.25	45.5	40.95
T-170		96.9	88.4	57.8	52.7
HET		113.3	106.7	68.2	63.8
SU4		30.78	27.81	18.36	16.47
SU5		34.72	31.31	20.77	18.91
SU6		38.573	35.0975	22.935	20.85
SU7		42.625	38.75	25.575	23.25
NRL		43.6	40	26	24

## Chapter 6: Conclusions

Dozens of KDOT bridges built in the early-to-mid 1900s exhibit a phenomenon known as reverse diagonal shear cracking, shown in Figure 1.1. Because this cracking is feared to result in a loss of bearing support at the girder ends, investigation must determine the cause of reverse diagonal cracking and its effects on girder capacity.

This study determined that this cracking is caused by unintended frictional forces acting at the girder-to-bearing pad interface. Girders are supported on steel-bearing pads and rockers instead of rubber-bearing pads, as is common in new construction. Steel-bearing pads and rockers rust and corrode due to decades of exposure to water and deicing salts, and this corrosion prevents the rocker from rotating, turning the once-pinned connection into a partially fixed connection. When girder rotation is prevented, a buildup of shear stress at the girder-to-bearing pad interface occurs due to the tendency of the bottom of the girder to expand towards the ends of the girder when subjected to tension during the loading process. This friction force, coupled with the girder reaction, causes reverse diagonal cracking.

Live- and dead-load reactions at the support, along with the friction force, act on the reverse diagonal crack, as shown in Figure 4.21. These forces cause the crack-driving and crack-clamping forces. Equation 4.30, based on Equation 2.2, was developed from these forces to calculate the RF of the bridge at the girder supports. In addition, SMCFT was used to find girder capacity without clamping forces. This method was chosen because it is widely accepted as a reliable method for finding the shear capacity of cracked concrete beams.

The BRIDGE program, used to load rate Bridge No. 54-104-15.45, yielded reasonable RFs for various trucks and reduced girder widths. The operating RFs were consistently above 1 and the inventory RFs were below 1, indicating that the decision to load post this bridge is based on the engineer's judgment.



## References

- Abouelleil, A. (2015). *Interaction domain in non-prestressed circular concrete bridge piers using simplified modified compression field theory* (Master's thesis). Kansas State University, Manhattan, KS.
- American Association of State Highway and Transportation Officials (AASHTO). (2002). *Standard specifications for highway bridges* (17th ed.). Washington, DC: Author.
- American Association of State Highway and Transportation Officials (AASHTO). (2011). Section 6: Load rating. In *Manual for bridge evaluation* (2nd ed., pp. 6-i-6-i). Washington, DC: Author.
- American Association of State Highway and Transportation Officials (AASHTO). (2014). *AASHTO LRFD bridge design specifications* (7th ed.). Washington, DC: Author.
- Beer, F. P., Johnston, E. R., Jr., DeWolf, J. T., & Mazurek, D. F. (2012). Chapter 7: Transformations of stress and strain. In *Mechanics of materials* (6th ed., pp. 438–445). New York, NY: McGraw-Hill.
- Bentz, E. C., Vecchio, F. J., & Collins, M. P. (2006). Simplified modified compression field theory for calculating shear strength of reinforced concrete elements. *ACI Structural Journal*, 103(4), 614–624.
- Bernica, A. (2016). *Rational load rating of deck-girder bridges with girder end shear cracks in reverse orientation* (Master's thesis). Kansas State University, Manhattan, KS.
- Dassault Systèmes. (2013). *Abaqus*. Providence, RI: Dassault Systèmes Simulia Corp.
- Kansas Department of Transportation (KDOT). (2011). *Special bridge inspection report: Special girder end inspection for bridge no. 54-104-317.27-(0005)* (Inspection). Topeka, KS: Author.
- Kansas Department of Transportation (KDOT). (2016). Bridge section - Chapter 15: Bridge load rating. In *KDOT design manual* (pp. 15-1–15-41). Topeka, KS: Author.
- Rabbat, B. G., & Russell, H. G. (1985). Friction coefficient of steel on concrete or grout. *Journal of Structural Engineering*, 111(3), 505–515.

RISA Technologies, Inc. (2012). *RISA-3D* (Version 10.0.1) [Software]. Foothill Ranch, CA: Author.

Vecchio, F. J., & Collins, M. P. (1982). *The response of reinforced concrete to in-plane shear and normal stresses*. Toronto, Canada: University of Toronto, Department of Civil Engineering.

## Appendix A: Truck Types

**Table A.1: Truck Axle Loads and Spacings**

Truck Type	Axle #	Axle Load (kips)	Axle Spacing (ft)	
			Minimum	Maximum
H 20	1	8	-	-
	2	32	14	14
Type 3	1	16	-	-
	2	17	15	15
	3	17	4	4
HS 20	1	8	-	-
	2	32	14	14
	3	32	14	30
Type 3S2	1	10	-	-
	2	15.5	11	11
	3	15.5	4	4
	4	15.5	22	22
	5	15.5	4	4
Type 3-3	1	12	-	-
	2	12	15	15
	3	12	4	4
	4	16	15	15
	5	14	16	16
	6	14	4	4
Type T130	1	10	-	-
	2	20	15	15
	3	20	4	4
	4	20	14	14
	5	20	4	4
	6	20	30	30
	7	20	4	4
Type T170	1	16	-	-
	2	18	15	15
	3	18	4	4
	4	18	4	4
	5	20	14	14
	6	20	4	4
	7	20	30	30
	8	20	4	4
	9	20	4	4

Truck Type	Axle #	Axle Load (kips)	Axle Spacing (ft)	
			Minimum	Maximum
HET	1	21.48	-	-
	2	21.35	12.92	12.92
	3	21.16	5	5
	4	19.23	5	5
	5	25.39	15.1	15.1
	6	27.84	5.94	5.94
	7	26.29	5.94	5.94
	8	27.42	5.94	5.94
	9	29.75	5.94	5.94
SU4	1	12	-	-
	2	8	10	10
	3	17	4	4
	4	17	4	4
SU5	1	12	-	-
	2	8	10	10
	3	8	4	4
	4	17	4	4
	5	17	4	4
SU6	1	11.5	-	-
	2	8	10	10
	3	8	4	4
	4	17	4	4
	5	17	4	4
	6	8	4	4
SU7	1	11.5	-	-
	2	8	10	10
	3	8	4	4
	4	17	4	4
	5	17	4	4
	6	8	4	4
	7	8	4	4
NRL	1	6	-	-
	2	8	6	14
	3	8	4	4
	4	17	4	4
	5	17	4	4
	6	8	4	4
	7	8	4	4
	8	8	4	4

## Appendix B: Stiffness Matrix

$$[K] = \begin{bmatrix}
 \frac{12EI}{L^3} & -\frac{6EI}{L^2}S & \frac{6EI}{L^2}C & -\frac{12EI}{L^3} & -\frac{6EI}{L^2}S & \frac{6EI}{L^2}C \\
 -\frac{6EI}{L^2}S & \frac{GJ}{L}C + \frac{4EI}{L}S^2 & (\frac{GJ}{L} - \frac{4EI}{L})SC & \frac{6EI}{L^2}S & -\frac{GJ}{L}C + \frac{2EI}{L}S^2 & -(\frac{GJ}{L} + \frac{2EI}{L})SC \\
 \frac{6EI}{L^2}C & (\frac{GJ}{L} - \frac{4EI}{L})SC & \frac{GJ}{L}S + \frac{4EI}{L}C^2 & -\frac{6EI}{L^2}C & -(\frac{GJ}{L} + \frac{2EI}{L})SC & -\frac{GJ}{L}S + \frac{2EI}{L}C^2 \\
 -\frac{12EI}{L^3} & \frac{6EI}{L^2}S & -\frac{6EI}{L^2}C & \frac{12EI}{L^3} & \frac{6EI}{L^2}S & -\frac{6EI}{L^2}C \\
 -\frac{6EI}{L^2}S & -\frac{GJ}{L}C + \frac{2EI}{L}S^2 & -(\frac{GJ}{L} + \frac{2EI}{L})SC & \frac{6EI}{L^2}S & \frac{GJ}{L}C + \frac{4EI}{L}S^2 & (\frac{GJ}{L} - \frac{4EI}{L})SC \\
 \frac{6EI}{L^2}C & -(\frac{GJ}{L} + \frac{2EI}{L})SC & -\frac{GJ}{L}S + \frac{2EI}{L}C^2 & -\frac{6EI}{L^2}C & (\frac{GJ}{L} - \frac{4EI}{L})SC & \frac{GJ}{L}S + \frac{4EI}{L}C^2
 \end{bmatrix}$$

Figure B.1: Stiffness Matrix as Function Member Properties

## Appendix C: Support Reactions: Program versus RISA

**Table C.1: Support Reaction Comparison #2: BRIDGE Input**

LOADING				
		Truck #1	Truck #2	
Truck Type		H Unit	H Unit	
Lane #		1	2	
Direction of Travel		Up-station	Down-station	
Truck Location		Exiting Bridge	Entering Bridge	
Position in Lane		Center	Center	
Analysis Level		Inventory	Inventory	
LANE ALIGNMENT		SECTION GEOMETRY		
# of Lanes	2	Girders	Height (inches)	48
Lane Width (ft)	12		Width (inches)	12
Cantilever Width (ft)	0	Exterior Diaphragms	Height (inches)	36
Ext. Shld. Width (ft)	0		Width (inches)	12
Ext. Barrier Width (inches)	12	Interior Diaphragms	Height (inches)	24
Median Shld. Width (ft)	0		Width (inches)	12
Median Barrier Width (inches)	0	Slab Thickness (inches)		8
BRIDGE MESH				
# of Girders	3	# of Interior Diaphragms		2
Length of Girders (ft)	50	# of Virtual Diaphragms		3
Tot. # of Diaphragms	7	Diaphragm Length (ft)		24
MATERIAL PROPERTIES		Concrete Strength (psi)		5000

**Table C.2: Support Reaction Comparison #2: Results**

Reactions at Supporting Nodes: Program vs RISA			
Node	Program (k)	RISA (k)	% Difference
1	4.871	4.871	-0.0044%
2	4.400	4.4	0.0092%
3	1.709	1.71	-0.0391%
19	12.143	12.261	-0.9665%
20	41.573	41.336	0.5734%
21	15.304	15.423	-0.7718%

**Table C.3: Support Reaction Comparison #3: BRIDGE Input**

<b>LOADING:</b>				
	<b>Truck #1</b>		<b>Truck #2</b>	
<b>Truck Type</b>	Heavy Equip. Trans.		H Unit	
<b>Lane #</b>	1		2	
<b>Direction of Travel</b>	Up-station		Down-station	
<b>Truck Location</b>	Exiting Bridge		Entering Bridge	
<b>Position in Lane</b>	Center		North Edge	
<b>Analysis Level</b>	Operating Posting		Operating Posting	
<b>LANE ALIGNMENT</b>		<b>SECTION GEOMETRY</b>		
<b># of Lanes</b>	2	<b>Girders</b>	<b>Height (inches)</b>	48
<b>Lane Width (ft)</b>	12		<b>Width (inches)</b>	5
<b>Cantilever Width (ft)</b>	1	<b>Exterior Diaphragms</b>	<b>Height (inches)</b>	36
<b>Ext. Shld. Width (ft)</b>	6		<b>Width (inches)</b>	12
<b>Ext. Barrier Width (inches)</b>	17	<b>Interior Diaphragms</b>	<b>Height (inches)</b>	24
<b>Median Shld. Width (ft)</b>	0		<b>Width (inches)</b>	12
<b>Median Barrier Width (in)</b>	0	<b>Slab Thickness (in.):</b>		8
<b>BRIDGE MESH</b>				
<b># of Girders</b>	3	<b># of Interior Diaphragms</b>		2
<b>Length of Girders (ft)</b>	120	<b># of Virtual Diaphragms</b>		0
<b>Tot. # of Diaphragms</b>	4	<b>Diaphragm Length (ft)</b>		36
<b>MATERIAL PROPERTIES</b>		<b>Concrete Strength (psi)</b>		4000

**Table C.4: Support Reaction Comparison #3: Results**

<b>Reactions at Supporting Nodes: Program vs RISA</b>			
<b>Node</b>	<b>Program (k)</b>	<b>RISA (k)</b>	<b>% Difference</b>
1	33.185	33.179	0.0186%
2	23.097	23.108	-0.0493%
3	10.153	10.147	0.0547%
10	67.873	67.867	0.0084%
11	86.973	86.984	-0.0124%
12	23.920	23.914	0.0240%

**Table C.5: Support Reaction Comparison #4: BRIDGE Input**

<b>LOADING</b>				
	<b>Truck #1</b>		<b>Truck #2</b>	
<b>Truck Type</b>	H Unit		H Unit	
<b>Lane #</b>	1		2	
<b>Direction of Travel</b>	Up-station		Down-station	
<b>Truck Location</b>	Entering Bridge		Entering Bridge	
<b>Position in Lane</b>	Center		Center	
<b>Analysis Level</b>	Inventory		Inventory	
<b>LANE ALIGNMENT</b>		<b>SECTION GEOMETRY</b>		
<b># of Lanes</b>	2	<b>Girders</b>	<b>Height (inches)</b>	36
<b>Lane Width (ft)</b>	12		<b>Width (inches)</b>	18
<b>Cantilever Width (ft)</b>	2	<b>Exterior Diaphragms</b>	<b>Height (inches)</b>	24
<b>Ext. Shld. Width (ft)</b>	6		<b>Width (inches)</b>	12
<b>Ext. Barrier Width (inches)</b>	12	<b>Interior Diaphragms</b>	<b>Height (inches)</b>	18
<b>Median Shld. Width (ft)</b>	3		<b>Width (inches)</b>	8
<b>Median Barrier Width (inches)</b>	12	<b>Slab Thickness (inches)</b>		10
<b>BRIDGE MESH</b>				
<b># of Girders</b>	4	<b># of Interior Diaphragms</b>		1
<b>Length of Girders (ft)</b>	25	<b># of Virtual Diaphragms</b>		4
<b>Tot. # of Diaphragms</b>	7	<b>Diaphragm Length (ft)</b>		38
<b>MATERIAL PROPERTIES</b>		<b>Concrete Strength (psi)</b>		4000

**Table C.6: Support Reaction Comparison #4: Results**

<b>Reactions at Supporting Nodes: Program vs RISA</b>			
<b>Node</b>	<b>Program (k)</b>	<b>RISA (k)</b>	<b>% Difference</b>
1	6.567	6.589	-0.3330%
2	30.591	30.533	0.1884%
3	1.926	1.977	-2.5971%
4	0.917	0.902	1.6364%
25	0.917	0.902	1.6364%
26	1.926	1.977	-2.5971%
27	30.591	30.533	0.1884%
28	6.567	6.589	-0.3330%



**Table C.7: Support Reaction Comparison #5: BRIDGE Input**

<b>LOADING:</b>				
	<b>Truck #1</b>	<b>Truck #2</b>		
<b>Truck Type</b>	Type 3S2 Unit	H Unit		
<b>Lane #</b>	1	2		
<b>Direction of Travel</b>	Up-station	Down-station		
<b>Truck Location</b>	Exiting Bridge	Entering Bridge		
<b>Position in Lane</b>	North Edge	South Edge		
<b>Analysis Level</b>	Operating Posting	Operating Posting		
<b>LANE ALIGNMENT</b>		<b>SECTION GEOMETRY</b>		
<b># of Lanes</b>	2	<b>Girders</b>	<b>Height (inches)</b>	24
<b>Lane Width (ft)</b>	12		<b>Width (inches)</b>	6
<b>Cantilever Width (ft)</b>	2	<b>Exterior Diaphragms</b>	<b>Height (inches)</b>	36
<b>Ext. Shld. Width (ft)</b>	6		<b>Width (inches)</b>	12
<b>Ext. Barrier Width (inches)</b>	12	<b>Interior Diaphragms</b>	<b>Height (inches)</b>	24
<b>Median Shld. Width (ft)</b>	3		<b>Width (inches)</b>	12
<b>Median Barrier Width (inches)</b>	12	<b>Slab Thickness (inches)</b>		12
<b>BRIDGE MESH</b>				
<b># of Girders</b>	4	<b># of Interior Diaphragms</b>	2	
<b>Length of Girders (ft)</b>	200	<b># of Virtual Diaphragms</b>	3	
<b>Tot. # of Diaphragms</b>	7	<b>Diaphragm Length (ft)</b>	40	
<b>MATERIAL PROPERTIES</b>		<b>Concrete Strength (psi)</b>	5000	

**Table C.8: Support Reaction Comparison #5: Results**

<b>Reactions at Supporting Nodes: Program vs RISA</b>			
<b>Node</b>	<b>Program (k)</b>	<b>RISA (k)</b>	<b>% Difference</b>
1	3.037	3.035	0.0628%
2	2.297	2.302	-0.2170%
3	2.444	2.439	0.2019%
4	0.590	0.592	-0.2763%
25	14.467	14.469	-0.0152%
26	37.972	37.974	-0.0047%
27	32.636	32.624	0.0373%
28	3.557	3.564	-0.2069%

**Table C.9: Support Reaction Comparison #6: BRIDGE Input**

<b>LOADING</b>				
	<b>Truck #1</b>		<b>Truck #2</b>	
<b>Truck Type</b>	Type 3S2 Unit		H Unit	
<b>Lane #</b>	1		2	
<b>Direction of Travel</b>	Up-station		Down-station	
<b>Truck Location</b>	Exiting Bridge		Entering Bridge	
<b>Position in Lane</b>	North Edge		South Edge	
<b>Analysis Level</b>	Operating Posting		Operating Posting	
<b>LANE ALIGNMENT</b>		<b>SECTION GEOMETRY</b>		
<b># of Lanes</b>	2	<b>Girders</b>	<b>Height (inches)</b>	36
<b>Lane Width (ft)</b>	12		<b>Width (inches)</b>	18
<b>Cantilever Width (ft)</b>	0	<b>Exterior Diaphragms</b>	<b>Height (inches)</b>	36
<b>Ext. Shld. Width (ft)</b>	3		<b>Width (inches)</b>	12
<b>Ext. Barrier Width (inches)</b>	12	<b>Interior Diaphragms</b>	<b>Height (inches)</b>	24
<b>Median Shld. Width (ft)</b>	0		<b>Width (inches)</b>	12
<b>Median Barrier Width (inches)</b>	0	<b>Slab Thickness (inches)</b>		8
<b>BRIDGE MESH</b>				
<b># of Girders</b>	4	<b># of Interior Diaphragms</b>		2
<b>Length of Girders (ft)</b>	75	<b># of Virtual Diaphragms</b>		0
<b>Tot. # of Diaphragms</b>	4	<b>Diaphragm Length (ft)</b>		53
<b>MATERIAL PROPERTIES</b>		<b>Concrete Strength (psi)</b>		4000

**Table C.10: Support Reaction Comparison #6: Results**

<b>Reactions at Supporting Nodes: Program vs RISA</b>			
<b>Node</b>	<b>Program (k)</b>	<b>RISA (k)</b>	<b>% Difference</b>
1	18.009	18.034	-0.1412%
4	7.991	7.988	0.0368%
5	34.088	34.027	0.1783%
8	6.507	6.52	-0.1956%
9	17.701	17.745	-0.2501%
12	6.092	6.075	0.2825%
13	5.887	5.878	0.1581%
16	0.726	0.733	-1.0164%

**Table C.11: Support Reaction Comparison #7: BRIDGE Input**

<b>LOADING</b>				
	<b>Truck #1</b>		<b>Truck #2</b>	
<b>Truck Type</b>	Type 3-3 Unit			
<b>Lane #</b>	1			
<b>Direction of Travel</b>	Up-station			
<b>Truck Location</b>	Exiting Bridge			
<b>Position in Lane</b>	Center			
<b>Analysis Level</b>	Operating Posting			
<b>LANE ALIGNMENT</b>		<b>SECTION GEOMETRY</b>		
<b># of Lanes</b>	2	<b>Girders</b>	<b>Height (inches)</b>	24
<b>Lane Width (ft)</b>	11		<b>Width (inches)</b>	12
<b>Cantilever Width (ft)</b>	3	<b>Exterior Diaphragms</b>	<b>Height (inches)</b>	36
<b>Ext. Shld. Width (ft)</b>	6		<b>Width (inches)</b>	12
<b>Ext. Barrier Width (inches)</b>	12	<b>Interior Diaphragms</b>	<b>Height (inches)</b>	24
<b>Median Shld. Width (ft)</b>	0		<b>Width (inches)</b>	6
<b>Median Barrier Width (inches)</b>	0	<b>Slab Thickness (inches)</b>		12
<b>BRIDGE MESH</b>				
<b># of Girders</b>	5	<b># of Interior Diaphragms</b>		1
<b>Length of Girders (ft)</b>	60	<b># of Virtual Diaphragms</b>		4
<b>Tot. # of Diaphragms</b>	7	<b>Diaphragm Length (ft)</b>		28
<b>MATERIAL PROPERTIES</b>		<b>Concrete Strength (psi)</b>		5000

**Table C.12: Support Reaction Comparison #7: Results**

<b>Reactions at Supporting Nodes: Program vs RISA</b>			
<b>Node</b>	<b>Program (k)</b>	<b>RISA (k)</b>	<b>% Difference</b>
1	9.695	9.755	-0.6154%
2	14.055	13.943	0.8045%
3	10.591	10.687	-0.9013%
4	6.794	6.698	1.4334%
5	-1.659	-1.608	3.1908%
31	8.890	8.955	-0.7237%
32	16.094	15.955	0.8738%
33	11.023	11.146	-1.1058%
34	5.879	5.789	1.5622%
35	-1.362	-1.322	3.0483%

**Table C.13: Support Reaction Comparison #8: BRIDGE Input**

<b>LOADING</b>					
	<b>Truck #1</b>		<b>Truck #2</b>		
<b>Truck Type</b>	HS Unit		Type 3 Unit		
<b>Lane #</b>	1		2		
<b>Direction of Travel</b>	Up-station		Down-station		
<b>Truck Location</b>	Exiting Bridge		Entering Bridge		
<b>Position in Lane</b>	Center		Center		
<b>Analysis Level</b>	Inventory		Inventory		
<b>LANE ALIGNMENT</b>			<b>SECTION GEOMETRY</b>		
<b># of Lanes</b>	2	<b>Girders</b>	<b>Height (inches)</b>	24	
<b>Lane Width (ft)</b>	12		<b>Width (inches)</b>	8	
<b>Cantilever Width (ft)</b>	1	<b>Exterior Diaphragms</b>	<b>Height (inches)</b>	36	
<b>Ext. Shld. Width (ft)</b>	3		<b>Width (inches)</b>	12	
<b>Ext. Barrier Width (inches)</b>	8	<b>Interior Diaphragms</b>	<b>Height (inches)</b>	24	
<b>Median Shld. Width (ft)</b>	0		<b>Width (inches)</b>	6	
<b>Median Barrier Width (inches)</b>	0	<b>Slab Thickness (inches)</b>		12	
<b>BRIDGE MESH</b>					
<b># of Girders</b>	5	<b># of Interior Diaphragms</b>		2	
<b>Length of Girders (ft)</b>	40	<b># of Virtual Diaphragms</b>		3	
<b>Tot. # of Diaphragms</b>	7	<b>Diaphragm Length (ft)</b>		28	
<b>MATERIAL PROPERTIES</b>			<b>Concrete Strength (psi)</b>		4000

**Table C.14: Support Reaction Comparison #8: Results**

<b>Reactions at Supporting Nodes: Program vs RISA</b>			
<b>Node</b>	<b>Program (k)</b>	<b>RISA (k)</b>	<b>% Difference</b>
1	8.256	8.325	-0.8242%
2	14.412	14.294	0.8288%
3	12.503	12.555	-0.4154%
4	10.304	10.274	0.2945%
5	3.207	3.235	-0.8564%
31	8.288	8.309	-0.2574%
32	18.231	18.155	0.4169%
33	30.655	30.966	-1.0047%
34	45.879	45.403	1.0494%
35	8.264	8.484	-2.5920%

**Table C.15: Support Reaction Comparison #9: BRIDGE Input**

<b>LOADING</b>				
	<b>Truck #1</b>		<b>Truck #2</b>	
<b>Truck Type</b>	Type 3-3 Unit		Type 3 Unit	
<b>Lane #</b>	1		2	
<b>Direction of Travel</b>	Up-station		Down-station	
<b>Truck Location</b>	Exiting Bridge		Entering Bridge	
<b>Position in Lane</b>	North Edge		South Edge	
<b>Analysis Level</b>	Inventory		Inventory	
<b>LANE ALIGNMENT</b>		<b>SECTION GEOMETRY</b>		
<b># of Lanes</b>	2	<b>Girders</b>	<b>Height (inches)</b>	30
<b>Lane Width (ft)</b>	10		<b>Width (inches)</b>	16
<b>Cantilever Width (ft)</b>	3	<b>Exterior Diaphragms</b>	<b>Height (inches)</b>	36
<b>Ext. Shld. Width (ft)</b>	3		<b>Width (inches)</b>	12
<b>Ext. Barrier Width (inches)</b>	8	<b>Interior Diaphragms</b>	<b>Height (inches)</b>	36
<b>Median Shld. Width (ft)</b>	2		<b>Width (inches)</b>	12
<b>Median Barrier Width (inches)</b>	12	<b>Slab Thickness (inches)</b>		12
<b>BRIDGE MESH</b>				
<b># of Girders</b>	5	<b># of Interior Diaphragms</b>		2
<b>Length of Girders (ft)</b>	75	<b># of Virtual Diaphragms</b>		0
<b>Tot. # of Diaphragms</b>	4	<b>Diaphragm Length (ft)</b>		23.6667
<b>MATERIAL PROPERTIES</b>		<b>Concrete Strength (psi)</b>		4000

**Table C.16: Support Reaction Comparison #9: Results**

<b>Reactions at Supporting Nodes: Program vs RISA</b>			
<b>Node</b>	<b>Program (k)</b>	<b>RISA (k)</b>	<b>% Difference</b>
1	21.891	21.827	0.2919%
4	26.221	26.172	0.1866%
5	12.280	12.407	-1.0226%
8	28.609	28.701	-0.3199%
9	12.698	12.74	-0.3309%
12	41.270	41.333	-0.1522%
13	13.681	13.472	1.5486%
16	47.749	47.546	0.4278%
17	1.451	1.555	-6.6917%
20	16.150	16.249	-0.6078%

**Table C.17: Support Reaction Comparison #10: BRIDGE Input**

<b>LOADING</b>				
		<b>Truck #1</b>	<b>Truck #2</b>	
<b>Truck Type</b>		H Unit	HS Unit	
<b>Lane #</b>		1	2	
<b>Direction of Travel</b>		Up-station	Up-station	
<b>Truck Location</b>		Entering Bridge	Entering Bridge	
<b>Position in Lane</b>		North Edge	South Edge	
<b>Analysis Level</b>		Operating Posting	Operating Posting	
		<b>Truck #3</b>	<b>Truck #4</b>	
<b>Truck Type</b>		Type 3 Unit	H Unit	
<b>Lane #</b>		3	4	
<b>Direction of Travel</b>		Left Bound	Left Bound	
<b>Truck Location</b>		Exiting Bridge	Exiting Bridge	
<b>Position in Lane</b>		South Edge	North Edge	
<b>Analysis Level</b>		Operating Posting	Operating Posting	
<b>LANE ALIGNMENT</b>		<b>SECTION GEOMETRY</b>		
<b># of Lanes</b>	4	<b>Girders</b>	<b>Height (inches)</b>	48
<b>Lane Width (ft)</b>	10		<b>Width (inches)</b>	18
<b>Cantilever Width (ft)</b>	5	<b>Exterior Diaphragms</b>	<b>Height (inches)</b>	24
<b>Ext. Shld. Width (ft)</b>	3		<b>Width (inches)</b>	12
<b>Ext. Barrier Width (inches)</b>	18	<b>Interior Diaphragms</b>	<b>Height (inches)</b>	12
<b>Median Shld. Width (ft)</b>	0		<b>Width (inches)</b>	8
<b>Median Barrier Width (inches)</b>	12	<b>Slab Thickness (inches)</b>		4
<b>BRIDGE MESH</b>				
<b># of Girders</b>	3	<b># of Interior Diaphragms</b>		1
<b>Length of Girders (ft)</b>	50	<b># of Virtual Diaphragms</b>		4
<b>Tot. # of Diaphragms</b>	7	<b>Diaphragm Length (ft)</b>		37
<b>MATERIAL PROPERTIES</b>		<b>Concrete Strength (psi)</b>		5000

**Table C.18: Support Reaction Comparison #10: Results**

<b>Reactions at Supporting Nodes: Program vs RISA</b>			
<b>Node</b>	<b>Program (k)</b>	<b>RISA (k)</b>	<b>% Difference</b>
1	24.483	24.538	-0.2243%
2	77.988	77.877	0.1421%
3	16.098	16.153	-0.3420%
19	2.309	2.315	-0.2594%
20	19.273	19.26	0.0653%
21	4.850	4.857	-0.1433%

**Table C.19: Support Reaction Comparison #11: BRIDGE Input**

<b>LOADING</b>				
		<b>Truck #1</b>	<b>Truck #2</b>	
<b>Truck Type</b>		Type T170 Unit	Heavy Equip. Trans.	
<b>Lane #</b>		1	2	
<b>Direction of Travel</b>		Up-station	Up-station	
<b>Truck Location</b>		Entering Bridge	Entering Bridge	
<b>Position in Lane</b>		Center	Center	
<b>Analysis Level</b>		Operating Posting	Operating Posting	
		<b>Truck #3</b>	<b>Truck #4</b>	
<b>Truck Type</b>		Type T130 Unit	Heavy Equip. Trans.	
<b>Lane #</b>		3	4	
<b>Direction of Travel</b>		Left Bound	Left Bound	
<b>Truck Location</b>		Exiting Bridge	Exiting Bridge	
<b>Position in Lane</b>		Center	Center	
<b>Analysis Level</b>		Operating Posting	Operating Posting	
<b>LANE ALIGNMENT</b>		<b>SECTION GEOMETRY</b>		
<b># of Lanes</b>	4	<b>Girders</b>	<b>Height (inches)</b>	36
<b>Lane Width (ft)</b>	12		<b>Width (inches)</b>	12
<b>Cantilever Width (ft)</b>	6	<b>Exterior Diaphragms</b>	<b>Height (inches)</b>	24
<b>Ext. Shld. Width (ft)</b>	6		<b>Width (inches)</b>	12
<b>Ext. Barrier Width (inches)</b>	8	<b>Interior Diaphragms</b>	<b>Height (inches)</b>	18
<b>Median Shld. Width (ft)</b>	0		<b>Width (inches)</b>	8
<b>Median Barrier Width (inches)</b>	0	<b>Slab Thickness (inches)</b>		10
<b>BRIDGE MESH</b>				
<b># of Girders</b>	3	<b># of Interior Diaphragms</b>	2	
<b>Length of Girders (ft)</b>	100	<b># of Virtual Diaphragms</b>	3	
<b>Tot. # of Diaphragms</b>	7	<b>Diaphragm Length (ft)</b>	47.333	
<b>MATERIAL PROPERTIES</b>		<b>Concrete Strength (psi)</b>		4000

**Table C.20: Support Reaction Comparison #11: Results**

<b>Reactions at Supporting Nodes: Program vs RISA</b>			
<b>Node</b>	<b>Program (k)</b>	<b>RISA (k)</b>	<b>% Difference</b>
1	114.990	115.043	-0.0464%
2	260.107	260.001	0.0408%
3	119.897	119.95	-0.0443%
19	64.663	64.679	-0.0241%
20	105.991	105.96	0.0294%
12	74.752	74.767	-0.0201%

**Table C.21: Support Reaction Comparison #12: BRIDGE Input**

<b>LOADING</b>				
		<b>Truck #1</b>	<b>Truck #2</b>	
<b>Truck Type</b>	Type T170 Unit		Heavy Equip. Trans.	
<b>Lane #</b>	1		2	
<b>Direction of Travel</b>	Up-station		Up-station	
<b>Truck Location</b>	Entering Bridge		Entering Bridge	
<b>Position in Lane</b>	Center		Center	
<b>Analysis Level</b>	Operating Posting		Operating Posting	
		<b>Truck #3</b>	<b>Truck #4</b>	
<b>Truck Type</b>	Type T130 Unit		Heavy Equip. Trans.	
<b>Lane #</b>	3		4	
<b>Direction of Travel</b>	Left Bound		Left Bound	
<b>Truck Location</b>	Exiting Bridge		Exiting Bridge	
<b>Position in Lane</b>	Center		Center	
<b>Analysis Level</b>	Operating Posting		Operating Posting	
<b>LANE ALIGNMENT</b>		<b>SECTION GEOMETRY</b>		
<b># of Lanes</b>	4	<b>Girders</b>	<b>Height (inches)</b>	36
<b>Lane Width (ft)</b>	12		<b>Width (inches)</b>	12
<b>Cantilever Width (ft)</b>	6	<b>Exterior Diaphragms</b>	<b>Height (inches)</b>	24
<b>Ext. Shld. Width (ft)</b>	6		<b>Width (inches)</b>	12
<b>Ext. Barrier Width (inches)</b>	8	<b>Interior Diaphragms</b>	<b>Height (inches)</b>	18
<b>Median Shld. Width (ft)</b>	0		<b>Width (inches)</b>	8
<b>Median Barrier Width (inches)</b>	0	<b>Slab Thickness (inches)</b>		10
<b>BRIDGE MESH</b>				
<b># of Girders</b>	3	<b># of Interior Diaphragms</b>		2
<b>Length of Girders (ft)</b>	100	<b># of Virtual Diaphragms</b>		0
<b>Tot. # of Diaphragms</b>	2	<b>Diaphragm Length (ft)</b>		47.333
<b>MATERIAL PROPERTIES</b>		<b>Concrete Strength (psi)</b>		4000

**Table C.22: Support Reaction Comparison #12: Results**

<b>Reactions at Supporting Nodes: Program vs RISA</b>			
<b>Node:</b>	<b>Program (k)</b>	<b>RISA (k)</b>	<b>% Difference:</b>
1	120.519	120.543	-0.0197%
2	249.081	249.034	0.0188%
3	125.393	125.417	-0.0188%
10	66.528	66.534	-0.0091%
11	102.229	102.215	0.0135%
12	76.650	76.657	-0.0095%



**Table C.23: Support Reaction Comparison #13: BRIDGE Input**

<b>LOADING</b>				
		<b>Truck #1</b>	<b>Truck #2</b>	
<b>Truck Type</b>		Type 3S2 Unit	H Unit	
<b>Lane #</b>		1	2	
<b>Direction of Travel</b>		Up-station	Up-station	
<b>Truck Location</b>		Entering Bridge	Exiting Bridge	
<b>Position in Lane</b>		Center	Center	
<b>Analysis Level</b>		Inventory	Inventory	
		<b>Truck #3</b>	<b>Truck #4</b>	
<b>Truck Type</b>		Type T130 Unit	Type T170 Unit	
<b>Lane #</b>		3	4	
<b>Direction of Travel</b>		Left Bound	Left Bound	
<b>Truck Location</b>		Entering Bridge	Exiting Bridge	
<b>Position in Lane</b>		Center	Center	
<b>Analysis Level</b>		Inventory	Inventory	
<b>LANE ALIGNMENT</b>		<b>SECTION GEOMETRY</b>		
<b># of Lanes</b>	4	<b>Girders</b>	<b>Height (inches)</b>	24
<b>Lane Width (ft)</b>	12		<b>Width (inches)</b>	8
<b>Cantilever Width (ft)</b>	0	<b>Exterior Diaphragms</b>	<b>Height (inches)</b>	24
<b>Ext. Shld. Width (ft)</b>	3		<b>Width (inches)</b>	8
<b>Ext. Barrier Width (inches)</b>	8	<b>Interior Diaphragms</b>	<b>Height (inches)</b>	16
<b>Median Shld. Width (ft)</b>	3		<b>Width (inches)</b>	8
<b>Median Barrier Width (inches)</b>	12	<b>Slab Thickness (inches)</b>		6
<b>BRIDGE MESH</b>				
<b># of Girders</b>	4	<b># of Interior Diaphragms</b>		1
<b>Length of Girders (ft)</b>	125	<b># of Virtual Diaphragms</b>		4
<b>Tot. # of Diaphragms</b>	7	<b>Diaphragm Length (ft)</b>		61
<b>MATERIAL PROPERTIES</b>		<b>Concrete Strength (psi)</b>		4000

**Table C.24: Support Reaction Comparison #13: Results**

<b>Reactions at Supporting Nodes: Program vs RISA</b>			
<b>Node</b>	<b>Program (k)</b>	<b>RISA (k)</b>	<b>% Difference</b>
1	45.792	45.793	-0.0014%
2	86.691	86.693	-0.0029%
3	104.374	104.367	0.0063%
4	118.311	118.314	-0.0029%
25	4.042	4.046	-0.0869%
26	86.718	86.718	-0.0004%
27	141.489	141.479	0.0074%
28	78.583	78.590	-0.0084%

**Table C.25: Support Reaction Comparison #14: BRIDGE Input**

<b>LOADING</b>				
		<b>Truck #1</b>	<b>Truck #2</b>	
<b>Truck Type</b>	Type 3-3 Unit		Type T130 Unit	
<b>Lane #</b>	1		2	
<b>Direction of Travel</b>	Up-station		Up-station	
<b>Truck Location</b>	Exiting Bridge		Exiting Bridge	
<b>Position in Lane</b>	Center		Center	
<b>Analysis Level</b>	Inventory		Inventory	
		<b>Truck #3</b>	<b>Truck #4</b>	
<b>Truck Type</b>	None		None	
<b>Lane #</b>	-		-	
<b>Direction of Travel</b>	-		-	
<b>Truck Location</b>	-		-	
<b>Position in Lane</b>	-		-	
<b>Analysis Level</b>	-		-	
<b>LANE ALIGNMENT</b>		<b>SECTION GEOMETRY</b>		
<b># of Lanes</b>	4	<b>Girders</b>	<b>Height (inches)</b>	24
<b>Lane Width (ft)</b>	10		<b>Width (inches)</b>	8
<b>Cantilever Width (ft)</b>	1	<b>Exterior Diaphragms</b>	<b>Height (inches)</b>	24
<b>Ext. Shld. Width (ft)</b>	3		<b>Width (inches)</b>	8
<b>Ext. Barrier Width (inches)</b>	8	<b>Interior Diaphragms</b>	<b>Height (inches)</b>	16
<b>Median Shld. Width (ft)</b>	0		<b>Width (inches)</b>	8
<b>Median Barrier Width (inches)</b>	0	<b>Slab Thickness (inches)</b>		6
<b>BRIDGE MESH</b>				
<b># of Girders</b>	4	<b># of Interior Diaphragms</b>		2
<b>Length of Girders (ft)</b>	125	<b># of Virtual Diaphragms</b>		3
<b>Tot. # of Diaphragms</b>	7	<b>Diaphragm Length (ft)</b>		44
<b>MATERIAL PROPERTIES</b>		<b>Concrete Strength (psi)</b>		5000

**Table C.26: Support Reaction Comparison #14: Results**

<b>Reactions at Supporting Nodes: Program vs RISA</b>			
<b>Node</b>	<b>Program (k)</b>	<b>RISA (k)</b>	<b>% Difference</b>
1	39.775	39.767	0.0201%
2	26.594	26.619	-0.0951%
3	28.497	28.472	0.0878%
4	2.917	2.925	-0.2708%
25	82.263	82.289	-0.0312%
26	117.950	117.897	0.0448%
27	56.182	56.209	-0.0486%
28	-0.178	-0.178	-0.2407%

**Table C.27: Support Reaction Comparison #15: BRIDGE Input**

<b>LOADING</b>				
		<b>Truck #1</b>	<b>Truck #2</b>	
<b>Truck Type</b>	Type 3-3 Unit		Type 3-3 Unit	
<b>Lane #</b>	1		2	
<b>Direction of Travel</b>	Up-station		Up-station	
<b>Truck Location</b>	Exiting Bridge		Exiting Bridge	
<b>Position in Lane</b>	Center		Center	
<b>Analysis Level</b>	Inventory		Inventory	
		<b>Truck #3</b>	<b>Truck #4</b>	
<b>Truck Type</b>	Type 3 Unit		H Unit	
<b>Lane #</b>	3		4	
<b>Direction of Travel</b>	Left Bound		Left Bound	
<b>Truck Location</b>	Entering Bridge		Entering Bridge	
<b>Position in Lane</b>	South Edge		North Edge	
<b>Analysis Level</b>	Inventory		Inventory	
<b>LANE ALIGNMENT</b>		<b>SECTION GEOMETRY</b>		
<b># of Lanes</b>	4	<b>Girders</b>	<b>Height (inches)</b>	36
<b>Lane Width (ft)</b>	12		<b>Width (inches)</b>	12
<b>Cantilever Width (ft)</b>	3	<b>Exterior Diaphragms</b>	<b>Height (inches)</b>	36
<b>Ext. Shld. Width (ft)</b>	3		<b>Width (inches)</b>	12
<b>Ext. Barrier Width (inches)</b>	8	<b>Interior Diaphragms</b>	<b>Height (inches)</b>	16
<b>Median Shld. Width (ft)</b>	3		<b>Width (inches)</b>	12
<b>Median Barrier Width (inches)</b>	12	<b>Slab Thickness (inches)</b>		8
<b>BRIDGE MESH</b>				
<b># of Girders</b>	4	<b># of Interior Diaphragms</b>		2
<b>Length of Girders (ft)</b>	60	<b># of Virtual Diaphragms</b>		0
<b>Tot. # of Diaphragms</b>	4	<b>Diaphragm Length (ft)</b>		54.333
<b>MATERIAL PROPERTIES</b>		<b>Concrete Strength (psi)</b>		5000

**Table C.28: Support Reaction Comparison #15: Results**

<b>Reactions at Supporting Nodes: Program vs RISA</b>			
<b>Node</b>	<b>Program (k)</b>	<b>RISA (k)</b>	<b>% Difference</b>
1	52.812	52.844	-0.0602%
4	49.858	49.911	-0.1066%
5	73.042	72.967	0.1030%
8	88.513	88.415	0.1112%
9	19.670	19.725	-0.2775%
12	84.281	84.318	-0.0439%
13	0.115	0.104	10.8286%
16	27.708	27.716	-0.0290%

**Table C.29: Support Reaction Comparison #16: BRIDGE Input**

<b>LOADING</b>				
		<b>Truck #1</b>	<b>Truck #2</b>	
<b>Truck Type</b>	Heavy Equip. Trans.		Type T170 Unit	
<b>Lane #</b>	1		2	
<b>Direction of Travel</b>	Up-station		Up-station	
<b>Truck Location</b>	Exiting Bridge		Exiting Bridge	
<b>Position in Lane</b>	North Edge		South Edge	
<b>Analysis Level:</b>	Inventory		Inventory	
		<b>Truck #3</b>	<b>Truck #4</b>	
<b>Truck Type</b>	Type 3-3 Unit		Type T130 Unit	
<b>Lane #</b>	3		4	
<b>Direction of Travel</b>	Left Bound		Left Bound	
<b>Truck Location</b>	Entering Bridge		Entering Bridge	
<b>Position in Lane</b>	South Edge		North Edge	
<b>Analysis Level</b>	Inventory		Inventory	
<b>LANE ALIGNMENT</b>		<b>SECTION GEOMETRY</b>		
<b># of Lanes</b>	4	<b>Girders</b>	<b>Height (inches)</b>	36
<b>Lane Width (ft)</b>	12		<b>Width (inches)</b>	18
<b>Cantilever Width (ft)</b>	3	<b>Exterior Diaphragms</b>	<b>Height (inches)</b>	24
<b>Ext. Shld. Width (ft)</b>	3		<b>Width (inches)</b>	12
<b>Ext. Barrier Width (inches)</b>	12	<b>Interior Diaphragms</b>	<b>Height (inches)</b>	24
<b>Median Shld. Width (ft)</b>	3		<b>Width (inches)</b>	12
<b>Median Barrier Width (inches)</b>	12	<b>Slab Thickness (inches)</b>		8
<b>BRIDGE MESH</b>				
<b># of Girders</b>	5	<b># of Interior Diaphragms</b>		1
<b>Length of Girders (ft)</b>	90	<b># of Virtual Diaphragms</b>		4
<b>Tot. # of Diaphragms</b>	7	<b>Diaphragm Length (ft.)</b>		54
<b>MATERIAL PROPERTIES</b>		<b>Concrete Strength (psi)</b>		5000

**Table C.30: Support Reaction Comparison #16: Results**

<b>Reactions at Supporting Nodes: Program vs RISA</b>			
<b>Node</b>	<b>Program (k)</b>	<b>RISA (k)</b>	<b>% Difference</b>
1	84.409	84.48	-0.0837%
2	132.906	132.735	0.1290%
3	75.796	75.912	-0.1524%
4	54.987	54.988	-0.0014%
5	46.302	46.285	0.0365%
31	107.212	107.322	-0.1029%
32	206.007	205.719	0.1398%
33	108.477	108.756	-0.2563%
34	105.658	105.520	0.1310%
35	86.045	86.083	-0.0436%

**Table C.31: Support Reaction Comparison #17: BRIDGE Input**

<b>LOADING</b>				
		<b>Truck #1</b>	<b>Truck #2</b>	
<b>Truck Type</b>	H Unit		Type 3 Unit	
<b>Lane #</b>	1		2	
<b>Direction of Travel</b>	Up-station		Up-station	
<b>Truck Location</b>	Exiting Bridge		Exiting Bridge	
<b>Position in Lane</b>	North Edge		South Edge	
<b>Analysis Level</b>	Inventory		Inventory	
		<b>Truck #3</b>	<b>Truck #4</b>	
<b>Truck Type</b>	HS Unit		Type 3 Unit	
<b>Lane #</b>	3		4	
<b>Direction of Travel</b>	Left Bound		Left Bound	
<b>Truck Location</b>	Entering Bridge		Entering Bridge	
<b>Position in Lane</b>	South Edge		North Edge	
<b>Analysis Level:</b>	Inventory		Inventory	
<b>LANE ALIGNMENT</b>		<b>SECTION GEOMETRY</b>		
<b># of Lanes</b>	4	<b>Girders</b>	<b>Height (inches)</b>	36
<b>Lane Width (ft)</b>	12		<b>Width (inches)</b>	18
<b>Cantilever Width (ft)</b>	3	<b>Exterior Diaphragms</b>	<b>Height (inches)</b>	24
<b>Ext. Shld. Width (ft)</b>	3		<b>Width (inches)</b>	12
<b>Ext. Barrier Width (inches)</b>	12	<b>Interior Diaphragms</b>	<b>Height (inches)</b>	24
<b>Median Shld. Width (ft)</b>	3		<b>Width (inches)</b>	12
<b>Median Barrier Width (inches)</b>	12	<b>Slab Thickness (inches)</b>		8
<b>BRIDGE MESH</b>				
<b># of Girders</b>	5	<b># of Interior Diaphragms</b>		2
<b>Length of Girders (ft)</b>	90	<b># of Virtual Diaphragms</b>		3
<b>Tot. # of Diaphragms</b>	7	<b>Diaphragm Length (ft)</b>		54
<b>MATERIAL PROPERTIES</b>		<b>Concrete Strength (psi)</b>		5000

**Table C.32: Support Reaction Comparison #17: Results**

<b>Reactions at Supporting Nodes: Program vs RISA</b>			
<b>Node</b>	<b>Program (k)</b>	<b>RISA (k)</b>	<b>% Difference</b>
1	5.164	5.167	-0.0501%
2	6.975	6.968	0.0998%
3	6.652	6.661	-0.1372%
4	7.026	7.021	0.0739%
5	4.864	4.866	-0.0378%
31	17.424	17.453	-0.1662%
32	77.635	77.564	0.0919%
33	48.463	48.556	-0.1914%
34	58.055	57.965	0.1557%
35	55.741	55.780	-0.0702%

**Table C.33: Support Reaction Comparison #18: BRIDGE Input**

LOADING				
		Truck #1	Truck #2	
Truck Type		H Unit	Type T170 Unit	
Lane #		1	2	
Direction of Travel		Up-station	Up-station	
Truck Location		Exiting Bridge	Exiting Bridge	
Position in Lane		North Edge	South Edge	
Analysis Level		Inventory	Inventory	
LANE ALIGNMENT		SECTION GEOMETRY		
# of Lanes	4	Girders	Height (inches)	36
Lane Width (ft)	12		Width (inches)	18
Cantilever Width (ft)	3	Exterior Diaphragms	Height (inches)	24
Ext. Shld. Width (ft)	3		Width (inches)	12
Ext. Barrier Width (inches)	12	Interior Diaphragms	Height (inches)	24
Median Shld. Width (ft)	3		Width (inches)	12
Median Barrier Width (inches)	12	Slab Thickness (inches)		8
BRIDGE MESH				
# of Girders	5	# of Interior Diaphragms	2	
Length of Girders (ft)	90	# of Virtual Diaphragms	0	
Tot. # of Diaphragms	4	Diaphragm Length (ft)	54	
MATERIAL PROPERTIES		Concrete Strength (psi)		5000

**Table C.34: Support Reaction Comparison #18: Results**

Reactions at Supporting Nodes: Program vs RISA			
Node	Program (k)	RISA (k)	% Difference
1	31.984	31.991	-0.0226%
4	45.123	45.138	-0.0338%
5	65.260	65.247	0.0203%
8	98.490	98.462	0.0282%
9	29.926	29.942	-0.0544%
12	35.817	35.836	-0.0522%
13	15.736	15.713	0.1477%
16	16.093	16.078	0.0922%
17	-5.983	-5.971	0.1939%
20	-6.446	-6.437	0.1391%

## Appendix D: ABAQUS Models: Shear and Normal Forces

Table D.1: Forces at One Support for ABAQUS Models with Girder Width of 12 inches

Beam Model	Normal Force (lbs)	Shear Force (lbs)
12-0.4-6-7	15999.7	2391.6
12-0.4-6-8	16001	3115.2
12-0.4-6-9	18002.2	4865
12-0.4-6-10	16002.5	4815.5
12-0.4-6-11	16003.5	5788.9
12-0.4-6-12	18006.9	8438.3
12-0.4-6-13	18009.2	9803.3
12-0.4-6-14	26024	14834
12-0.4-6-17	26042.4	14842
12-0.4-8-7	15980.7	2406.1
12-0.4-8-12	18006.9	8537.2
12-0.4-8-17	26038.7	14842
12-0.4-10-7	16000.63	2417.6
12-0.4-10-12	18007.1	8639.2
12-0.5-6-7	16000.74	2321.3
12-0.5-6-12	16006.54	6856.4
12-0.5-8-7	16000.77	2344
12-0.5-8-12	16006.82	6969.4
12-0.5-10-7	16000.76	2348
12-0.5-10-12	16007.02	7044.3
12-0.6-6-7	8000.11	593.26
12-0.6-6-12	16008	6842.8
12-0.6-8-7	8000.125	599.09
12-0.6-8-12	15988.45	6966.7
12-0.6-10-7	8000.133	599.24
12-0.6-10-12	16008.95	7022

**Table D.2: Forces at One Support for ABAQUS Models with Girder Width of 15 inches**

<b>Beam Model</b>	<b>Normal Force (lbs)</b>	<b>Shear Force (lbs)</b>
15-0.4-6-7	16000.38	2067.6
15-0.4-6-12	26010.25	13897
15-0.4-8-7	16000.4	2066.2
15-0.4-8-12	26010.06	13949
15-0.4-10-7	16000.43	2076.5
15-0.4-10-12	26010.22	14085
15-0.5-6-7	16000.43	2020.5
15-0.5-6-12	18005.22	7253.5
15-0.5-8-7	16000.49	2030.6
15-0.5-8-12	18005.24	7328.8
15-0.5-10-7	16000.44	2042
15-0.5-10-12	18005.4	7420.2
15-0.6-6-7	16000.56	1969.2
15-0.6-6-12	16004.75	5866.1
15-0.6-8-7	16000.54	1981.3
15-0.6-8-12	16004.86	5950.4
15-0.6-10-7	16000.54	1996
15-0.6-10-12	16005.04	6031.4



**Table D.3: Forces at One Support for ABAQUS Models with Girder Width of 18 inches**

<b>Beam Model</b>	<b>Normal Force (lbs)</b>	<b>Shear Force (lbs)</b>
18-0.4-6-7	16000.3	1826.9
18-0.4-6-8	18000.7	2936.3
18-0.4-6-9	18000.9	3685.5
18-0.4-6-10	26157.5	8900.4
18-0.4-6-11	26005	10518
18-0.4-6-12	26006.9	12317
18-0.4-6-13	34016.6	19389
18-0.4-8-7	16000.28	1814.3
18-0.4-8-12	26006.61	12275
18-0.4-10-7	16000.23	1815.4
18-0.4-10-12	26006.58	12333
18-0.5-6-7	16000.28	1788.5
18-0.5-6-12	26008.83	12376
18-0.5-8-7	16000.28	1786.7
18-0.5-8-12	26008.84	12417
18-0.5-10-7	16000.32	1794
18-0.5-10-12	26008.84	12535
18-0.6-6-7	16000.34	1755.4
18-0.6-6-12	18004.13	6380.4
18-0.6-8-7	16000.37	1762.2
18-0.6-8-12	18004.16	6438.1
18-0.6-10-7	16000.39	1772.3
18-0.6-10-12	18004.31	6518

## Appendix E: RF and Truck Ratings for Bridge # 54-104-15.45

**Table E.1: Rating Factors for Spans #2 and #4 for 50% and 100% Girder Width**

Rating	Operating		Inventory		
	b <sub>w</sub> used	100%	50%	100%	50%
H Unit		1.24	1.09	0.74	0.65
T 3		1.19	1.05	0.71	0.63
HS		1.12	1.01	0.67	0.61
3S2		1.19	1.05	0.71	0.63
T 3-3		1.24	1.09	0.74	0.66
T-130		1.18	1.06	0.71	0.64
T-170		1.13	1.04	0.68	0.62
HET		0.97	1.03	0.58	0.62
SU4		1.16	1.04	0.69	0.62
SU5		1.13	1.02	0.68	0.61
SU6		1.12	1.01	0.67	0.61
SU7		1.1	1.01	0.66	0.6
NRL		1.1	1	0.66	0.6

**Table E.2: Truck Ratings for Spans #2 and #4 for 50% and 100% Girder Width**

Rating	Operating		Inventory		
	b <sub>w</sub> used	100%	50%	100%	50%
H Unit		15.5	13.625	9.25	8.125
Type 3		29.75	26.25	17.75	15.75
HS		40.32	36.36	24.12	21.96
3S2		42.84	37.8	25.56	22.68
Type 3-3		49.6	43.6	29.6	26.4
T-130		76.7	68.9	46.15	41.6
T-170		96.05	88.4	57.8	52.7
HET		106.7	113.3	63.8	68.2
SU4		31.32	28.08	18.63	16.74
SU5		35.03	31.62	21.08	18.91
SU6		38.92	35.0975	23.2825	21.198
SU7		42.625	39.1375	25.575	23.25
NRL		44	40	26.4	24

**Table E.3: Rating Factors for Span #3 for 50% and 100% Girder Width**

Rating	Operating		Inventory		
	$b_w$ used	100%	50%	100%	50%
H Unit		1.28	1.11	0.77	0.67
T 3		1.21	1.07	0.73	0.64
HS		1.13	1.02	0.68	0.61
3S2		1.19	1.06	0.71	0.64
T 3-3		1.25	1.11	0.75	0.66
T-130		1.19	1.07	0.71	0.64
T-170		1.14	1.04	0.68	0.62
HET		1.03	0.97	0.62	0.58
SU4		1.18	1.05	0.71	0.63
SU5		1.15	1.04	0.69	0.62
SU6		1.13	1.03	0.68	0.61
SU7		1.12	1.02	0.67	0.61
NRL		1.11	1.01	0.66	0.61

**Table E.4: Truck Ratings for Span #3 for 50% and 100% Girder Width**

Rating	Operating		Inventory		
	$b_w$ used	100%	50%	100%	50%
H Unit		16	13.875	9.625	8.375
Type 3		30.25	26.75	18.25	16
HS		40.68	36.72	24.48	21.96
3S2		42.84	38.16	25.56	23.04
Type 3-3		50	44.4	30	26.4
T-130		77.35	69.55	46.15	41.6
T-170		96.9	88.4	57.8	52.7
HET		113.3	106.7	68.2	63.8
SU4		31.86	28.35	19.17	17.01
SU5		35.65	32.24	21.39	19.22
SU6		39.268	35.7925	23.63	21.198
SU7		43.4	39.525	25.9625	23.638
NRL		44.4	40.4	26.4	24.4

# K-TRAN

## KANSAS TRANSPORTATION RESEARCH AND NEW-DEVELOPMENT PROGRAM

